PONTIFÍCIA UNIVERSIDADE CATÓLICA
DO RIO DE JANEIRO

Jose Adriano Bento de Souza Cardoso

Pressure and Temperature transiente response in a coupled stratified wellbore-reservoir model

Dissertação de Mestrado

Dissertation presented to the Programa de Pós-Graduação em Engenharia Mecânica of PUC-Rio in partial fulfillment of the requirements for the degree of Mestre em Engenharia Mecânica.

Advisor : Prof. Márcio da Silveira Carvalho
Co-advisor: Dr. Danmer Maza Quinones

Rio de Janeiro
July 2020

PONTIFÍCIA UNIVERSIDADE CATÓLICA
DO RIO DE JANEIRO

Jose Adriano Bento de Souza Cardoso

Pressure and Temperature transiente response in a coupled stratified wellbore-reservoir model

Dissertation presented to the Programa de Pós-Graduação em Engenharia Mecânica of PUC-Rio in partial fulfillment of the requirements for the degree of Mestre em Engenharia Mecânica. Approved by the Examination Committee.

Prof. Márcio da Silveira Carvalho
Advisor
Departamento de Engenharia Mecânica PUC-Rio

Dr. Danmer Maza Quinones
Co-advisor
Laboratório de Microhidrodinâmica e Escoamento em Meios Porosos LMMP/PUC-Rio

Prof. Angela Ourivio Nieckele
Departamento de Engenharia Mecânica PUC-Rio

Prof. Abelardo Borges Barreto Junior
Departamento de Engenharia Mecânica PUC-Rio

Rio de Janeiro, July 27th, 2020

Jose Adriano Bento de Souza Cardoso

Bachelor in Mechanical Engineering with emphasis in Automobile Mechanics by Instituto Militar de Engenharia - IME (1989)

To God and my family for their love.

Acknowledgments

First, I would like to thank God for giving me strength and courage to overcome challenges.

To my advisor, Prof. Marcio Carvalho, for trusting on me.

To my children for understanding my absence, You can be sure that all I want is to be an example for you.

To my co-advisor Dr. Danmer Maza, who was tireless always ready to support me.

To my friends Alandmara, Rafael and Vinicius for your help, support and patience.

To my parents, for even don't understanding what and why I was studying , always encouraged me.

Abstract

Bento de Souza Cardoso, Jose Adriano; Carvalho, Márcio da Silveira (Advisor); Maza, Danmer Quinones (Co-Advisor). **Pressure and Temperature transiente response in a coupled stratified wellbore-reservoir model**. Rio de Janeiro, 2020. 113p. Dissertação de Mestrado – Departamento de Mechanical Engineering, Pontifícia Universidade Católica do Rio de Janeiro.

Well formation tests are usually performed to determine rock properties of a reservoir and the obtained data has often been interpreted based on an assumption that the reservoir is homogeneous in the vertical direction and described by a 1-D model. However, many reservoirs are found to be composed of different number of layers that have different characteristics. Production wells in such reservoirs may receive oil from more than one layer. In stratified reservoir system, the pressure and temperature behavior are not necessarily the same as in single layered system, and rarely reveals the same average properties of the entire system. The prediction of the characteristics of the individual layers is important to describe properly the reservoir and improve production management. This work presents a numerical transient-thermal model for a coupled wellbore/2D-reservoir considering Joule-Thompson heating/cooling, adiabatic fluid expansion/compression, conduction and convection effects for both wellbore and reservoir for a single-phase fluid flow. The two-dimensional reservoir model allows the analysis of stratified zones and barriers. The model allows cross flow between the adjacent layers with different rock properties. Wellbore temperature and pressure at a certain gauge depth are evaluated along the time. Results show how pressure transient analysis (PTA) and temperature transient analysis (TTA) can be used to characterize different configuration of stratified reservoirs.

Keywords

Non-isothermal; coupled wellbore-reservoir; stratified reservoir; wellbore test; temperature transient analysis;

Resumo

Bento de Souza Cardoso, Jose Adriano; Carvalho, Márcio da Silveira; Maza, Danmer Quinones. **Resposta transiente de pressão e temperatura em um modelo acoplado poço- reservatório estratificado**. Rio de Janeiro, 2020. 113p. Dissertação de Mestrado – Departamento de Engenharia Mecânica, Pontifícia Universidade Católica do Rio de Janeiro.

Testes de formação são normalmente realizados para determinar as propriedades rochosas do reservatório e os dados obtidos costumam ser interpretados com base no pressuposto que o reservatório é homogêneo na direção vertical e descrito por um modelo uni dimensional. No entanto, muitos reservatórios são compostos por diversas camadas que possuem características diferentes. Os poços de produção nesses reservatórios podem receber óleo de mais de uma camada. Em um sistema de reservatório estratificado, o comportamento da pressão e da temperatura não é necessariamente o mesmo de um sistema em camada única e raramente revela as mesmas propriedades médias de todo o sistema. Prever as características das camadas individuais é importante para descrever adequadamente o reservatório e melhorar o gerenciamento da produção. Este trabalho apresenta um modelo numérico, transiente-térmico para um sistema acoplado poço - reservatório 2D, levando-se em consideração efeitos Joule-Thompson responsáveis pelo aquecimento / resfriamento do fluido, expansão/compressão adiabática, além de efeitos de condução e convecção para o poço e o reservatório em um escoamento monofásico. A análise bidimensional do reservatório permite que se simule zonas de estratificação e barreiras. O modelo permite fluxo através de camadas adjascentes com propriedades de rocha diferentes. Pressão e temperatura a uma certa posição no poço produtor são avaliadas ao longo do tempo. Resultados mostram que a análise do transiente de pressão (PTA) e a análise do transiente de temperatura (TTA) podem ser utilizadas para caracterizar diferentes configurações de um reservatório estratificado.

Palavras-chave

Não isotérmico; poço-reservatório acoplado; reservatório estratificado; teste de poço; análise do transiente de temperatura;

Table of contents

List of figures

List of tables

List of Symbols

Greek Symbols

α	Wellbore inclination
α_{te}	Earth total Thermal diffusive
δ	Roughness
ε_{JT}	Joule-Thompson coefficient
ϕ	Effective porosity
ρ	Density
θ	Time discretization constant
μ	Viscosity
ν	Kinematic viscosity
φ	Effective adiabatic-expansion coefficient
λ_e	Thermal conductivity of the earth
λ_{an}	Thermal conductivity of material in annulus
λ_{cem}	Thermal conductivity of cement
λ_t	Thermal conductivity of the saturated porous medium

Acronyms

A	Cross-Section area of the pipe
C_T	Lumped parameter, thermal storage constant
C_p	Specific heat
D	Inside pipe diameter
E_w	Wellbore energy per unit length
E_f	Fluid energy per unit length
f_D	Dimensionless function
g	Gravity acceleration
g_t	Geothermal Gradient
H	Internal Enthalpy
L_R	Relaxation distance
p	Pressure
r	Radial coordinate
Re	Reynold's number

r_{ti}	Inside tubbing radius
r_{to}	Outside tubbing radius
r_{ci}	Inside casing radius
r_{co}	Outside casing radius
r_{wb}	Wellbore radius
s	Saturation, fraction
T	Temperature, K
t	Time, seconds
t_D	Dimensionless time
T_{ei}	Earth Temperature distribution
T_{eibh}	T_{ei} at bottom hole
q	Flow rate
c	Compressibility
U	Internal Energy
U_t	Overall heat transfer coefficient
$\mathbf{v}$	Velocity vector
r, z	Radial and vertical coordinate

subscript

e	Energy source term
JT	Joule-Thompson
m	Component
o	Oil
p	constant pressure or isobaric
r	Rock
s	Mass source term
sf	Sand face
t	Total
T	Constant Temperature or isotherm
w	Water
wb	Wellbore

*"Never turn away from your dreams. Because
if they are gone, you will continue to live, but
you will no longer exist"*

Mark Twain .

1
Introduction

1.1
Motivation

Oil and gas are hydrocarbons found in nature in sedimentary basins formed by processes of deposition and decomposition of organic and inorganic materials. Due to their formation and storage process, reservoirs are often formed by more than one layer of rocks, giving rise to stratified reservoirs, with layers with different properties. Well test is used to characterize the reservoir in order to improve reserve estimation and the production management. The test consists in analysing the pressure transient behavior inside the wellbore after successive opening and closing the production valve. Commonly, well test assumes an isothermal fluid flow, i.e., small temperature change during the test. However, this assumption can lead to misinterpretation of pressure signal and as a consequence errors in the reservoir characterization. Moreover, the characteristic pressure response during a formation test is evaluated assuming a homogeneous reservoir in the vertical direction. Therefore, they provide average properties of the different layers of a stratified reservoir, not the characteristics of each individual layer.

Many reservoirs are stratified, with layers with very different properties. Optimized production strategies and more precise estimation of reserves can be developed with detailed of information of each individual layer is available. Current strategies of well test provide average information. Therefore, there is a great need for the development of models and characterization procedures for stratified reservoirs.

1.2
Well-Tests

Formation tests consist of changing the flow rate and record the pressure transient response in the flow in a well. They have three main objectives:

1. Reservoir evaluation

   In order to make the best production decisions for a given reservoir, we need to know its properties, deliverability and size. For this, it is important to determine the conductivity of the reservoir (product Kh), initial pressure and its boundaries. At the same time, samples of the fluid are taken to determine its physical properties. Damage formation and storage effects are also assessed.

2. Reservoir management

   During the productive life of a reservoir, it is desirable to know the conditions of the producing well. It is useful to monitor changes in pressure and so it's possible to refine the forecast production.

3. Reservoir description

   Geological formations hosting oil, gas, water and geothermal reservoirs are complex, and may contain different rock types, stratigraphics interfaces, faults, barriers and fluid fronts. Some of these features may influence the transient behavior to a measurable extent, and most will affect the reservoir performance.

If properly designed, well tests can be used to estimate the reservoir properties. The type of test performed is usually governed by the test objective or practical limitations or expediencies, Horne (1990)[1]. Usually there are six types of well test :

1. Drawdown test

   In this test the wellbore top valve which is initially closed, is suddenly opened to let the oil flow at a constant rate. The pressure will drop with time, as sketched in Fig. 1.1. In this kind of test, the flow rate control is very important. This is a very good method to evaluate the boundaries of a reservoir because the long time behavior, the fluctuations in flow rate are less significant, Horne (1990)[1].

2. Buildup test

   In this test, a wellbore which is producing is shut down and as a consequence the pressure start to buildup. A constant flow rate (zero) is easier achieved as can be seen in Fig. 1.2. On the other hand, production time is lost.
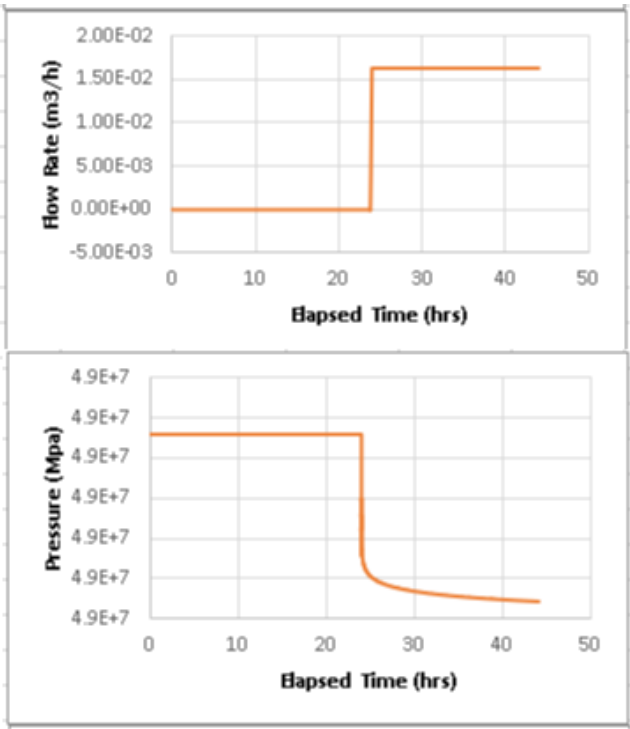
Figure 1.1: Drawdown test - Pressure and flow rate.
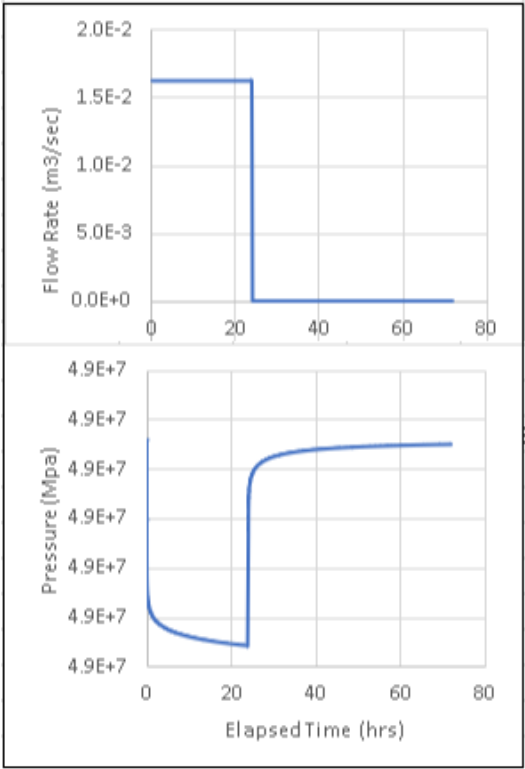
Figure 1.2: Build Up Test - Pressure and Flow Rate.

3. Injection test

   An injection test is conceptually identical to a drawdown test, except that flow is into the well rather than out of it [1]. Flow rate control is easier than in production rates, however analysis of the tests can be complicated by multi phase effects due to water/gas injection.

4. Falloff test

   After a injection test, the wellbore is shut down. It is conceptually the same as the buildup test. The falloff test measures the decline of pressure. The interpretation is more difficult if the injected fluid is different from the original reservoir fluid.

5. Interference test

   The pressure is measured in a well while a flow rate variation is imposed in a different well of the same reservoir. This test is useful to characterize long reservoirs. Interference test can be used regardless of the flow rate variation sequence (drawdown, buildup, falloff or injection).

6. Drill stem test

   A special tool is mounted in the end of the drill string, it is only performed while a rig is over the well. Analysis of DST requires special techniques since the flow is not constant.

1.3
Well-test interpretation

The analytical process of interpreting a well test is based on the identification of flow behavior over time, and the adoption of a simplified mathematical model to describe it. Thus, it is possible to estimate parameters that lead to the observed behavior of the reservoir (permeability, storage, skin effect, porosity, boundaries, etc).

In the beginning, well tests were based on straight lines and applied to middle time semi log data (Miller et al. (1950); Horner (1951); Warren and Root (1963); Odeh and Jones (1965); Horner (1951)) and were solved using Laplace Transform. The emphasis was on production operations, and well test analysis results were limited to the reservoir permeability, skin effect or productivity index, drainage area and average reservoir pressure. Straight lines analysis techniques rely on the existence of a straight line on a plot of the pressure response by some function of the elapsed time when a particular flow regime dominates.

Table 1.1: Well test behavior - Agarwall, (2008)

	Early time	**Intermediate time**	**Late time**
radial flow	storage	infinite acting radial flow	close boundary sealing fault constant pressure
fractures	storage/ bilinear flow	radial flow	close boundary sealing fault constant pressure
double porosity	storage	double porosity behavior transition radial flow	closed boundary sealing fault constant pressure

During 1960's and 70's type-curve or log-log analysis were introduced (Ramey (1970); Agarwal ey al. (1970); Gringarten and Ramey (1974); Cinco-Ley et al. (1978); MacKinley (1971)). The initial objective was to identify the correct infinite-acting radial flow (IARF) straight line on a Miller, Dyes, Hutchinson (MDH) method or Horner semi-log plot.

The introduction of derivatives by Bourdet et al. (1983) made well tests analysis a characterization tool.

Although different reservoirs present different physical properties, the different flow behaviors (pressure response) can be used to evaluate different properties (Perez-Rozales, (1978)), as illustrated in tab. 1.1.

Formation test analysis is an inverse problem (Gringarten, 2008[2]). Parameters of the flow (reservoir properties) are estimated based on the system response to an external perturbation, as sketched in Fig. 1.3.
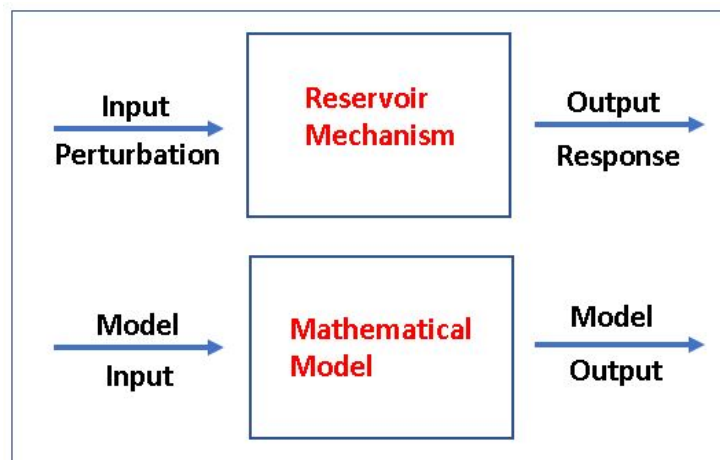
Figure 1.3: Modeling Flowchart of a Well-test

One limitation of inverse problems is the lack of a unique solution, that is, local minimums can be found, which do not correspond to the correct characterization.

1.4
Derivative methods in Well-Test interpretation

During the 80's the emergence of derivative methods allowed the analysis of heterogeneous reservoirs. This method emphasizes the pressure derivative over the derivative of the logarithm of time. This plot is generally referred to as the diagnostic chart. Table 1.2 presents a summary of the evolution of well tests over time.

Table 1.2: Evolution of well-tests- Gringarten (2008).

Date	Interpretation Method	Tools	Enphasis
50s	Straight lines	Laplace transform	Homogeneous reservoir behavior
Late 60s Early 70s	Pressure type-curve analysis	Greens's functions	Near wellbore effects
Late 70s	Type curves with independent variables	Integrated methodology Stehfest algorithm	Dual-porosity behavior
Early 80s	Derivatives	Computerized analysis	Heterogeneous reservoir behavior and reservoir boundaries
90s		Computer-aided analysis downhole rate measurements integration with interpretation models from other data	Multilayered reservoir
Early 00s		Deconvolution	Enhanced radius of investigation boundaries

In the past, the main obstacle to this test was the accuracy and frequency of the data obtained, as it is the processing of primary pressure and test time data. The advantage of the derivative plot is that it is able to display in a single graph many different characteristics that would otherwise require different plots (Horner (1990)[1]). Figure 1.4 shows an example of a pressure derivative plot where the different flow regimes and the different characteristics of the reservoir can be observed in only one single graphic.
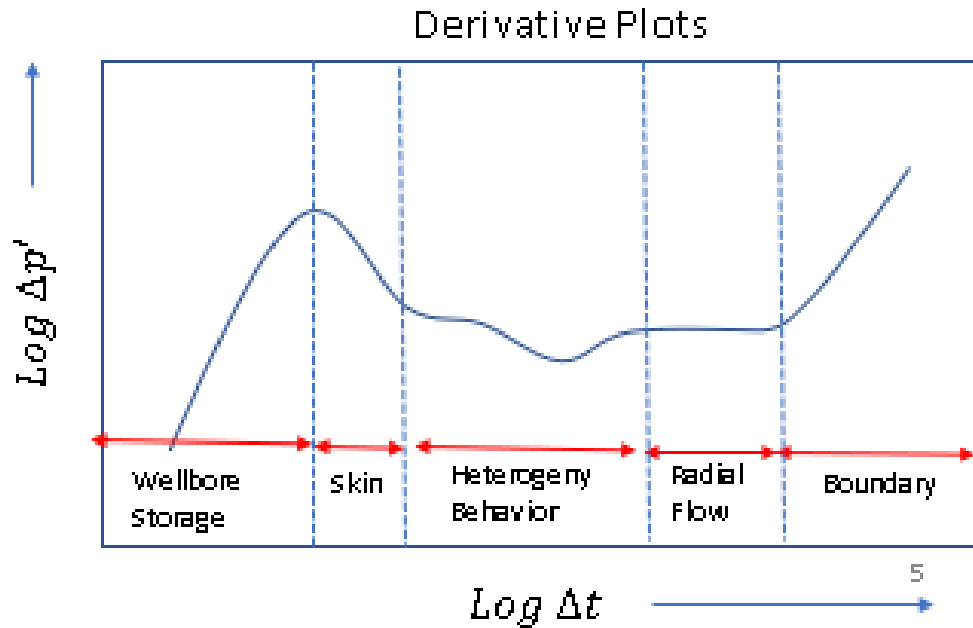
Figure 1.4: Schematic derivative plot of a heterogeneous reservoir with storage and skin.

Fig.1.5 presents the derivative graph for two different reservoirs, one homogeneous and other stratified with double permeability. This graph consist of 2 curves: the upper one is the pressure variation curve (discontinuous red line for the stratified reservoir and continuous in blue line for the homogeneous reservoir) and the bottom is the Bourdet derivative (blue in continuous line for homogeneous and red in discontinuous line for the stratified reservoir). The pressure derivative allows the identification of the flow regimes achieved during the test and heterogeneity's.
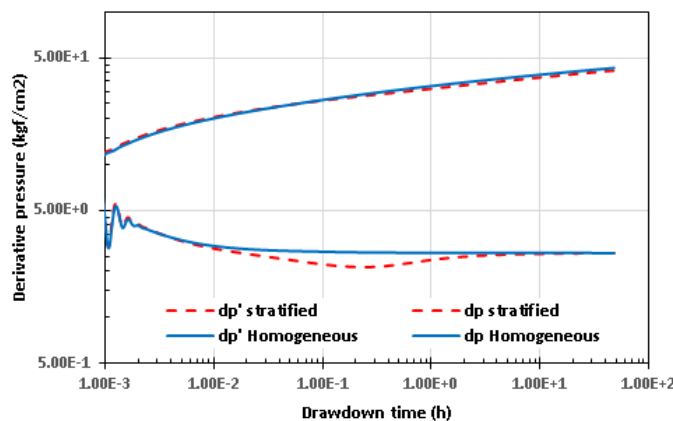
Figure 1.5: Derivative plot of a stratified and a homogeneous reservoir.

The diffusivity equation solved for infinite acting radial flow (IARF), with reference pressure p_o , has the following solution :

$$p\left(r, t = 0\right) = p_o$$

$$\frac{\Delta p}{q} = \frac{p_o - p_w\left(t\right)}{q} = \frac{qB\mu}{4\pi kh} \ln\left(\frac{4}{e^\gamma} \frac{kt}{\phi\mu c_t r_w^2}\right) \tag{1-1}$$

where $\Delta p/q$ is the normalized pressure drop, which varies linearly with the logarithm of time.

By definition, the derivative pressure is given by:

$$\Delta p'\left(t\right) = \frac{d\Delta p(t)}{d\left(Ln\left(t\right)\right)}$$

so

$$\Delta p'\left(t\right) = \frac{qB\mu}{4\pi kh} \tag{1-2}$$

The logarithmic derivative in the infinite radial regime test is observed as a constant value in the diagnostic graph, as shown in Fig. 1.5 above 10h.

In this graph, the up and down of the derivative curve represent, respectively, losses and gains in transmissibility, Kh/μ in different positions of the reservoir. In the diagnostic graph, the transmissibility increases in the negative direction of the vertical axis. With this understanding, one can also observe the behavior of the transient from a numerical model and the diagnostic graph simultaneously.

In practice, the following algorithm proposed by Bourdex (1989) [3] is used:

$$\Delta p'(t_j) = \frac{\Delta p(t_{j+1}) - \Delta p(t_j)}{ln(t_{j+1}/t_j)} \frac{ln(t_j/t_{j-1})}{ln(t_{j+1}/t_{j-1})} + \frac{\Delta p(t_j) - \Delta p(t_{j-1})}{ln(t_j/t_{j-1})} \frac{ln(t_{j+1}/t_j)}{ln(t_{j+1}/t_{j-1})}. \tag{1-3}$$

Where the subindex j is the point where is calculated $\Delta p'$ and $j+1$ and $j-1$ are the points on the right and left sides respectively.

1.5
Literature Review

1.5.1
Layered Reservoirs

The first work on pressure response in multilayer reservoirs was proposed by Lefkovits, et al. (1961)[4]. They presented a rigorous analytical study on reservoirs without communication between the layers (commingled). The pressure evolution was solved for layers with different properties. They also did a complete mathematical analysis for a two-layer system and found that early-time layer flow rate was governed basically by permeability-thickness product Kh and skin, and the late-time flow rate depends on oil-filled volume and compressibility. Nevertheless, individual layer properties could be determined from the proposed methodology.

Bourdet (1985)[5] extended Levkovits' work to systems with cross-layer communication (crossflow) and included storage and skin effects. He showed that his solution recovered general forms of many reservoir models by showing that the solution was identical to the solutions of other problems when some reservoir parameters took limiting values.

Park (1989)[6] made a detailed analysis of the behavior of early and late times for each layer.

A semipermeable wall model was proposed by Deans and Gao (1983)[7]. The model assumes all the vertical resistance to flow is concentrated on the wall between the layers so there is no vertical variation of pressure in each layer. Fluid flow through the barrier is assumed to be proportional to the local pressure difference across the wall, and inversely proportional to the viscosity of the fluid.

Russell and Prats (1962 b)[8] published a separate paper about practical aspects of cross flow, in which they concluded that crossfow between communicating adjacent layers was of great economic significance, and was beneficial by shortening the operating life of a reservoir and by raising primary ultimate recovery.

Pendergrass and Berry (1962)[9] also solved the same problem, concentrating on the efect of permeability distribution between the layers. They concluded that it was not possible to diagnose stratification from wellbore pressure data except at early time. As it will be discussed later in this work, their conclusion may be due to the negligence of the vertical permeabilities of the layers.

Kucuk, et al. (1984)[10] used the technique of nonlinear parameter estimation by coupling sandface production rate of each layer with wellbore pressure. The coupling of layer production rate is very significant for multilayered reservoirs because rate transient of each layer reveals information about the layer, while wellbore pressure is determined more by average reservoir pa-

rameters.

Kuchuk et al. (1986a)[11] first presented a new testing analysis technique called "multilayer test", which made it possible to uniquely determine individual-layer permeabilities and skin factors for reservoirs with commingled layers. Their multilayer testing technique starts with the well flowing at a constant production or injection rate. A production log (PL) flow rate survey is acquired during stabilized flow, then the flow meter is stationed above one of the layers to be characterized, and a step change in surface rate is made while the PL string is kept in a stationary position. After some time, usually several hours, another flow rate survey is acquired, the PL string is stationed above another of the layers, and the surface flow rate is changed again. The test continues repeating these same steps until transient measurements of pressure and flow rate have been made above each of the layers to be characterized. It is important to note that this method to determine the characteristics of individual layers of a stratified reservoir is complex and expensive.

Ehlig-Economides and Joseph (1987)[12] did a complete review of previous works and extended the results of two layers to a multilayer model, presented a new test for determination of individual layer properties, the key of the method is the interpretation of each layer following a change in the total wellbore flow rate. Interpreting the results, it's possible to determine each layer properties. Such analytical solutions provided the theoretical support for multilayer test technique. Formation crossflow was modeled as in the semipermeable-wall model of Gao and Deans [7], which assumes that all resistance to vertical flow is concentrated in the walls (layer top, bottom).

Shah et al. (1988)[13] by introducing step-wise changes in the surface flow rates made the Ehlig-Economides model (1987) [12] applicable in practice.

Kuchuk and Wilkinson (1991)[14] presented a more generic method. Their solutions are applicable to a variety of commingled reservoir systems (no flow between different layers) in which individual layers may have different initial and outer-boundary conditions. The vertical wellbore can commingle layers with completely general model characterizations including partially penetrated or vertically fractured wellbores. Their study extended the application of the multilayer test in practice. Multilayer test models are important in determining individual layer. The testing techniques depend on the acquisition of transient downhole pressure and layer flow rate data that are sensitive to layer properties.

Sui et al. (2008)[15] presented a numerical model to evaluate the individual layer permeability and skin from transient temperature measurements of a commingled production well penetrating a multilayer gas reservoir. Under the

condition of no layer communication (commingled reservoir), they found that the temperature solution is sensitive to permeability and skin.

Several researchers have published results showing the need for coupled simulation in wellbore and reservoir systems. Sarica et al. (2001)[16] showed in their isothermal model that the traditional decoupling approach between the well and the reservoir in horizontal wells does not capture the initial transients interaction between them. Belfroid et al. (2007)[17] analyzed the dynamic behavior in the well and the reservoir, identifying the time and space scales in which the reservoir coupling becomes important. They created a temporal space map showing the importance of coupling in different production processes.

1.5.2
Thermal Model

During most of all oil production processes, temperature variations in the reservoir and wellbore are minor, so the hypothesis of treating the problem as isothermal was an acceptable approach.

Muradov and Davies (2012) [18] reported that the resolution of array temperature sensing, permanent downhole gauges (PDG) and distributed temperature sensing (DTS) allow measurements of very small temperature changes in the orders of 0.002 , 0.005 and 0.01 deg C, respectively.

As reported by Duru and Horne (2011a)[19] and Sidorova et al. (2015)[20], temperatures can be measured with a resolution better than 0.01K and pressure better than 0.07 kPa.

Initial applications of the use of temperature data in the oil industry date back to the 1930´s when the first electronic thermometer was developed for underground wellbore applications. Schlumberger et al. (1936) [21] was one of the pioneers who indicated the usefulness of measuring fluid temperature.

The first analytical solutions taking into account thermal effects in reservoirs were developed by Lauwerier (1955)[22] and Malofeev (1963)[23]. They show results of temperature distribution in reservoirs due to purely convective heat transfer in linear and radial flow systems respectively.

An initial attempt to develop mathematical models for the behavior of heat transfer in a porous medium was presented by Ramey (1962)[24], who developed a model for predicting the temperature of the well fluid as a function of the depth of the injection well. Atkinson and Ramey (1977)[25] developed a model that estimates the temperature distribution caused by non-isothermal flow in a reservoir, assuming a constant fluid velocity within the reservoir. However, the model was simplified to obtain an analytical solution

and did not take into account variations that could happen due to the effects of compressibility and viscous dissipation.

Horne and Shinohara (1979)[26] presented heat transfer equations in wells for the production and injection of a single-phase fluid, modifying the Ramey model. With these modifications, the model considers heat losses between the well and the reservoir, and thus is able to evaluate the temperature of the reservoir.

Crookston et al. (1979)[27] presented a model to numerically simulate thermal recovery processes, taking into account the flow of water, oil and gas. Their results showed the evolution of temperature with time. In the proposed model, the effects of gravity and capillarity were considered, however the effect arising from the velocity of the formation fluid and the velocity of the vapor in the injection were not considered.

Garg and Pritchett (1977)[28] presented an analytical solution for temperature variation at the outlet of a reservoir with single-phase flow of a lightly compressible fluid.

Shiu and Beggs (1980)[29] presented another modification of the Ramey model to predict the temperature profile for a producing well, where the temperature of the fluid entering the well from the reservoir is known using a correlation method to estimate the relaxation distance. This wellbore model considers heat transfer strictly from convection and conduction, with the fluid entering at a constant temperature equal to that of the reservoir. Maubeuge et al. (1994)[30] presented an initial attempt to analyze the possible heating or cooling of the reservoir's fluid before it entered the wellbore and incorporated the Joule-Thomson effect in their two-dimensional reservoir model using a two-dimensional finite volume method.

Chekalyuk[31] presented the first work on sandface transient temperature. He decoupled the pressure diffusion equation and the thermal energy balance and presented an analytical temperature solution for constant rate drawdown using the Boltzmann transformation for a line-sink well.

Ramazanov and Nagimov (2007)[32] using the same assumptions of Ckekalyuk (1985) used the method of characteristics to predict sandface temperature for a slight compressible single-phase fluid flow in an homogeneous reservoir.

App (2010)[33] studied the Joule-Thompson effect in high flow reservoirs. Several authors concluded that the temperature transient measured during build up and drawdown tests at a constant flow rate provide important information to evaluate formation properties: Sui et al. (2008a, 2008b)[15]; App (2009); Duru and Horne (2010a,2010b, 2011a, 2011b)[19, 34]; Ramazanov

et al. (2010)[35];App an Yoshioka(2013)[36]; Sidorova et al (2015); Onur and Palabiyik (2015)[37].

All the works cited consider local thermal equilibrium, which is realistic for flow in porous media with low velocity. They include Joule-Thompson (J-T) heating-cooling effects, transient adiabatic expansion/compression and heat transfer by convection and conduction. Pressure and temperature are decoupled by using constant coefficients involving rock, fluid and thermal parameters in the thermal energy balance equation.

Onur and Çinar (2016)[38] presented a semi-log and log-log interpretation method to analise the temperature transient data from drawdown and build up tests for a coupled Wellbore-reservoir system.

App and Yoshioka (2013)[36] presented a steady-state analytical solution and a transient numerical simulation to evaluate the temperature signals.

Mao and Zeidouni (2017)[39] presented an analytical solution to determine the individual layer temperature signal associated with constant rate production of slightly compressible fluid from a fully penetrating vertical well in a multilayered reservoir. They provide semi-log temperature interpretation techniques to characterize the layer permeability and porosity, and damage zone radius considering the availability of adequate data. The simplified characterization method are also developed in the case of insufficient or inaccurate data to obtain permeability and production rate between layers which helps to identify the layers contributing the most to well production.

Galvao et al (2019)[40] showed that in high transmissivity reservoirs the isothermal analysis may lead to the interpretation of false geological heterogeneities, since the heat loss during the buildup period provides an increase in the pressure exerted by the static fluid, due to an increase in the oil mass density, and a change in tubing length, leading to change in the gauge position. These effects can make a homogeneous reservoir be wrongly interpreted as a double-porosity reservoir, yielding invalid conclusions to the geological modeling.

Izgec et al. (2006)[41] presented a model that applies to a well and reservoir coupled system. Their study took into account heat transfer mechanism in the well and the interaction with the surrounding environment, without considering possible changes in the temperature of the reservoir fluid before entering the well. Kocabas (2004)[42] developed an analytical model that considered linear flow in a steady state capable of calculating temperature transients caused by non-isothermal injection of fluids. The effect of advection in the porous medium and thermal exchanges with the adjacent rock formations were included.

Hossaim et al. (2007)[43] solved numerically the non-isothermal problem of the injection of fluids, considering two situations: first, the existence of the local thermal balance between the fluid and the rock and second, the absence of the local thermal balance between the fluid and the rock (fluid and rock with different temperatures). The results show that the temperature difference between the fluid and the rock is negligible.

Dawkrajai and Yoshioca (2006)[44] developed a complete energy balance equation for the temperature distribution inside the reservoir for horizontal production wells. Both presented heat transfer equations for both the well and reservoir and developed numerical models for the calculation of pressure and temperature taking into account Joule-Thomson effects and viscous dissipation. However, they assume a constant flow and permanent conditions to obtain the solution in their models.

1.6
Objectives

The main objective of this work is to develop a computational model for the analysis of transient fluid flow and heat transfer that occur between a production well and its adjacent stratified reservoir area. The model is used to analyse the effect of individual reservoir layer properties in the transient pressure and temperature response. The results can be used in the development of formation test for stratified reservoirs.

The dissertation is organized in 6 chapters including the introduction and the conclusion. The second chapter describes the mathematical model that describes the transient flow and heat transfer that occur in a well and a stratified reservoir. The third chapter presents the numerical solution of the fully coupled wellbore-reservoir system. In the fourth chapter, the numerical implementation is validated by comparing the predictions to results available in the literature for limiting cases. In the fifth chapter, synthetic cases are analyzed in order to show the effect of stratified reservoirs and it's impacts on pressure transient analysis (PTA) interpretations and how temperature transient analysis (TTA) can help the interpretation of the pressure signals. In chapter sixth, the conclusion of this work are presented.

.

2
Mathematical Model

2.1
Introduction

This chapter presents the mathematical model that describes the transient flow and heat transfer that occur in a well and in a stratified reservoir. Figure 2.1 shows a schematic representation of the system to be analyzed.

The reservoir model consists of a mass balance and energy conservation equations in two dimensions (radial and vertical direction). The momentum conservation equation, in the case of porous media, represented by the Darcy equation, is already considered in the mass and energy conservation equations.

The wellbore model is described by three one-dimensional conservation equations: Mass, momentum and energy.
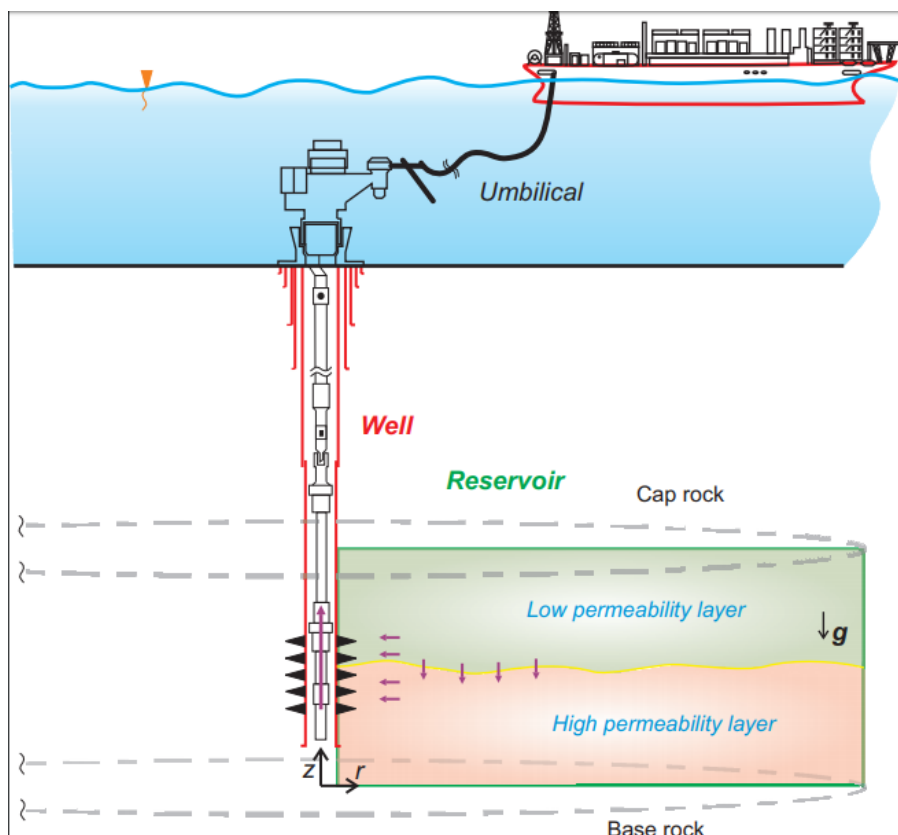
Figure 2.1: Cross section schematic drawing of a two-layer radial reservoir with cross-flow between layers

2.2
Wellbore Model

In this work, the following hypothesis for the wellbore model were considered:

1. Axial flow of slightly compressible single phase fluid.

2. Wellbore storage (WBS) is considered.

3. Heat transfer to the surroundings occurs due to radial diffusion. There is no axial heat diffusion.

4. Density is function of temperature and pressure. Others fluid properties are constant.

5. Wellbore materials have constant thermal conductivities.

The wellbore has two distinct zones: One that is in contact with the reservoir, in which it fully penetrates. The second zone, above of the reservoir, which is sealed with respect to the formation. Fig. 2.2 shows a diagram of the coupled system, where the radial flow from the reservoir enters the well.
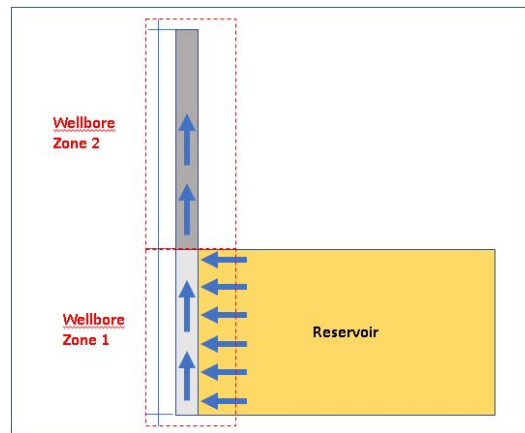
Figure 2.2: Coupled Wellbore-reservoir model.

2.2.1
Wellbore Mass Balance

The differential mass conservation equation assuming an axial flow is written as:

$$\frac{\partial \rho}{\partial t} + \frac{\partial (\rho v_z)}{\partial z} + q_s = 0. \tag{2-1}$$

Where q_s is a mass source term, which represents the radial flow that comes from the reservoir.

Using the definitions of coefficients of isothermal compressibility and isobaric thermal expansion of the fluid:

$$c_o = \frac{1}{\rho}\left(\frac{\partial \rho_o}{\partial p}\right)\bigg|_T, \tag{2-2}$$

$$\beta_o = -\frac{1}{\rho}\left(\frac{\partial \rho_o}{\partial T}\right)\bigg|_p, \tag{2-3}$$

and assuming that density is only function of temperature and pressure, equation (2-1) can be combined with (2-2) and (2-3) , leading to:

$$c_o\rho\frac{\partial p}{\partial t} + (-\beta_o)\rho\frac{\partial T}{\partial t} + \rho\frac{\partial v}{\partial z} + v\left(c_o\rho\frac{\partial p}{\partial z} + (-\beta_o)\rho\frac{\partial T}{\partial z}\right) + q_s = 0. \tag{2-4}$$

Introducing the volumetric flow rate, $q(z,t) = v_z A$, and considering positive the upward flow direction, the mass conservation equation is written as:

$$\frac{\partial p}{\partial t} + (-\frac{\beta_o}{c_o})\frac{\partial T}{\partial t} + \frac{1}{Ac_o}\frac{\partial q}{\partial z} + \frac{q}{Ac_o}\left(c_o\frac{\partial p}{\partial z} + (-\beta_o)\frac{\partial T}{\partial z}\right) + \frac{q_s}{\rho c_o} = 0. \tag{2-5}$$

This form of the mass conservation equation is similar to the one used by Ulker et al. (2017) [45].

The source term q_s represents the flow from the reservoir, and is given by:

$$q_s = (2/R)(\rho v)_r. \tag{2-6}$$

2.2.2
Wellbore Momentum

In this work, the conservation equations presented by Chaudhry (1979) and Mansoori et al. (2015), cited by Onur (2017) [45], are used. These models consider the momentum balance in addition to the mass balance in the wellbore. This approach is more general than the WBS model (Wellbore Storage model, Van Everdingen and Hurst (1949)), which only considers the

mass balance and ignores the momentum balance in the wellbore, and the thermal expansion of the fluid.

The flow is one dimensional (only "z" direction, vertical) in the wellbore, so, in the "r" (radial) direction momentum is neglected. The tube cross section is constant (rigid).

Under these conditions, Ulker et al. (2017) [45] writes the momentum balance equations as:

$$\frac{1}{A}\frac{\partial q}{\partial t} + \frac{q}{A^2}\frac{\partial q}{\partial z} + \frac{1}{\rho_o}\frac{\partial p}{\partial z} + gsin\alpha + \frac{fq\,|q|}{2\left(A^2\right)D} = 0. \tag{2-7}$$

Where D is the pipe inside diameter, α is the angle that the wellbore makes with the horizontal and f is the Darcy-Weishbach friction factor. Although results presented here are for vertical wellbore, $\alpha = 90^o$, here is presented in a more general form. For laminar flow, it is a function of the Reynolds number Re:

$$f = \frac{64}{R_e}. \tag{2-8}$$

For turbulent flow (Re>4000), the friction factor is given by Colebrook (1939).

$$\frac{1}{\sqrt{f}} = -2.0log\left(\frac{\delta/D}{3.7} + \frac{2.51}{R_e\sqrt{f}}\right), \tag{2-9}$$

where: δ/D represents the relative roughness of the tube and

$$R_e = \frac{\rho v_z D}{\mu} = \frac{v_z D}{\nu} = \frac{qD}{A\nu},$$

is the Reynold number. The kinematic viscosity is:

$$\nu = \frac{\mu}{\rho}.$$

2.2.3
Wellbore Energy conservation

The energy conservation model used in the present work is similar to the one presented by Hasan et al. (2005) [46].

The mass balance equation for a wellbore control volume takes account the conductive heat loss to the formation (Q), the convective energy transport into and out of the control volume, z is positive in the upward direction and the length of the control volume is Δz, as scketched in Fig. 2.3 . The energy-balance equation is written taking account to the lost energy to the formation and the convective energy transport into and out to the control volume.

E - Fluid internal energy;

H_f-Fluid enthalpy;

w- Fluid mass rate;

T_o - Inlet fluid temperature;

r_1- Inside radius of the tubing;

T_1 -Temperature of the fluid in the tubing, $T_1 = T_1(z,t)$;

m- Fluid mass in the control volume;

r_2- Outside radius of the casing;

T_2 -Temperature of the casing outer surface, $T_2 = T_2(z,t)$;

$(mE)_w$ - Mass and internal energy of the wellbore system;

$(mE)_w$ - Mass and internal energy of the fluid inside the control volume.

$$Q = \frac{\partial (mE)_{cv}}{\partial t} + \frac{\partial (mE)_w}{\partial t} - \frac{\partial}{\partial z}\left[w\left(H_f + \frac{1}{2}v^2 + gz\right)\right] \qquad \text{(2-10)}$$
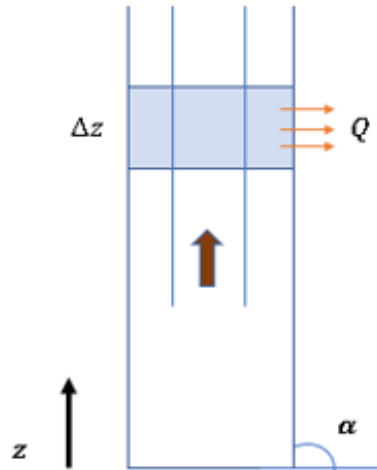
Figure 2.3: Wellbore heat problem scheme.

The first lumped term represents the rise in fluid temperature at any time. The second term on the right side of the equation (2.3) represents the

energy absorbed or released by the tubular material and cement sheaths in the wellbore. Omitting this term can lead to serious error because it accounts for a significant fraction of the total energy exchange between the wellbore and the formation. The temperature rises of the cement/tubular material, at any time, may be considered as a fraction of the rise of the fluid temperature (Hasan ad Kabir, (2005) [46]), so we can write:

$$(mE)_w = C_T(mE)_{cv} \tag{2-11}$$

Thus , the thermal storage parameter $C_T = (mE)_w/(mE)_{cv}$ represents the capacity of the wellbore to store or release heat as a function of the fluid mass and fluid heat capacity.

$$\frac{\partial}{\partial t} \left(\, (mE)_{cv} + \, (mE)_w \right) = \frac{\partial}{\partial t} \left(mc_p T_f \left(1 + C_T \right) \right) = \left(mc_p \left(1 + C_T \right) \right) \frac{\partial T_f}{\partial t} \tag{2-12}$$

During the early periods, w varies with depth (z), so:

$$\frac{d}{dz} \left(w H_f \right) \neq w \frac{d}{dz} \left(H_f \right)$$

However, a steady state in the fluid flow is attained much more rapidly than stabilization of fluid temperature. For this analysis, we will consider w independent of depth (z). Therefore, the third term on the right side is rewritten as:

$$\frac{\partial}{\partial z} \left[w \left(H_f + \frac{1}{2} v^2 + gz \right) \right] = w \left(\frac{\partial H_f}{\partial z} + v \frac{\partial v}{\partial z} + g \sin \alpha \right) =$$
$$w \left(c_p \frac{\partial T_f}{\partial z} - c_p \epsilon_{JT} \frac{\partial p}{\partial z} + v \frac{\partial v}{\partial z} + g \sin \alpha \right) \tag{2-13}$$

Defining:

$$\varphi \left(z, t \right) = \epsilon_{JT} \frac{\partial p}{\partial z} - \frac{v}{c_p} \frac{\partial v}{\partial z} \tag{2-14}$$

So, the heat loss by the control volume to the formation is:

$$Q = \left(mc_p \left(1 + C_T \right) \right) \frac{\partial T_f}{\partial t} - w \left(c_p \frac{\partial T_f}{\partial z} - \varphi \left(z, t \right) + g \sin \alpha \right) \tag{2-15}$$

Usual procedure for flow problems of this type is to solve the total-energy and mechanical-energy equations simultaneously. The solution may be approximated by the following considerations:

Total energy equation:

$$dH + gdz + udu = dQ - dW_f$$

Assuming steady state flow of a single-phase fluid in a pipe, flow-work W_f is zero, so:

$$dH + gdz + udu = dQ$$

If the fluid is noncompressible, the kinetic-energy term becomes zero.

$$dH + gdz = dQ$$

By enthalpy definition,

$$dH = dE + d\left(PV\right) = dE + VdP$$

For a noncompressible fluid

$$dH = cdT + VdP$$

Neglecting the flowing friction, the term VdP is equal to the change in fluid head

$$dH \approx cdT + gdz$$

Considering flow down the well, the increase in enthalpy due to increase in pressure is equal to the loss in potential energy. Conversely, for flow up the well, the loss of enthalpy due to the decrease in pressure is approximately equal to the increase in potential energy.

As a result, the total-energy becomes:

$$c_p dT \approx dQ$$

for a noncompressible liquid flowing vertically in a constant-diameter tube. Assuming no phase changes, an approximate energy balance over the differential element of depth dz , yields: heat loss by liquid = heat transferred to the casing or surrounding formation

$$dq = -wc_p dT = 2\pi r_1 U \left(T_1 - T_2\right) dz \tag{2-16}$$

The rate of heat conduction from the casing to the surrounding formation may be expressed as:

$$dq = \frac{2\pi\lambda_e \left(T_2 - T_e\right) dz}{f\left(t\right)} \tag{2-17}$$

Assumption that the heat transfers radially away from the wellbore Assuming geothermal temperature is a linear function of depth,

$$T_e = az + b \tag{2-18}$$

Equations (2-17) and (2-18) may be substituted in (2-16) to yield:

$$\frac{\partial T_1}{\partial z} + (T_1 - T_e)L_R = 0 \tag{2-19}$$

and

$$L_R = \frac{2\pi}{c_p w} \left[\frac{r_{to}U_{to}\lambda_e}{\lambda_e + (r_{to}U_{to}T_D)}\right] \tag{2-20}$$

An energy balance on the formation leads to the partial differential equation, derived in cylindrical coordinates, for the variation of formation temperature with radial distance from the well.

$$\frac{\partial^2 T_e}{\partial r^2} + \frac{1}{r}\frac{\partial T_e}{\partial r} = \frac{\rho_e c_e}{k_e}\frac{\partial T_e}{\partial t} \tag{2-21}$$

T_e is the formation temperature at a certain depth at time t, and distance r, measured from the center of the wellbore. At very early times, the formation temperature retains its initial value, except near the wellbore. As time increases, heat transferred from the warm wellbore fluid raise the formation temperature in its vicinity. The heat flow rate at the wellbore/formation interface is governed by Fourier´s law of heat conduction. This equation can be solved in terms of dimensionless variables. Hasan and Kabir solved the resulting equation with the Laplace transform, following the approach suggested by van Everdingen and Husrt [47].

If $t_D > 1.5$:

$$T_D = \left[0.4063 + \frac{1}{2}lnt_D\right]\left[1 + \frac{0.6}{t_D}\right]$$

If $t_D < 1.5$:

$$T_D = 1.1281\sqrt{t_D}\left(1 - 0.3\sqrt{t_D}\right)$$

The above expressions for dimensionless become discontinuous around

1.5. The continuous expression for the same expression is provided as:

$$T_D = ln\left[e^{(-0.2t_D)} + \left(1.5 - 0.3719e^{-t_D}\right)\sqrt{t_D}\right] \tag{2-22}$$

The heat received or lost for the formation is:

$$Q = wc_p\left(T_{ei} - T_f\right)L_R,$$

so:

$$Q = wc_p\left(T_{ei} - T_f\right)L_R = \left(mc_p\left(1 + C_T\right)\right)\frac{\partial T_f}{\partial t} - w\left(c_p\frac{\partial T_f}{\partial z} - \varphi\left(z,t\right) + gsin\alpha\right) \tag{2-23}$$

and can be rearranged in terms of flow rate (q):

$$\frac{\partial T_f}{\partial t} = \frac{qL_R}{A\left(1 + C_T\right)}\left(T_{ei} - T_f\right) - \frac{q}{A\left(1 + C_T\right)}\left(\frac{\partial T_f}{\partial z} - \varphi\left(z,t\right) + \frac{gsin\alpha}{c_p}\right) \tag{2-24}$$

The convection heat from the reservoir will be treated the same way as the mass flux, as a source term q_e.

$$\rho_o AC_{po}(1 + C_T)\frac{\partial T}{\partial t} = \rho_o qC_{po}L_R\left[T_{ei}(z) - T(z,t)\right] - $$
$$\rho_o qC_{po}\left[\frac{\partial T}{\partial z} - \varphi(z,t) + \frac{gsin\alpha}{C_{po}}\right] + q_e. \tag{2-25}$$

$T_{ei}(z)$ is the initial earth temperature distribution, due to geothermal gradient, defined by

$$T_{ei}(z) = T_{eibh} - zg_tsin\alpha, \tag{2-26}$$

and T_{eibh} is the earth temperature at $z = 0$ and $t = 0$, and g_t is the geothermal gradient taken as 0.03 K/m.

$$\varphi(z,t) = \varepsilon_{JTo}\frac{\partial p}{\partial z} - \frac{q}{\left(A\right)^2 C_p}\frac{\partial q}{\partial z}, \tag{2-27}$$

and L_R is referred as Thermal Relaxation distance, defined as:

$$L_R = \frac{2\pi r_{to}U_t\lambda_e}{\rho_o qc_{po}\left[\lambda_e + r_{to}U_tf_D(t_D)\right]},$$

$f_D(t_D)$ is the dimensionless heat transfer function. The approximation given by Hasan an Kabir (2002) [48]is used in the present work.

$$f_D(t_D) = ln \left[e^{-0.2t_D} + \left(1.5 - 0.3719e^{-t_D}\right) \sqrt{t_D} \right],$$

t_D is the dimensionless time, defined by :

$$t_D = \frac{\alpha_{te}}{r_{co}^2}t,$$

α_{te} is the effective/total thermal diffusive constant of earth. U_t is the overall heat transfer coefficient, which determines the heat transfer from the wellbore to the surroundings. This was presented by Sagar et al (1991) [49] the model is derived from the steady-state energy equation that considers the heat-transfer mechanisms found in a wellbore, and if flow occurs inside a tubing, as sketched in Fig. 2.4, is given by:

$$U_t = \frac{1}{r_{ti}} \left[\frac{ln\left(r_{ci}/r_{co}\right)}{\lambda_{an}} + \frac{ln\left(r_{wb}/r_{co}\right)}{\lambda_{cem}} \right]^{-1},$$

r_{ti} is the inside tubbing radius

r_{to} is the outside tubbing radius

r_{ci} is the inside casing radius

r_{co} is the outside casing radius

r_{wb} is the wellbore radius

λ_e is the thermal conductivity of the earth

λ_{an} is the thermal conductivity of material in anulus

λ_{cem} is the thermal conductivity of cement
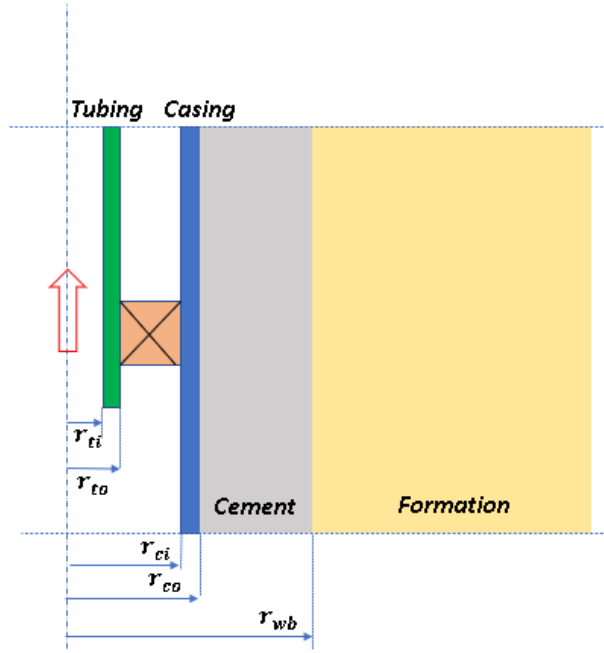
Figure 2.4: wellbore with a production column scheme.

The energy source term that represents the convective heat transfer from the reservoir is:

$$q_e = \frac{2}{R} \frac{\rho_r v_r}{\rho_w} \frac{1}{Cp_o(T_r - T_w)}. \tag{2-28}$$

2.3
Reservoir

The reservoir model used in this work is based on the model presented by Onur and Cinar (2016) [38] for one dimension and will be extended to two-dimensional reservoir. The reservoir is heterogeneous, i.e. the values of porosity and permeability may vary as function of z and r coordinates.

The following hypotheses are considered:

1. Flow in two dimensions (radial and vertical),

2. Single phase oil with connate water,

3. Fluid flow is governed by Darcy's Law, both for radial and vertical directions,

4. Reservoir parameters and thermal properties of fluid (except density and porosity) do not vary with temperature and pressure,

5. Wellbore is vertical and fully penetrates the reservoir.

6. Solid matrix is rigid and is in local thermal equilibrium with surrounding fluids (oil and water),

7. The reservoir is thermally isolated on the bottom and top boundaries,

8. There is no fluid flow from upper and lower boundaries,

9. Capillary effects are negligible,

10. Gravity effects are considered.

2.3.1
Mass Balance

The fluid phases in the reservoir is composed of oil and connate water. The mass balance of each phase is written as:

$$\frac{\partial}{\partial t}\left(\phi s_m \rho_m\right) + \nabla \cdot \left(\rho_m \mathbf{v}_m\right) = 0, \tag{2-29}$$

where $m = w, o$ and s_m is the saturation .

Since the aqueous phase is immobile, the saturation of both phases are constant.

$$(s_m) = cte.$$

$$s_w + s_o = 1.$$

Expanding equation (2-29):

$$\phi s_m \frac{\partial}{\partial t}\left(\rho_m\right) + s_m \rho_m \frac{\partial}{\partial t}\left(\phi\right) + \rho_m \nabla \cdot \left(\mathbf{v}_m\right) + \mathbf{v}_m \cdot \nabla\left(\rho_m\right) = 0. \tag{2-30}$$

The isothermal compressibility and isobaric thermal expansion coefficients for oil and water phases are defined as:

$$C_m = \frac{1}{\rho_m}\frac{\partial \rho_l}{\partial p}\bigg|_T, \tag{2-31}$$

$$\beta_m = -\frac{1}{\rho_m}\frac{\partial \rho_l}{\partial T}\bigg|_p. \tag{2-32}$$

The effective isothermal compressibility and isobaric thermal expansion coefficients for the rock are defined as:

$$C_r = \frac{1}{\phi}\frac{\partial \phi}{\partial p}\bigg|_T, \tag{2-33}$$

$$\beta_r = -\frac{1}{\phi}\frac{\partial \phi}{\partial T}\bigg|_p. \tag{2-34}$$

Assuming density as function of pressure and temperature, replacing (2-31), (2-32), (2-33) and (2-34) in (2-30):

$$\phi\left(C_m\frac{\partial p}{\partial t} - \beta_m\frac{\partial T}{\partial t}\right) + s_m\frac{\partial}{\partial t}\left(\phi\right) + \nabla\cdot\left(\mathbf{v}_m\right) + \frac{1}{\rho_m}\mathbf{v}_m\cdot\nabla(\rho_m) = 0. \tag{2-35}$$

Equation (2-35) for water, $m = w$

$$\phi s_w\left(C_w\frac{\partial p}{\partial t} - \beta_w\frac{\partial T}{\partial t}\right) + s_w\frac{\partial\left(\phi\right)}{\partial t} + \nabla\cdot\left(\mathbf{v}_w\right) + \frac{1}{\rho_w}\mathbf{v}_w\cdot\nabla(\rho_w) = 0. \tag{2-36}$$

Equation (2-35) for oil, $m = o$

$$\phi s_o\left(Co\frac{\partial p}{\partial t} - \beta o\frac{\partial T}{\partial t}\right) + s_o\frac{\partial\left(\phi\right)}{\partial t} + \nabla\cdot\left(\mathbf{v}_o\right) + \frac{1}{\rho_o}\mathbf{v}_o\cdot\nabla\left(\rho_o\right) = 0. \tag{2-37}$$

Since we assume connate water, $\mathbf{v}_w = 0$.

Combining the oil and water mass balance equations, (2-36) and (2-37):

$$\phi\left(C_r + C_w s_w + s_o C_o\right)\frac{\partial p}{\partial t} - \phi\left(\beta_r + \beta_w s_w + s_o\beta_o\right)\frac{\partial T}{\partial t} + \nabla\cdot(\mathbf{v_o}) + \frac{1}{\rho_o}\mathbf{v_o}\cdot\nabla(\rho_o) = 0. \tag{2-38}$$

The definition of C_t and β_t as the total system (fluid + rock) isothermal and thermal expansion coefficients are:

$$C_t = C_r + s_w C_w + s_o C_o, \tag{2-39}$$

$$\beta_t = \beta_r + s_w \beta_w + s_o \beta_o. \tag{2-40}$$

Replacing in equation (2-38):

$$\phi C_t \frac{\partial p}{\partial t} - \phi \beta_t \frac{\partial T}{\partial t} + \nabla \cdot (\mathbf{v}_o) + \frac{1}{\rho_o} \mathbf{v}_o \cdot \nabla(\rho_o) = 0. \tag{2-41}$$

Darcy's law, radial direction :

$$v_r = -\frac{K_r}{\mu} \frac{\partial p}{\partial r}, \tag{2-42}$$

Darcy's law, vertical direction:

$$v_z = -\frac{K_z}{\mu} \left(\frac{\partial p}{\partial z} - \rho g \right). \tag{2-43}$$

Where K_r and K_z are the components related to principal directions of the permeability tensor **K**.

The final form of the mass conservation equation for a two-dimensional reservoir in cylindrical coordinates is:

$$\begin{aligned}
\frac{\partial p}{\partial t} - \frac{\beta_t}{C_t} \frac{\partial T}{\partial t} =& \frac{1}{C_t \phi \mu} \frac{1}{r} \frac{\partial}{\partial r} \left(r K_r \frac{\partial p}{\partial r} \right) + \left(\frac{1}{C_t \phi \mu} \right) \frac{\partial}{\partial z} \left(K_z \left(\frac{\partial p}{\partial z} - \right) \right) + \\
& (\frac{K_r}{\phi \mu} \frac{C_o}{C_t})(\frac{\partial p}{\partial r}) \left(\frac{\partial p}{\partial r} \right) - (\frac{K_r}{\phi \mu} \frac{\beta o}{C_t})(\frac{\partial p}{\partial r}) \frac{\partial T}{\partial r} + \\
& \left(\frac{K_z}{\mu \phi} \frac{C_o}{C_t} \right) \left(\frac{\partial p}{\partial z} - \rho g \right) \left(\frac{\partial p}{\partial z} \right) - \left(\frac{K_z}{\mu \phi} \frac{\beta o}{C_t} \right) \left(\frac{\partial p}{\partial z} - \rho g \right) \frac{\partial T}{\partial z}.
\end{aligned} \tag{2-44}$$

2.3.2
Energy Model

The energy conservation equation model used in this work is based on the model presented by Onur and Cinar (2017a) [45] and was derived from

Barenblatt et al (1990).

$$\frac{\partial}{\partial t}\left[\phi\left(s_w\rho_w U_w + s_o\rho_o U_o\right) + (1-\phi)\rho_s U_s\right] + \nabla\cdot(\rho_o U_o\mathbf{v_o}) + \nabla\cdot(p\mathbf{v_o}) -$$

$$\nabla\cdot(\lambda_t\nabla T) = 0.$$

$$(2\text{-}45)$$

Using the relation between specific internal energy and specific internal enthalpy:

$$\rho_m H_m = \rho_m U_m + p. \tag{2-46}$$

For $m = o, w$, the second and third terms of Eq. (2-45) can be written as:

$$\nabla\cdot(\rho_o U_o\mathbf{v_o}) + \nabla\cdot(p\mathbf{v_o}) = \nabla\cdot((\rho_o U_o + p)\mathbf{v_o}) = \nabla\cdot(\rho_o H_o\mathbf{v_o}). \tag{2-47}$$

Returning to equation 2-45:

$$\frac{\partial}{\partial t}\left[\phi\left(s_w\rho_w U_w + s_o\rho_o U_o\right) + (1-\phi)\rho_s U_s\right] + \nabla\cdot(\rho_o H_o\mathbf{v_o}) - \nabla\cdot(\lambda_t\nabla T) = 0. \tag{2-48}$$

The convection term of Eq. 2-48:

$$\nabla\cdot(\rho_o H_o\vec{v}_o) = \rho_o\mathbf{v_o}\nabla H_o + H_o\nabla\cdot(\rho_o\mathbf{v_o}). \tag{2-49}$$

The accumulation term for each phase from Eq. (2-48) is written as:

$$\frac{\partial}{\partial t}(\phi s_m\rho_m U_m) = \frac{\partial}{\partial t}(\phi s_m\rho_m H_m - \phi s_m p) =$$
$$H_m\frac{\partial}{\partial t}(\phi s_m\rho_m) + \phi s_m\rho_m\frac{\partial H_m}{\partial t} + \frac{\partial}{\partial t}(\phi s_m p). \tag{2-50}$$

For $m = o, w$

$$\frac{\partial}{\partial t}(\phi s_m\rho) = s_m\frac{\partial}{\partial t}(\phi\rho) + \phi\rho\frac{\partial s_m}{\partial t}. \tag{2-51}$$

Thus:

$$\frac{\partial}{\partial t}\left(\phi s_m \rho_m U_m\right) = H_m \frac{\partial}{\partial t}(\phi s_m \rho_m) + \phi s_m \rho_m \frac{\partial H_m}{\partial t} - s_m \frac{\partial}{\partial t}\left(\phi p\right) - \phi p \frac{\partial s_m}{\partial t}. \quad (2\text{-}52)$$

If the matrix solid is rigid, so $H_s = U_s$

$$\frac{\partial}{\partial t}\left[(1-\phi)\rho_s U_s\right] = \frac{\partial}{\partial t}\left[(1-\phi)\rho_s H_s\right] = \frac{\partial}{\partial t}\left[(1-\phi)\rho_s\right] + (1-\phi)\rho_s \frac{\partial[H_s]}{\partial t}. \quad (2\text{-}53)$$

$$\phi s_o \rho_o \frac{\partial H_o}{\partial t} + \phi s_w \rho_w \frac{\partial H_w}{\partial t} - \frac{\partial(\phi p)}{\partial t} + (1-\phi)\rho_s \frac{\partial[H_s]}{\partial t} + \rho_o \mathbf{v_o} \nabla H_o - \quad (2\text{-}54)$$
$$\nabla(\lambda_t \nabla T) = 0.$$

Enthalpy is a function of pressure and temperature, and using the definitions of heat capacity of the fluid at constant pressure and Joule-Thompson coefficient:

$$c_p = \left(\frac{\partial H}{\partial T}\right)_p \quad (2\text{-}55)$$

$$\varepsilon_{JT} = \left(\frac{\partial T}{\partial p}\right)_H \quad (2\text{-}56)$$

$$\partial H = \left(\frac{\partial H}{\partial T}\right)_p \partial T + \left(\frac{\partial H}{\partial p}\right)_T \partial p \quad (2\text{-}57)$$

Thus,

$$\partial H = c_p \left(\partial T - \varepsilon_{JT}\partial p\right).$$

For $m = oil$ and $water$,

$$\nabla H_m = c_{pm}\left(\nabla T - \varepsilon_{JTo}\nabla p\right).$$

And for $m = rock$,
$$\nabla H_m = c_{pm}\left(\nabla T\right).$$

The model presented by Onur and Cinar (2017a) [45] assume that

porosity is constant, so the third of term equation (2-54) is simplified as:

$$\frac{\partial}{\partial t}(\phi p) = \phi \frac{\partial p}{\partial t}.$$

Rearranging:

$$\left[\phi \left(s_p \rho_o c_{po} + s_w \rho_w c_{pw}\right) + (1 - \phi) \rho_s c_{ps}\right] \frac{\partial T}{\partial t} - \left[\phi \left(s_p \rho_o c_{po} + s_w \rho_w c_{pw} \varphi_w\right)\right] \frac{\partial p}{\partial t} +$$
$$\rho_o c_{po} \mathbf{v_o} \left(\nabla T - \varepsilon_{JTo} \nabla p\right) - \nabla \left(\lambda_t\right) = 0.$$
$$(2\text{-}58)$$

Using Darcy's law, equations (2-42) and (2-43):

$$\left[\phi \left(s_p \rho_o c_{po} + s_w \rho_w c_{pw}\right) + (1 - \phi) \rho_s c_{ps}\right] \frac{\partial T}{\partial t} - \left[\phi \left(s_p \rho_o c_{po} + s_w \rho_w c_{pw} \varphi_w\right)\right] \frac{\partial p}{\partial t} +$$
$$\rho_o c_{po} \left(\frac{-K_r}{\mu} \frac{\partial p}{\partial r}\right) \left(\frac{\partial T}{\partial r}\right) + \rho_o c_{po} \left(\frac{K_z}{\mu} \frac{\partial p}{\partial z} - \rho_o g\right) \left(\frac{\partial T}{\partial z}\right) - \rho_o c_{po} \varepsilon_{JTo} \left(\frac{-K_r}{\mu} \frac{\partial p}{\partial r}\right) \left(\frac{\partial p}{\partial r}\right) +$$
$$\rho_o c_{po} \varepsilon_{JTo} \left(\frac{K_z}{\mu} \frac{\partial p}{\partial z} - \rho_o g\right) \left(\frac{\partial p}{\partial z}\right) - \nabla \left(\lambda_t\right) = 0.$$
$$(2\text{-}59)$$

Defining:

$$\left(\rho c_p\right)_t = \left[\phi \left(s_o \rho_o c_{po} + s_w \rho_w c_{pw}\right) + (1 - \phi) \rho_s c_{ps}\right].$$

As the volumetric heat capacity of the fluid-saturated rock.

$$\left(\rho c_p \varphi\right)_t = \phi \left(s_o \rho_o c_{po} + s_w \rho_w c_{pw} \varphi_w\right).$$

As adiabatic-expansion coefficient of fluid system.

$$\varphi^* = \frac{\left(\rho c_p \varphi\right)_t}{\left(\rho c_p\right)_t}. \tag{2-60}$$

$$C_{pRo} = \frac{\rho_o c_{po}}{\left(\rho c_p\right)_t}. \tag{2-61}$$

$$\alpha_t = \frac{\lambda_t}{(\rho c_p)_t}.$$ (2-62)

If we consider that porosity is function of temperature and pressure and using the definitions of isothermal compressibility and isobaric thermal expansion coefficients of the rock, equations (2-33) and (2-34), the third term of equation (2-54) becomes:

$$\frac{\partial}{\partial t}(\phi p) = \phi\frac{\partial p}{\partial t} + p\frac{\partial \phi}{\partial t} = \phi\frac{\partial p}{\partial t} + \phi p C_r\frac{\partial p}{\partial t} - \phi p \beta_r\frac{\partial T}{\partial t}.$$ (2-63)

Although some studies shows that porosity variation with temperature and pressure is small and does not change the results (Palabiyik et al., 2016) [50], we present the formulation including porosity variation:

$$\varphi^* = \frac{(\rho c_p \varphi)_t + \phi p C_r}{(\rho c_p)_t + \phi p \beta_r}.$$ (2-64)

$$C_{pRo} = \frac{\rho_o c_{po}}{(\rho c_p)_t + \phi p \beta_r}.$$ (2-65)

$$\alpha_t = \frac{\lambda_t}{(\rho c_p)_t + \phi p \beta_r}.$$ (2-66)

$$\frac{\partial T}{\partial t} - \varphi^*\frac{\partial p}{\partial t} + C_{pRo}\left(\frac{-K_r}{\mu}\frac{\partial p}{\partial r}\right)\left(\frac{\partial T}{\partial r}\right) + C_{pRo}\left(\frac{K_z}{\mu}(\frac{\partial p}{\partial z} - \rho_o g)\right)\left(\frac{\partial T}{\partial z}\right) - \\ C_{pRo}\varepsilon_{JTo}\left(\frac{-K_r}{\mu}\frac{\partial p}{\partial r}\right)\left(\frac{\partial p}{\partial r}\right) + C_{pRo}\varepsilon_{JTo}\left(\frac{K_z}{\mu}(\frac{\partial p}{\partial z} - \rho_o g)\right)\left(\frac{\partial p}{\partial z}\right) - \\ \frac{1}{r}\frac{\partial}{\partial r}\left(r\alpha_t\frac{\partial T}{\partial r}\right) + \frac{\partial}{\partial z}\left(\alpha_t\frac{\partial T}{\partial z}\right) = 0.$$ (2-67)

2.4
Coupling between reservoir and wellbore

The coupling between the wellbore and the reservoir will be carried out through the proper use of boundary conditions at the boundary to which the

systems connect and the addition of the source terms of mass and energy. Figure 2.5 shows a diagram of the wellbore-reservoir coupling.

Wellbore / Reservoir Coupling

For $0 < z \leq h$

$$p_r(r = r_w, z, t) = p_w(z, t)$$

$$\lim_{r \to r_w} r \frac{\partial}{\partial r} T_r(r, z, t) = 0$$

h

q_s
q_θ

$$p_w(z = 0, t) = p_r(r = r_w, z = 0, t)$$
$$T_w(z = 0, t) = T_r(r = r_w, z = 0, t)$$

$$\lim_{r \to r_w} r \frac{\partial}{\partial r} p_r(r, z = 0, t) = \frac{q_w(z = 0, t)\mu_o}{2\pi K \Delta z}$$

$$\lim_{r \to r_w} r \frac{\partial}{\partial r} T_r(r, z = 0, t) = 0$$
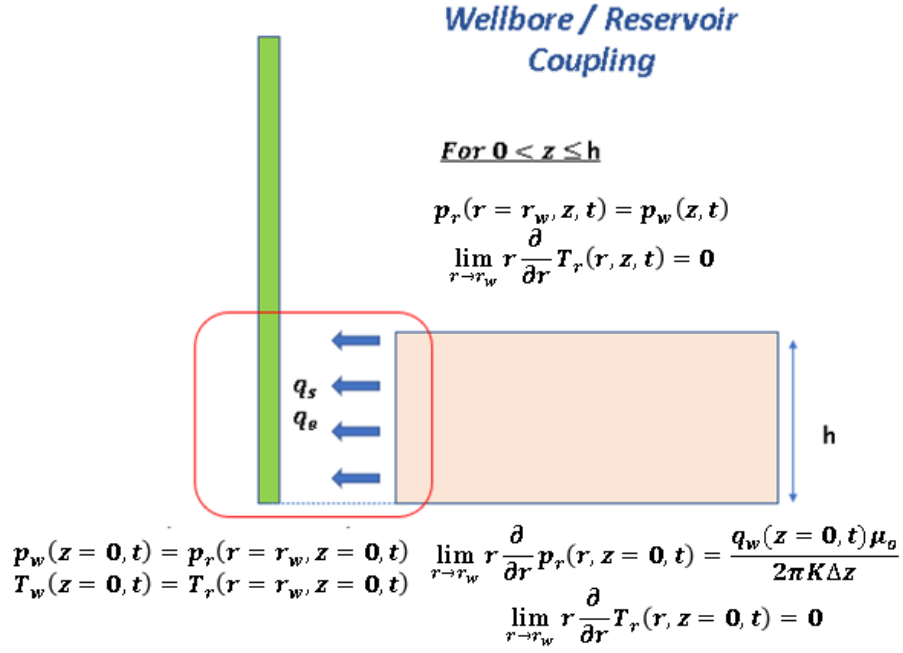
Figure 2.5: Wellbore / reservoir coupling scheme.

The coupling takes place through:

1- At the bottom-hole, the wellbore and the reservoir has the same pressure and temperature.:

$$P_w(z = 0, t) = P_r(r = r_w, z = 0, t).$$

$$T_w(z = 0, t) = T_r(r = r_w, z = 0, t).$$

2- Contact region between the wellbore and the reservoir have the same pressure. The heat exchange by diffusion between the reservoir and the wellbore is negligible:

For $z = 0$ despite the wellbore and reservoir pressures being identical, a flow condition to the reservoir is necessary.

$$\lim_{r \to r_w} \left(r \frac{\partial P_r}{\partial r}(r, z = 0, t) \right) = \frac{q_w(z = 0)\mu_o}{2\pi K \Delta z}.$$

For $0 < z \leq h$

$$P_r(r = r_w, z, t) = P_w(z, t).$$

For $0 \leq z \leq h$

$$\lim_{r \to r_w} (r \frac{\partial T_r}{\partial r}(r, z, t)) = 0.$$

3- The mass and energy source terms of the wellbore will be determined directly through the flows from the reservoir.

Mass source term:

$$q_s = (\frac{2}{R})(\rho v)_r. \tag{2-68}$$

Energy source term:

$$q_e = \frac{2}{R} \frac{\rho_r v_r}{\rho_w} \frac{1}{Cp_o(T_r - T_w)}. \tag{2-69}$$

2.5
Initial condition

Wellbore initial conditions

Before the wellbore top valve is opened, it's assumed that the wellbore is fully filled with oil, so initial pressure condition will be the hydrostatic gradient. Assuming that the wellbore bottom pressure $(P_w (z = 0))$ for the gradient is the same as the bottom pressure for the reservoir $(P_r(r, z = 0))$.

$$P_w (z, t = 0) = P_{wbh} - \rho g z sin(\theta).$$

And P_{wbh} is the initial pressure at z=0 and t=0.

Initially it will be considered that the wellbore and the oil inside it are in local equilibrium with the neighborhood, so the initial temperature of the wellbore and oil will be the geothermal gradient, assuming the wellbore bottom temperature $(T_w (z = 0))$ for the geothermal gradient is the same as the temperature of the reservoir at the same level $(T_r(r = r_w, z = 0))$.

$$T_w (z, t = 0) = T_{eibh} - g_t z sin(\theta).$$

And T_{eibh} is the earth temperature at z=0 and t=0.

Initially the oil is static in the wellbore, so

$$q_w (z, t = 0) = 0.$$

Reservoir Initial conditions

The reservoir initially is static, in local equilibrium so, the pressure distribution will be the hydrostatic gradient , assuming P_{wbh} as the reference level at z=0, and constant at the end of the reservoir.

$$p_r(r, z, t = 0) = P_{wbh} - \rho g z.$$

For temperature, the geothermal gradient will be considered, assuming T_{eibh} as the reference level, and constant at the end of the reservoir.

$$T_r(r, z, t = 0) = T_{eibh} - g_t z.$$

2.6
Boundary conditions

After coupling, it remains to define the boundary conditions of the coupled system: flow rate at the top of the wellbore, pressure and temperature at the top, bottom and at the end of the reservoir, as shown in Fig. 2.6

Top of the wellbore
Prescribed flow rate

Boundary Conditions
Of The coupled system

Upperr Border:
No flow rate or heat flux

Right Border:
Geothermal gradiente
Hydrostatic gradient

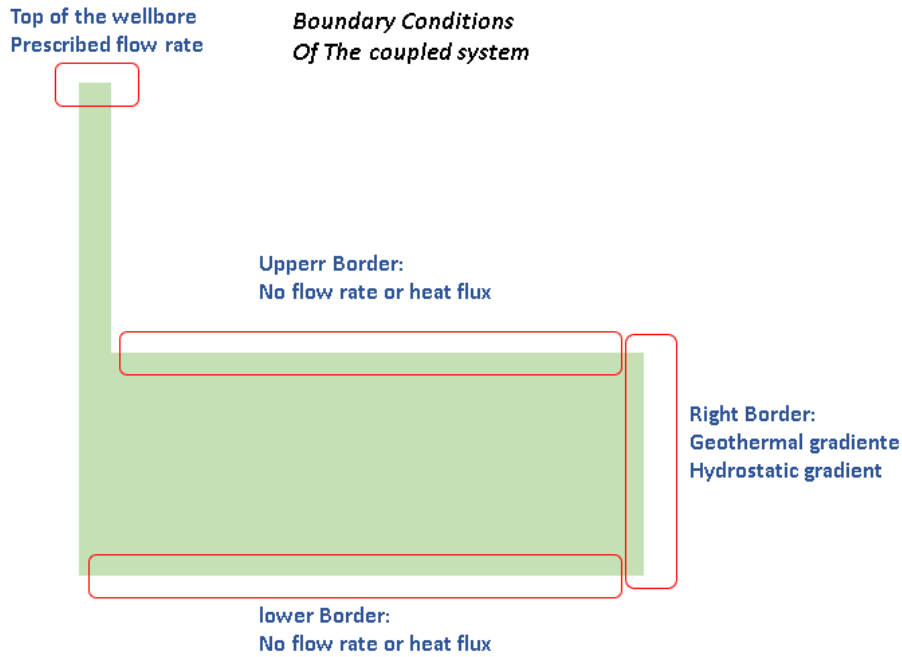**lower Border:**
No flow rate or heat flux

Figure 2.6: Wellbore-reservoir boundary scheme.

Wellbore

The boundary condition for flow rate is defined at the top of the wellbore. During the drawdown, the flow rate is set to a constant value Q_w; during the build up, it is set to zero, $Q_w = 0$.

$$q_w(z = h_{top}) = Q_w.$$

Reservoir

In the reservoir boundaries, far away from the wellbore (right side), we have the geothermal gradient for the temperature and hydrostatic gradient for the pressure.

$$P_r(r = \infty, z, t) = P_\infty - \rho g z.$$

$$T_r(r = \infty, z, t) = T_\infty - g_t z.$$

The top and the bottom boundaries are isolated, both for heat and flow.
Bottom:

$$\frac{\partial T_r}{\partial z}(r, z = 0, t) = 0.$$

$$\frac{\partial P_r}{\partial z}(r, z = 0, t) - \rho g = 0.$$

Top:

$$\frac{\partial T_r}{\partial z}(r, z = h, t) = 0.$$

$$\frac{\partial P_r}{\partial z}(r, z = h, t) - \rho g = 0.$$

2.7
Model summary

Below is summarized the system of equations that describe the flow and the heat transfer into the reservoir and into the well, all equations are coupled together. In the present model, density and porosity vary with pressure and temperature, other properties of oil and rock are constant.

Wellbore mass equation

$$\frac{\partial p}{\partial t} + (-\frac{\beta_o}{c_o})\frac{\partial T}{\partial t} + \frac{1}{Ac_o}\frac{\partial q}{\partial z} + \frac{q}{Ac_o}\left(c_o\frac{\partial p}{\partial z} + (-\beta_o)\frac{\partial T}{\partial z}\right) + \frac{q_s}{\rho c_o} = 0 \quad (2\text{-}70)$$

$$q_s = (\frac{2}{R})(\rho v)_r \tag{2-71}$$

Wellbore momentum equation

$$\frac{1}{A}\frac{\partial q}{\partial t} + \frac{q}{A^2}\frac{\partial q}{\partial z} + \frac{1}{\rho_o}\frac{\partial p}{\partial z} + g sin\alpha + \frac{fq\,|q|}{2\,(A^2)\,D} = 0 \tag{2-72}$$

Wellbore energy equation

$$\rho_o A C_{po}(1 + C_T)\frac{\partial T}{\partial t} = \rho_o q C_{po} L_R \left[T_{ei}(z) - T(z,t)\right] -$$
$$\rho_o q C_{po} \left[\frac{\partial T}{\partial z} - \varphi(z,t) + \frac{gsin\alpha}{C_{po}}\right] + q_e \tag{2-73}$$

Where:

$$T_{ei}(z) = T_{eibh} - z g_g sin\theta \tag{2-74}$$

$$\varphi(z,t) = \varepsilon_{JTo}\frac{\partial p}{\partial z} - \frac{q}{(A)^2 C_p}\frac{\partial q}{\partial z} \tag{2-75}$$

$$L_R = \frac{2\pi r_{to} U_t \lambda_e}{\rho_o q c_{po} \left[\lambda_e + r_{to} U_t f_D(t_D)\right]}$$

$$f_D(t_D) = ln\left[e^{-0.2t_D} + \left(1.5 - 0.3719e^{-t_D}\right)\sqrt{t_D}\right]$$

$$t_D = \frac{\alpha_{te}}{r_{co}^2}t.$$

$$U_t = \frac{1}{r_{ti}}\left[\frac{ln\left(r_{ci}/r_{co}\right)}{\lambda_{an}} + \frac{ln\left(r_{wb}/r_{co}\right)}{\lambda_{cem}}\right]^{-1}$$

$$q_e = \frac{2}{R}\frac{\rho_r v_r}{\rho_w}\frac{1}{Cp_o(T_r - T_w)} \tag{2-76}$$

Reservoir mass equation

$$\frac{\partial p}{\partial t} - \frac{\beta_t}{C_t}\frac{\partial T}{\partial t} = \frac{1}{C_t\phi\mu}\frac{1}{r}\frac{\partial}{\partial r}\left(rK_r\frac{\partial p}{\partial r}\right) + \left(\frac{1}{Ct\phi\mu}\right)\frac{\partial}{\partial z}\left(K_z\left(\frac{\partial p}{\partial z} - \rho g\right)\right) +$$
$$(\frac{K_r}{\phi\mu}\frac{C_o}{C_t})(\frac{\partial p}{\partial r})\left(\frac{\partial p}{\partial r}\right) - (\frac{K_r}{\phi\mu}\frac{\beta_o}{C_t})(\frac{\partial p}{\partial r})\frac{\partial T}{\partial r} +$$
$$\left(\frac{K_z}{\mu\phi}\frac{C_o}{C_t}\right)\left(\frac{\partial p}{\partial z} - \rho g\right)\left(\frac{\partial p}{\partial z}\right) - \left(\frac{K_z}{\mu\phi}\frac{\beta o}{Ct}\right)\left(\frac{\partial p}{\partial z} - \rho g\right)\frac{\partial T}{\partial z}. \tag{2-77}$$

Reservoir Energy equation

$$\frac{\partial T}{\partial t} - \varphi^* \frac{\partial p}{\partial t} + C_{pRo} \left(\frac{-K_r}{\mu} \frac{\partial p}{\partial r} \right) \left(\frac{\partial T}{\partial r} \right) + C_{pRo} \left(\frac{K_z}{\mu} (\frac{\partial p}{\partial z} - \rho_o g) \right) \left(\frac{\partial T}{\partial z} \right) -$$
$$C_{pRo} \varepsilon_{JTo} \left(\frac{-K_r}{\mu} \frac{\partial p}{\partial r} \right) \left(\frac{\partial p}{\partial r} \right) + C_{pRo} \varepsilon_{JTo} \left(\frac{K_z}{\mu} (\frac{\partial p}{\partial z} - \rho_o g) \right) \left(\frac{\partial p}{\partial z} \right) -$$
$$\frac{1}{r} \frac{\partial}{\partial r} \left(r \alpha_t \frac{\partial T}{\partial r} \right) + \frac{\partial}{\partial z} \left(\alpha_t \frac{\partial T}{\partial z} \right) = 0.$$
$$(2\text{-}78)$$

$$\varphi^* = \frac{(\rho c_p \varphi)_t + \phi p C_r}{(\rho c_p)_t + \phi p \beta_r}. \tag{2-79}$$

$$C_{pRo} = \frac{\rho_o c_{po}}{(\rho c_p)_t + \phi p \beta_r} \tag{2-80}$$

$$\alpha_t = \frac{\lambda_t}{(\rho c_p)_t + \phi p \beta_r}. \tag{2-81}$$

Wellbore initial conditions

$$P_w (z, t = 0) = P_{wbh} - \rho g z sin(\theta)$$

$$T_w (z, t = 0) = T_{eibh} - g_t z sin(\theta)$$

Reservoir Initial conditions

$$p_r (r, z, t = 0) = P_{wbh} - \rho g z$$

$$T_r (r, z, t = 0) = T_{eibh} - g_t z$$

Coupling

$$P_w (z = 0, t) = P_r (r = r_w, z = 0, t).$$

$$T_w(z = 0, t) = T_r(r = r_w, z = 0, t)$$

$$\lim_{r \to r_w} \left(r \frac{\partial P_r}{\partial r}(r, z = 0, t) \right) = \frac{q_w(z = 0)\mu_o}{2\pi K \Delta z}$$

$$\lim_{r \to r_w} \left(r \frac{\partial T_r}{\partial r}(r, z = 0, t) \right) = 0$$

for $0 < z \leq h$

$$P_r(r = r_w, z, t) = P_w(z, t).$$

$$\lim_{r \to r_w} \left(r \frac{\partial T_r}{\partial r}(r, z, t) \right) = 0$$

Boundary conditions

A schematic summary can be seen in Fig.2.7.

Wellbore:

$$q_w(z = h_{top}) = Q_w$$

$$P_w(z = 0, t) = P_r(r = r_w, z = 0, t)$$

$$T_w(z = 0, t) = T_r(r = r_w, z = 0, t)$$

Reservoir:

Boundary far away from the wellbore

$$P_r(r = \infty, z, t) = P_\infty - \rho g z$$

$$T_r(r = \infty, z, t) = T_\infty - g_t z$$

Upper and lower Boundaries

Bottom:

$$\frac{\partial T_r}{\partial z}(r, z = 0, t) = 0$$

$$\frac{\partial P_r}{\partial z}(r, z = 0, t) - \rho g = 0$$

Top:

$$\frac{\partial T_r}{\partial z}(r, z = h, t) = 0$$

$$\frac{\partial P_r}{\partial z}(r, z = h, t) - \rho g = 0$$

$q_w(z = H, t) = Q_w$

Upper Boundary

$P_R(r,, z = h, t) \Rightarrow \frac{\partial P}{\partial z} = 0$

$T_R(r,, z = h, t) \Rightarrow \frac{\partial T}{\partial z} = 0$

Right boundary

$P_R(r = r_\infty, z \geq 0, t) = P_\infty \text{-}\rho g z$

$T_R(r = r_\infty, z \geq 0, t) = T_\infty \text{-} g_t z$

lower Boundary

$P_R(r,, z = 0, t) \Rightarrow \frac{\partial P}{\partial z} = 0$

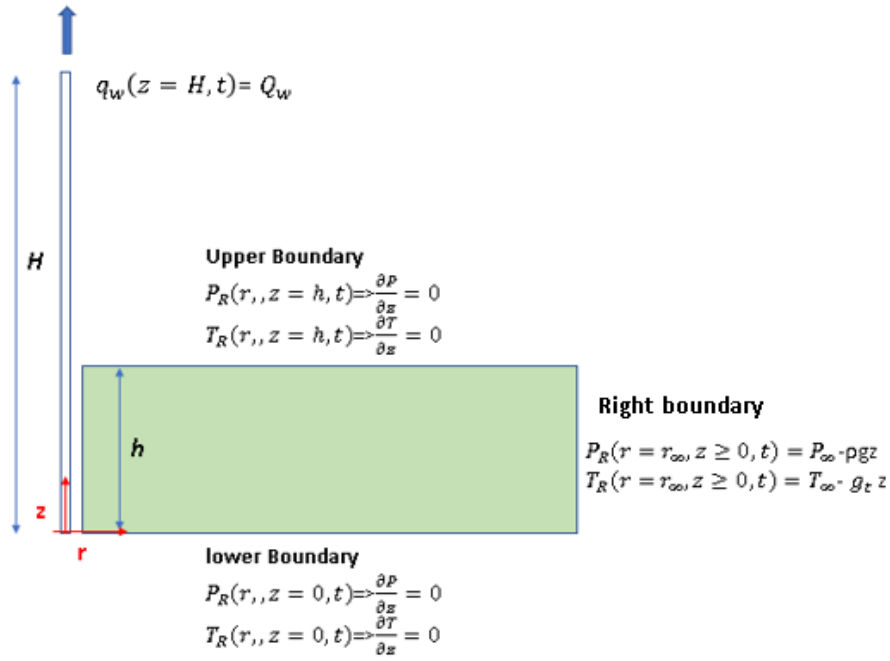$T_R(r,, z = 0, t) \Rightarrow \frac{\partial T}{\partial z} = 0$

Figure 2.7: Wellbore/reservoir boundary condition scheme.

3
Numerical Solution

The mathematical model formulated in Chapter 2 provides a system of five differentials conservation equations:

1- Wellbore Mass Balance

2- Wellbore Energy balance

3- Wellbore Momentum balance

4- Reservoir mass balance

5- Reservoir Energy balance

The set of differential equation is solved using a second order finite difference method. The time derivative is discretized using a second order implicit scheme.

3.1
Finite Difference Method

In numerical analysis, the finite difference method is used for solving differential equations by approximating the differential operators by difference equations. The differential equation is transformed into a set of algebraic equations.

The derivatives are approximated using a truncated Taylor series.

$$F_{i+1} = F_i + \Delta x F_i' + \frac{h^2}{2} F_i'' + ...$$

$$F_{i-1} = F_i - \Delta x F_i' + \frac{h^2}{2} F_i'' - ...$$

The first and second derivatives can be approximated using central difference considering a non-uniform mesh, according to the diagram shown in Fig. 3.1:

$$\frac{dF}{dx} \cong \frac{F_{i+1} - F_{i-1}}{x_{i+1} - x_{i-1}}.$$

$$F'' = \frac{\partial}{\partial x}\left(\frac{\partial F}{\partial x}\right) \cong \frac{\frac{\Delta F_r}{\Delta x_r} - \frac{\Delta F_l}{\Delta x_l}}{x_r - x_l} = \frac{\frac{F_{i+1} - F_i}{\Delta x_r} - \frac{F_i - F_{i-1}}{\Delta x_l}}{\Delta x}$$
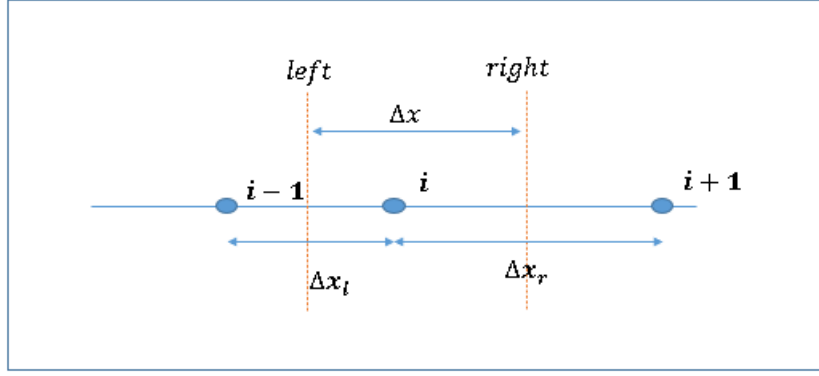
Figure 3.1: Finite Difference scheme.

An implicit formulation is used to descritize the time derivative term. A second order scheme, also known as theta method, was employed in this work, Morton et al. (2005) [51].

Convention: ϕ_i^t

ϕ- Variable

t − time

i − node/position

$$\frac{\delta \phi_i}{\delta t} = \frac{\phi_i^{t+1} - \phi_i^t}{\Delta t} = \theta F_i^{t+1}\left(u, x, t, \frac{\delta u}{\delta x}, \frac{\delta^2 u}{\delta x^2}\right) + (1 - \theta) F_i^t\left(u, x, t, \frac{\delta u}{\delta x}, \frac{\delta^2 u}{\delta x^2}\right).$$

t represents the previous instant, where the variables of the problem are known and $t + 1$ is the current instant. F is the right hand-side of the initial value problem. In this work $\theta = 1.0$ was used.
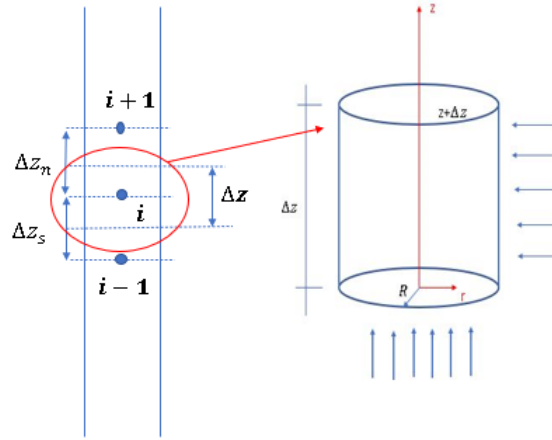
3.2
Discretization of the wellbore system equations

Figure 3.2: Wellbore discretization scheme

Wellbore Mass Equation

The wellbore mass conservation, equation (2-5) will be linearized by using a semi implicit method where the flow rate is based in the previous time step.

$$\frac{\partial p}{\partial t} - (\frac{\beta_o}{c_o})\frac{\partial T}{\partial t} + \frac{1}{Ac_o}\frac{\partial q}{\partial z} + \frac{q}{Ac_o}\left(c_o\frac{\partial p}{\partial z} + (-\beta_o)\frac{\partial T}{\partial z}\right) + \frac{q_s}{\rho c_o} = 0.$$

This equation will be discretized as follows:

Temporal terms:

$$\frac{\partial p}{\partial t} - \left(\frac{\beta_o}{c_o}\right)\frac{\partial T}{\partial t} = \frac{p_i^{t+1} - p_i^t}{\Delta t} - \left(\frac{\beta_o}{c_o}\right)\frac{T_i^{t+1} - T_i^t}{\Delta t}.$$

Pressure term:

$$\frac{q}{A}\frac{\partial p}{\partial z} = \theta\left(\frac{q_i^t}{A}\frac{p_{z+1}^{t+1} - p_{z-1}^{t+1}}{\Delta z_s + \Delta z_n}\right) + (1-\theta)\left(\frac{q_i^t}{A}\frac{p_{z+1}^t - p_{z-1}^t}{\Delta z_s + \Delta z_n}\right).$$

Temperature term:

$$\frac{-\beta_o q}{Ac_o}\frac{\partial T}{\partial z} = \theta\left(\frac{-\beta_o q_i^t}{Ac_o}\frac{T_{z+1}^{t+1} - T_{z-1}^{t+1}}{\Delta z_s + \Delta z_n}\right) + (1-\theta)\left(\frac{-\beta_o q_i^t}{Ac_o}\frac{T_{z+1}^t - T_{z-1}^t}{\Delta z_s + \Delta z_n}\right).$$

Flow term:

$$\frac{1}{Ac_o}\frac{\partial q}{\partial z} = \theta\left(\frac{1}{Ac_o}\frac{q_{z+1}^{t+1} - q_{z-1}^{t+1}}{\Delta z_n + \Delta z_s}\right) + (1-\theta)\left(\frac{1}{Ac_o}\frac{q_{z+1}^t - q_{z-1}^t}{\Delta z_n + \Delta z_s}\right).$$

Wellbore Momentum Equation

Similar linearization is used in equation 2-8. The non-linearities are removed by using the flow rate from the previous time step.

$$\frac{1}{A}\frac{\partial q}{\partial t} + \frac{q}{A^2}\frac{\partial q}{\partial z} + \frac{1}{\rho_o}\frac{\partial p}{\partial z} + g\sin\alpha + \frac{fq\,|q|}{2\,(A^2)\,D} = 0.$$

Temporal term:

$$\frac{1}{A}\frac{\partial q}{\partial t} = \frac{1}{A}\frac{q_z^{t+1} - q_z^t}{\Delta t}.$$

Pressure term:

$$\frac{1}{\rho_o}\frac{\partial p}{\partial z} = \theta\left(\frac{1}{\rho_o}\frac{p_{z+1}^{t+1} - p_{z-1}^{t+1}}{\Delta z_n + \Delta z_s}\right) + (1-\theta)\left(\frac{1}{\rho_o}\frac{p_{z+1}^t - p_{z-1}^t}{\Delta z_n + \Delta z_s}\right).$$

Flow term:

$$\begin{aligned}\frac{q}{A^2}\frac{\partial q}{\partial z} + \frac{f\,|\,q\,|\,q}{2A^2 D} &= \theta\left(\frac{q_z^t}{A^2}\frac{q_{z+1}^{t+1} - q_{z-1}^{t+1}}{2\Delta z} + \frac{f\,|\,q_z^t\,|\,q_z^{t+1}}{2A^2 D}\right) + \\ &\quad (1-\theta)\left(\frac{q_z^t}{A^2}\frac{q_{z+1}^t - q_{z-1}^t}{2\Delta z} + \frac{f\,|\,q_z^t\,|\,q_z^t}{2A^2 D}\right).\end{aligned}$$

(3-1)

There is no temperature term in the wellbore momentum equation.

Wellbore Energy Equation

Using the same criteria, the wellbore energy equation (2-25), will be linearized by taking the previous time step value for the flow rate.

$$\rho_o A C_{po}(1 + C_T)\frac{\partial T}{\partial t} = \rho_o q C_{po} L_R\left[T_{ei}(z) - T(z,t)\right] -$$
$$\rho_o q C_{po}\left[\frac{\partial T}{\partial z} - \varphi(z,t) + \frac{gsin\alpha}{C_{po}}\right].$$

$$\varphi(z,t) = \varepsilon_{JTo}\frac{\partial p}{\partial z} - \frac{q}{A^2 C_p g_c J}\frac{\partial q}{\partial z},$$

and it will be discretized as follow:

Temporal term:

$$\rho_o A C_{po}(1 + C_T)\frac{\partial T}{\partial t} = \rho_o A C_{po}(1 + C_T)\frac{T_z^{t+1} - T_z^t}{\Delta t}.$$

Pressure term:

$$\rho_o q C_{po}\varepsilon_{JTo}\frac{\partial p}{\partial z} = \theta(\rho_o q_z^t C_{po}\varepsilon_{JTo}\frac{p_{z+1}^{t+1} - p_{z-1}^{t+1}}{\Delta z_n + \Delta z_s}) +$$
$$(1 - \theta)(\rho_o q_z^t C_{po}\varepsilon_{JTo}\frac{p_{z+1}^t - p_{z-1}^t}{\Delta z_n + \Delta z_s}).$$

Temperature term:

$$\rho_o q C_{po}L_R[-T] - \rho_o q C_{po}(\frac{\partial T}{\partial z}) = \theta(-\rho_o C_{po}q_z^t L_R T_z^{t+1} - \rho_o C_{po}q_z^t\frac{T_{z+1}^{t+1} - T_{z-1}^{t+1}}{\Delta z_n + \Delta z_s}) +$$
$$(1 - \theta)(-\rho_o C_{po}q_z^t L_R T_z^t - \rho_o C_{po}q_z^t\frac{T_{z+1}^t - T_{z-1}^t}{\Delta z_n + \Delta z_s}).$$

Flow term:

$$\rho_o q C_{po}(-\frac{q}{A^2 C_{po}g_c J}\frac{\partial q}{\partial z}) = \theta(\frac{-\rho_o C_{po}(q_z^t)^2}{A^2 C_p g_c J}\frac{q_{z+1}^{t+1} - q_{z-1}^{t+1}}{\Delta z_n + \Delta z_s}) +$$
$$(1 - \theta)(\frac{-\rho_o C_{po}(q_z^t)^2}{A^2 C_p g_c J}\frac{q_{z+1}^t - q_{z-1}^t}{\Delta z_n + \Delta z_s}).$$

3.3
Discretization of the reservoir system equations.

The reservoir is treated two-dimensionally, the variables temperature and pressure are set at the node position of the mesh, fig. 3.3. Again, central finite difference method is used.
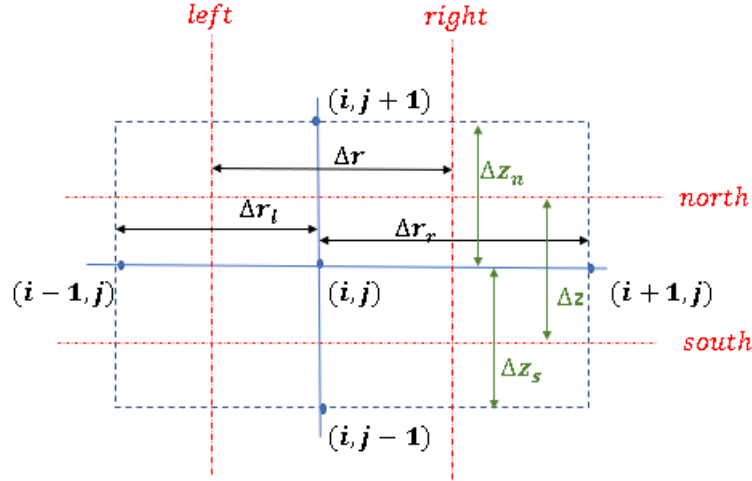

Figure 3.3: Reservoir discretization scheme

Reservoir Mass Equation:

The equation (2-44) presents the conservation of mass for the reservoir in two dimensions, in cylindrical coordinates.

$$\frac{\partial p}{\partial t} - \frac{\beta_t}{C_t}\frac{\partial T}{\partial t} = \frac{1}{C_t\phi\mu}\frac{1}{r}\frac{\partial}{\partial r}\left(rK_r\frac{\partial p}{\partial r}\right) + \left(\frac{1}{C_t\phi\mu}\right)\frac{\partial}{\partial z}\left(K_z\left(\frac{\partial p}{\partial z} - \rho g\right)\right) +$$
$$(\frac{K_r}{\phi\mu}\frac{C_o}{C_t})(\frac{\partial p}{\partial r})\left(\frac{\partial p}{\partial r}\right) - (\frac{K_r}{\phi\mu}\frac{\beta_o}{C_t})(\frac{\partial p}{\partial r})\frac{\partial T}{\partial r} +$$
$$\left(\frac{K_z}{\mu\phi}\frac{C_o}{C_t}\right)\left(\frac{\partial p}{\partial z} - \rho g\right)\left(\frac{\partial p}{\partial z}\right) - \left(\frac{K_z}{\mu\phi}\frac{\beta o}{Ct}\right)\left(\frac{\partial p}{\partial z} - \rho g\right)\frac{\partial T}{\partial z}.$$

As can be seen, this is a non-linear equation, and the non-linear terms have their origin from the product of a velocity (from Darcy in the radial or vertical direction) by pressure or temperature derivatives.

Adopting a procedure analogous to that used in the wellbore, a semi-implicit linearization method will be used through the adoption of Darcy's velocity values referring to the previous time step.

Temporal terms:

$$\frac{\partial p}{\partial t} - \frac{\beta_t}{C_t}\frac{\partial T}{\partial t} = \frac{p_{r,z}^{t+1} - p_{r,z}^{t}}{\Delta t} - \frac{\beta_t}{C_t}\frac{T_{r,z}^{t+1} - T_{r,z}^{t}}{\Delta t}.$$

Pressure terms:

$$\frac{1}{C_t\phi\mu}\frac{1}{r}\frac{\partial}{\partial r}\left(rK_r\frac{\partial p}{\partial r}\right) + \left(\frac{1}{C_t\phi\mu}\right)\frac{\partial}{\partial z}\left(K_z\left(\frac{\partial p}{\partial z} - \rho g\right)\right) +$$
$$(\frac{K_r}{\phi\mu}\frac{C_o}{C_t})(\frac{\partial p}{\partial r})\left(\frac{\partial p}{\partial r}\right) + \left(\frac{K_z}{\mu\phi}\frac{C_o}{C_t}\right)\left(\frac{\partial p}{\partial z} - \rho g\right)\left(\frac{\partial p}{\partial z}\right).$$

First pressure term:

$$\frac{1}{C_t\phi\mu}\frac{1}{r}\frac{\partial}{\partial r}\left(rK_r\frac{\partial p}{\partial r}\right) = \frac{1}{C_t\phi\mu}\frac{1}{r}\left[\theta\left(\frac{r_rK_r\frac{p_{r+1,z}^{t+1}-p_{r,z}^{t+1}}{\Delta r_r} - r_lK_l\frac{p_{r,z}^{t+1}-p_{r-1,z}^{t+1}}{\Delta r_l}}{\Delta r}\right)+\right.$$
$$\left.(1-\theta)\left(\frac{r_rK_r\frac{p_{r+1,z}^{t}-p_{r,z}^{t}}{\Delta r_r} - r_lK_l\frac{p_{r,z}^{t}-p_{r-1,z}^{t}}{\Delta r_l}}{\Delta r}\right)\right].$$

Second pressure term:

$$\left(\frac{1}{C_t\phi\mu}\right)\frac{\partial}{\partial z}\left(K_z\left(\frac{\partial p}{\partial z} - \rho g\right)\right) = \left(\frac{1}{C_t\phi\mu}\right)\left[\theta\left(\frac{K_n\frac{(p_{z+1}^{t+1}-\rho_ng)-(p_z^{t+1}-\rho_zg)}{\Delta z_n} - K_s\frac{(p_z^{t+1}-\rho_zg)-(p_{z-1}^{t+1}-\rho_sg)}{\Delta z_s}}{\Delta z}\right)+\right.$$
$$\left.(1-\theta)\left(\frac{K_n\frac{(p_{z+1}^{t}-\rho_ng)-(p_z^{t}-\rho_zg)}{\Delta z_n} - K_s\frac{(p_z^{t}-\rho_zg)-(p_{z-1}^{t}-\rho_sg)}{\Delta z_s}}{\Delta z}\right)\right].$$

Third pressure term:

$$(\frac{K_r}{\phi\mu}\frac{C_o}{C_t})(\frac{\partial p}{\partial r})\left(\frac{\partial p}{\partial r}\right) = \left(\frac{K_r}{\phi\mu}\frac{C_o}{C_t}\right)\left(\frac{p_{r+1,z}^{t}-p_{r-1,z}^{t}}{\Delta r_r + \Delta r_l}\right)\left[\theta\left(\frac{p_{r+1,z}^{t+1}-p_{r-1,z}^{t+1}}{\Delta r_r + \Delta r_l}\right)+\right.$$
$$\left.(1-\theta)\left(\frac{p_{r+1,z}^{t}-p_{r-1,z}^{t}}{\Delta r_r + \Delta r_l}\right)\right].$$

Fourth pressure term:

$$\left(\frac{K_z}{\mu\phi}\frac{C_o}{C_t}\right)\left(\frac{\partial p}{\partial z}-\rho g\right)\left(\frac{\partial p}{\partial z}\right)=\left(\frac{K_z}{\mu\phi}\frac{C_o}{C_t}\right)\left(\frac{p_{r,z+1}^t-p_{r,z-1}^t}{\Delta z_n+\Delta z_s}-\rho g\right)\left[\theta\left(\frac{p_{r,z+1}^{t+1}-p_{r,z-1}^{t+1}}{\Delta z_n+\Delta z_s}-\rho g\right)+\right.$$
$$\left.(1-\theta)\left(\frac{p_{r,z+1}^t-p_{r,z-1}^t}{\Delta z_n+\Delta z_s}-\rho g\right)\right].$$

Temperature terms:

$$-\left(\frac{K_r}{\phi\mu}\frac{\beta_o}{C_t}\right)\left(\frac{\partial p}{\partial r}\right)\frac{\partial T}{\partial r}-\left(\frac{K_z}{\mu\phi}\frac{\beta o}{Ct}\right)\left(\frac{\partial p}{\partial z}+\rho g\right)\frac{\partial T}{\partial z}.$$

Again, it will be used the previous step time in the portion related to Darcy's velocity $\partial p/\partial r$ or $\partial p/\partial z-\rho g$

Radial term:

$$-\left(\frac{K_r}{\phi\mu}\frac{\beta_o}{C_t}\right)\left(\frac{\partial p}{\partial r}\right)\frac{\partial T}{\partial r}=-\left(\frac{K_r}{\phi\mu}\frac{\beta_o}{C_t}\right)\left(\frac{p_{r+1,z}^t-p_{r-1,z}^t}{\Delta r_r+\Delta r_l}\right)\left[\theta\left(\frac{T_{r+1,z}^{t+1}-T_{r-1,z}^{t+1}}{\Delta r_r+\Delta r_l}\right)+\right.$$
$$\left.(1-\theta)\left(\frac{T_{r+1,z}^t-T_{r-1,z}^t}{\Delta r_r+\Delta r_l}\right)\right].$$

Vertical term:

$$-\left(\frac{K_z}{\mu\phi}\frac{\beta o}{Ct}\right)\left(\frac{\partial p}{\partial z}-\rho g\right)\frac{\partial T}{\partial z}=-\left(\frac{K_z}{\mu\phi}\frac{\beta o}{Ct}\right)\left(\frac{p_{r,z+1}^t-p_{r,z-1}^t}{\Delta z_n+\Delta z_s}-\rho g\right)\left[\theta\left(\frac{T_{r,z+1}^{t+1}-T_{r,z-1}^{t+1}}{\Delta z_n+\Delta z_s}\right)+\right.$$
$$\left.(1-\theta)\left(\frac{T_{r,z+1}^t-T_{r,z-1}^t}{\Delta z_n+\Delta z_s}\right)\right].$$

Reservoir Energy Equation:

The reservoir energy equation, equation (2-67), will be taken the terms relative to the Darcy velocity from the previous step time.

Temporal terms:

$$\frac{\partial T}{\partial t}-\varphi^*\frac{\partial p}{\partial t}=\frac{T_{r,z}^{t+1}-T_{r,z}^t}{\Delta t}-\varphi^*\frac{p_{r,z}^{t+1}-p_{r,z}^t}{\Delta t}.$$

Pressure terms:

$$C_{pRo}\varepsilon_{JTo}\left(\frac{-K_r}{\mu}\frac{\partial p}{\partial r}\right)\left(\frac{\partial p}{\partial r}\right) + C_{pRo}\varepsilon_{JTo}\left(\frac{-K_z}{\mu}(\frac{\partial p}{\partial z}+\rho_o g)\right)\left(\frac{\partial p}{\partial z}\right).$$

Radial pressure term:

$$C_{pRo}\varepsilon_{JTo}\left(\frac{-K_r}{\mu}\frac{\partial p}{\partial r}\right)\left(\frac{\partial p}{\partial r}\right) = C_{pRo}\varepsilon_{JTo}\left(\frac{-K_r}{\mu}\frac{p^t_{r+1,z}-p^t_{r-1,z}}{\Delta r_r+\Delta r_l}\right)\left[\theta\left(\frac{p^{t+1}_{r+1,z}-p^{t+1}_{r-1,z}}{\Delta r_r+\Delta r_l}\right)+\right.$$
$$\left.(1-\theta)\left(\frac{p^t_{r+1,z}-p^t_{r-1,z}}{\Delta r_r+\Delta r_l}\right)\right].$$

Vertical pressure term:

$$C_{pRo}\varepsilon_{JTo}\left(\frac{K_z}{\mu}(\frac{\partial p}{\partial z}-\rho g)\right)\left(\frac{\partial p}{\partial z}\right) = C_{pRo}\varepsilon_{JTo}\left(\frac{K_z}{\mu}(\frac{p^t_{r,z+1}-p^t_{r,z-1}}{\Delta z_n+\Delta z_s}-\rho g)\right)$$
$$\left[\theta\left(\frac{p^{t+1}_{r,z+1}-p^{t+1}_{r,z-1}}{\Delta z_n+\Delta z_s}\right)+(1-\theta)\left(\frac{p^t_{r,z+1}-p^t_{r,z-1}}{\Delta z_n+\Delta z_s}\right)\right].$$

Temperature terms:

$$C_{pRo}\left(\frac{-K_r}{\mu}\frac{\partial p}{\partial r}\right)\left(\frac{\partial T}{\partial r}\right) + C_{pRo}\left(\frac{-K_z}{\mu}(\frac{\partial p}{\partial z}-\rho g)\right)\left(\frac{\partial T}{\partial z}\right) - \frac{1}{r}\frac{\partial}{\partial r}\left(r\alpha_t\frac{\partial T}{\partial r}\right) + \frac{\partial}{\partial z}\left(\alpha_t\frac{\partial T}{\partial z}\right).$$

First term:

$$C_{pRo}\left(\frac{-K_r}{\mu}\frac{\partial p}{\partial r}\right)\left(\frac{\partial T}{\partial r}\right) = C_{pRo}\left(\frac{-K_r}{\mu}\frac{p^t_{r+1,z}-p^t_{r-1,z}}{\Delta r_r+\Delta r_l}\right)\left[\theta\left(\frac{T^{t+1}_{r+1,z}-T^{t+1}_{r-1,z}}{\Delta r_r+\Delta r_l}\right)+\right.$$
$$\left.(1-\theta)\left(\frac{T^t_{r+1,z}-T^t_{r-1,z}}{\Delta r_r+\Delta r_l}\right)\right].$$

Second term:

$$C_{pRo}\left(\frac{-K_z}{\mu}(\frac{\partial p}{\partial z}-\rho g)\right)\left(\frac{\partial T}{\partial z}\right) = C_{pRo}\left(\frac{-K_z}{\mu}\left(\frac{p^t_{r,z+1}-p^t_{r,z-1}}{\Delta z_n+\Delta z_s}-\rho g\right)\right)\left[\theta\left(\frac{T^{t+1}_{r,z+1}-T^{t+1}_{r,z-1}}{\Delta z_n+\Delta z_s}\right)+\right.$$
$$\left.(1-\theta)\left(\frac{T^t_{r,z+1}-T^t_{r,z-1}}{\Delta z_n+\Delta z_s}\right)\right].$$

Third term:

$$\frac{1}{r}\frac{\partial}{\partial r}\left(r\alpha_{te}\frac{\partial T}{\partial r}\right) = \theta\left(\frac{\alpha_{te}}{r}\frac{r_r\frac{T_{r+1,z}^{t+1}-T_{r,z}^{t+1}}{\Delta r_r} - r_l\frac{T_{r,z}^{t+1}-T_{r-1,z}^{t+1}}{\Delta r_l}}{\Delta r}\right) +$$

$$(1-\theta)\left(\frac{\alpha_{te}}{r}\frac{r_r\frac{T_{r+1,z}^{t}-T_{r,z}^{t}}{\Delta r_r} - r_l\frac{T_{r,z}^{t}-T_{r-1,z}^{t}}{\Delta r_l}}{\Delta r}\right).$$

Fourth term:

$$\frac{\partial}{\partial z}\left(\alpha_{te}\frac{\partial T}{\partial z}\right) = \theta\left(\frac{\alpha_{te}\frac{T_{r,z+1}^{t+1}-T_{r,z}^{t+1}}{\Delta z_n} - \alpha_{te}\frac{T_{r,z}^{t+1}-T_{r,z-1}^{t+1}}{\Delta z_s}}{\Delta z}\right) +$$

$$(1-\theta)\left(\frac{\alpha_{te}\frac{T_{r,z+1}^{t}-T_{r,z}^{t}}{\Delta z_n} - \alpha_{te}\frac{T_{r,z}^{t}-T_{r,z-1}^{t}}{\Delta z_s}}{\Delta z}\right).$$

3.4
Brief program description

In the wellbore, three information are computed in each node: pressure, temperature and the flow rate. In the reservoir, only two variables are computed: pressure and temperature. The flow rate in the reservoir is later calculated using the Darcy equation over the pressure values obtained for the reservoir nodes.

The finite difference method establishes equations for each variable for each node.

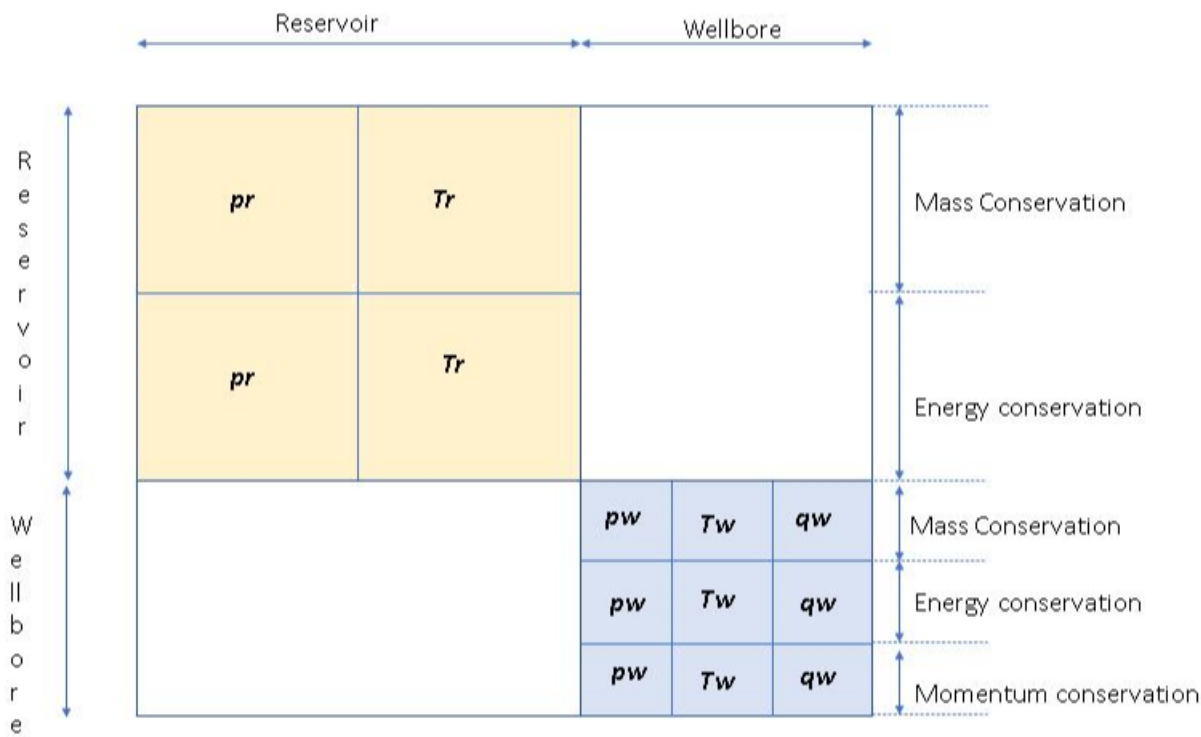Fig. 3.4 shows a schematic model of the assembly of the system of equations.

Figure 3.4: Scheme of discretized equations sequence to obtain the matrix coefficient.

The characteristic structure of the complete coefficient matix is shown in Fig. 3.5 where the dots are represented by non null coefficient. The resulting sparse matriz was stored properly in order to reduce the computer memory and time to solve the linear system. The numerical code was implemented in a Matlab environment which directly solves the system through LU decomposition.
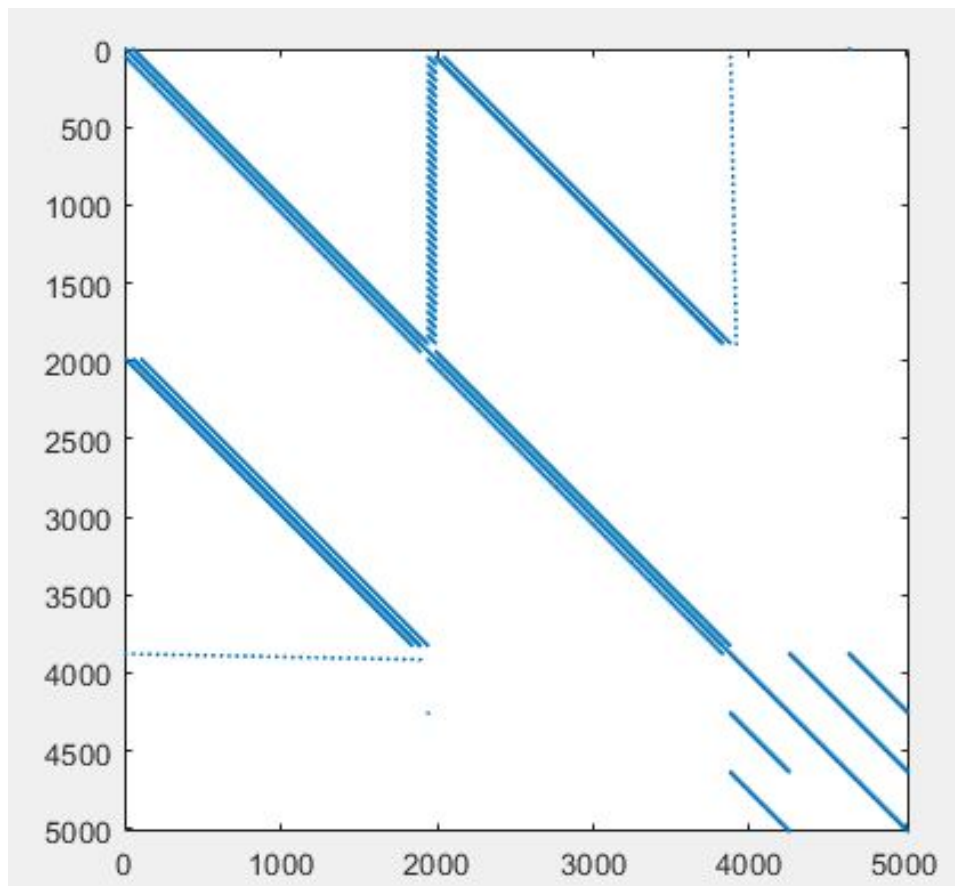
Figure 3.5: Position in the coefficients matrix, non-zero elements.

4
Program Validation

4.1
Mesh Grid Test

The wellbore-reservoir system is composed of two distinct meshes that must be coupled in the region where the wellbore fully penetrates the reservoir. For the wellbore a one-dimensional mesh is used in the vertical direction. The reservoir needs a two-dimensional mesh, in the vertical and radial directions. Since the systems are coupled, it is necessary that the wellbore nodes located in the reservoir region have the same vertical coordinates as the reservoir nodes, as shown in Fig. 4.1.
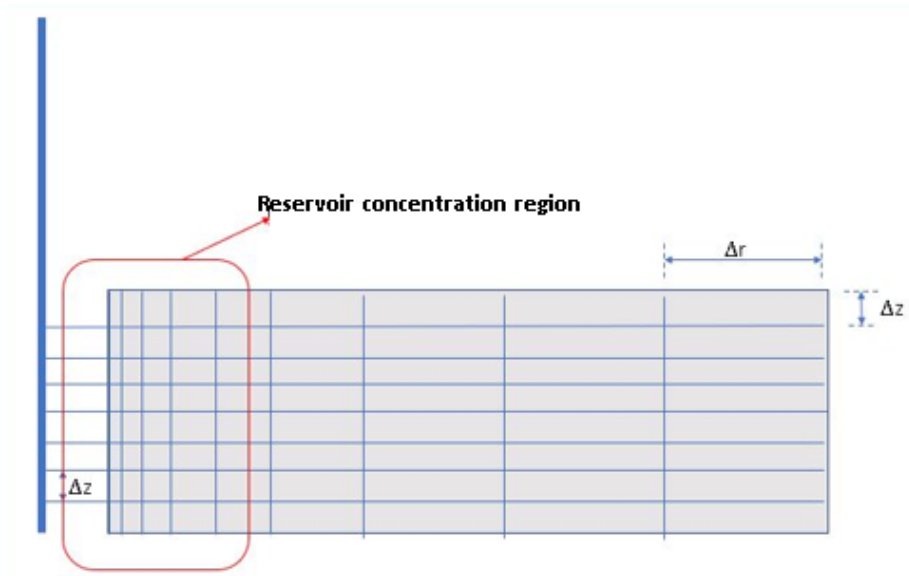
Figure 4.1: Concentration Factor Scheme

Preliminary results of the numerical model showed that the reservoir solution is very sensitive to the mesh concentration in radial direction near the wellbore when the pressure gradient is high. A series of tests were made to reach the minimum number of nodes and mesh concentration parameter that makes the solution for temperature and pressure independent to the mesh.

Figure 4.2 shows significant variations in pressure and temeperature near the wellbore measured at late times. In the other hand, there is no variation in value of p and T after some radial distance.
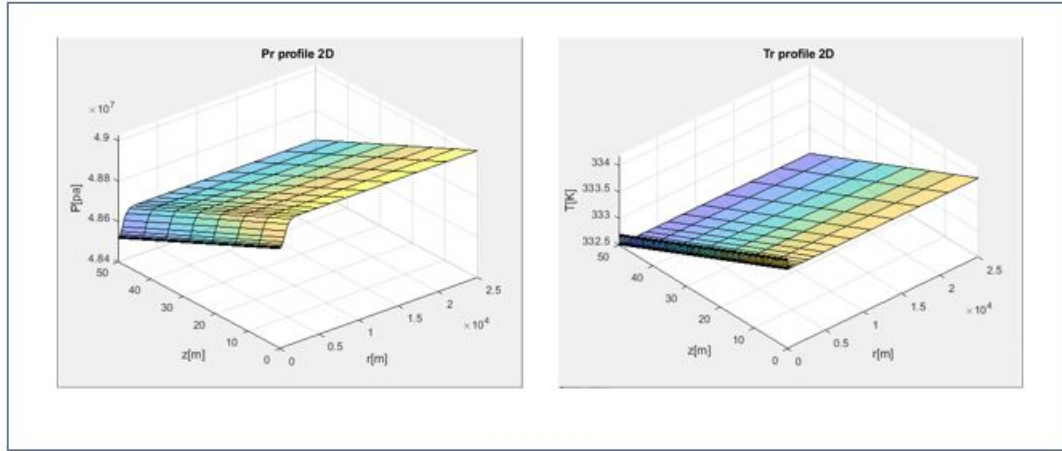

Figure 4.2: Pressure and Temperature distribution inside the reservoir measured after an interval of time.

Reservoir mesh grid

It is required to find a mesh that is capable of representing the variations occurring in the reservoir and at the same time is not too large to make the program computationally expensive.

In order to automatic generate the grid in radial direction that meets the requirements of being refined near the wellbore, a hyperbolic function that easily allowed variations in the total number of nodes and their concentration in a given region was chosen. The distribution of nodes in the radial direction follows Vinokur M.(1983) [52]. :

$$r\left(i\right) = r_w + \left(L - r_w\right)\left(1 + \tanh\left(CF\frac{(i-1)}{(NEX-2)}\right)/\tanh CF\right) \qquad (4\text{-}1)$$

Where:

$r(i)$ is the position of the node i;

r_w is the wellbore radius;

L is the reservoir length;

CF is the nodes concentration factor;

NEX is the total nodes number in radial direction;

Figure 4.3 presents a coupled wellbore-reservoir system that was used for the mesh grid test and later program validation. During the mesh grid tests, when the reservoir was considered homogeneous, the permeability of the

two layers was the same, $K_1 = K_2 = 100mD$. The wellbore high was 512.5m measured from bottom of reservoir, the flow rate was set in the upper boundary of the wellbore, $800m^3/day$. The Drawdown and Build up periods were both 48 hours.
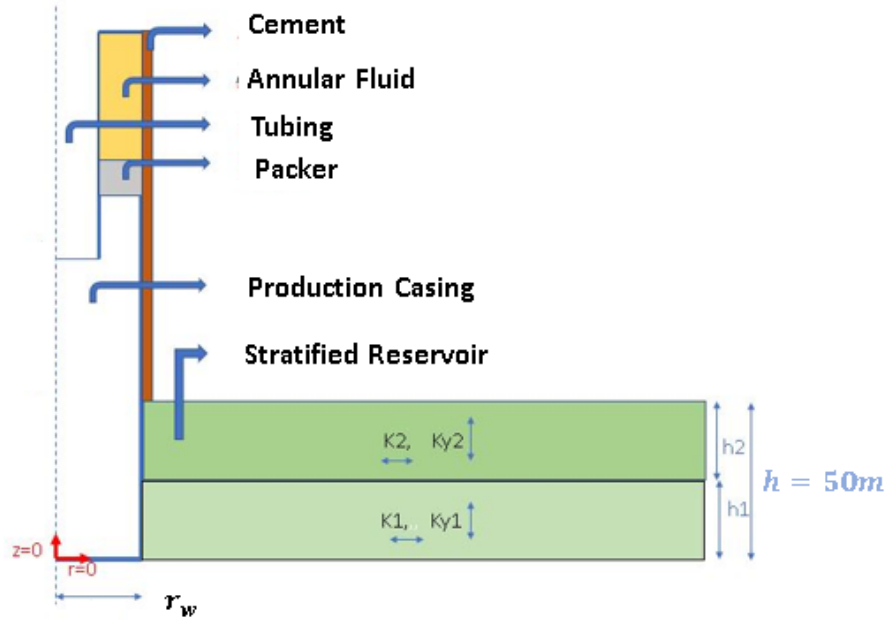
Figure 4.3: Wellbore-Reservoir System Scheme

Tables 4.1 and 4.2 presents the reservoir and fluid properties respectively. Table 4.3 presents the constants given in equations (2-60), (2-61) and (2-62) and Table 4.4, the wellbore properties and dimensions .

Table 4.1: Reservoir properties

Property	Units	Value
p_i	MPa	49.03
T_i	K	334.0
r_e	m	25,000.0
ϕ	fraction	0.12
c_r	cm^2 / kgf	3.0e-5
s_w	fraction	0.15
g_t	K/m	0.03
$c_p r$	$J/m^3/K$	2.347e+6
λ_r	J/m/K	1.396e+4
λ_e	J/m/K	1.396e+4
α_e	m^2/h	5.894e-3

Table 4.2: Fluid properties

Property	Units	Oil	Water
B	$m^3/stdm^3$	1.4	1.0
c	cm^2/kgf	1.10e-4	3.96e-5
μ	cP	0.9	1.0
λ	$J/m//h/K$	5.833e+2	2.229e+3
ρ	Kg/m^3	770.0	998.2
β	K^{-1}	1.11e-3	5.27e-4
c_p	$J/Kg/K$	2252.9	4209.35
ε_{JT}	$K/Kgf/cm^2$	-3.374e-2	-1.921e-2
φ	$K/(Kgf/cm^2)$	2.279e-2	4.132e-3

Table 4.3: Reservoir constants

Constant	Units	Value
λ_t	$J/m/h/K$	1.238e+4
ϕ_t^*	$K/(Kgf/cm^2)$	1.874e-3
α_t	m^2/h	5.342e-3

Table 4.4: Wellbore Properties and dimensions

Properties	Units	Value
r_w	m	0.156
r_{co}	m	0.12224
r_{ci}	m	0.10839
r_{to}	m	0.06985
r_{ti}	m	0.05931
λ_{cem}	$J/m/h/K$	6.833e+3
λ_{wall}	$J/m/h/K$	1.617e+5
$\lambda_{wall-cem}$	$J/m/h/K$	9.995e+3
λ_{an}	$J/m/h/K$	5.833e+2
Skin factor		0
θ	$degree$	90^0

Initially the number of elements in the vertical direction of the reservoir (NEY) and the mesh concentration factor(CF) was fixed at 6 and the number of elements in the radial direction (NEX) was successively modified, Table 4.5. The vertical mesh was considered uniform. The number of elements in the wellbore (Ny) will be a function of the number of elements in the vertical direction of the reservoir (NEY) and the wellbore height.

Table 4.5: Mesh grid test, variation in reservoir element number in radial direction

Parameter	Test1	Test2	Test3	Test4	Test5	Test6
NEX	50	100	200	400	600	800
NEY	6	6	6	6	6	6
CF	6	6	6	6	6	6
Ny	62	62	62	62	62	62

Figure 4.4 (a) and (b) shows the evolution of pressure and temperature measured in the sandface during the draw down and build up period for the different cases listed in table 4.5. The solutions became mesh independent for $NEX \geqslant 400$ for $CF = 6$.
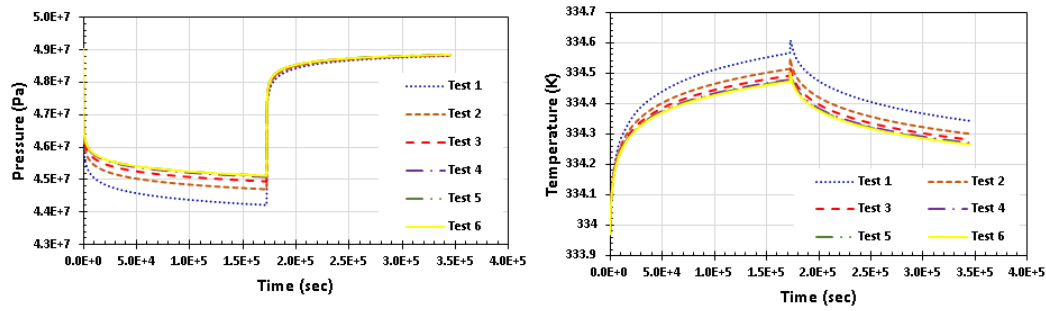

Figure 4.4: Bottom hole Pressure and Temperature results varying the number of nodes in the radial direction

In order to control the precision and reduce the number of nodes in the radial direction a concentration factor test is necessary.

As can be seen in fig. 4.5, increasing the concentration factor from 6 to 8 in equation (4-1), according to table 4.6, allows a significant reduction in the number of nodes in the radial direction.
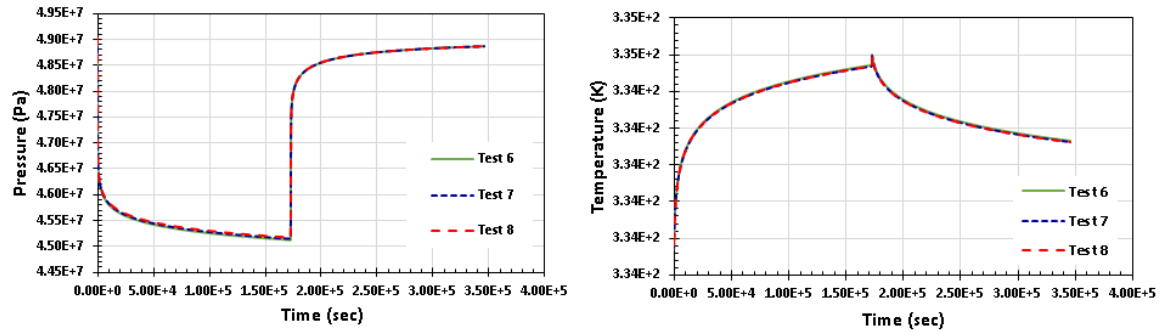
Figure 4.5: Bottom hole pressure and temperature results varying the concentration factor in the radial direction

Table 4.6: Mesh grid test, variation in the concentration factor in the radial direction

Parameter	Test6	Test7	Test8
NEX	800	100	50
NEY	6	6	6
CF	6	7	8
Ny	62	62	62

The same procedure was carried out to determine the number of elements in the vertical direction of the reservoir. The number of elements in the vertical direction was gradually increased until the result no longer presented changes, figure 4.6(a) and (b) and table 4.7.
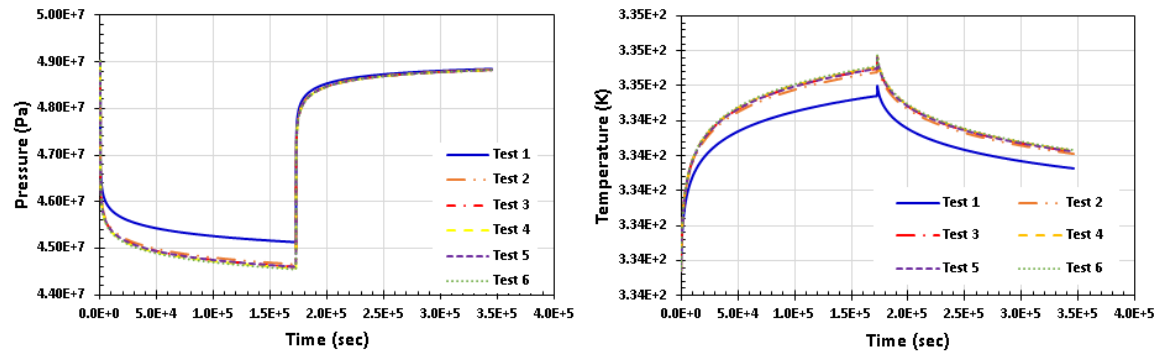

Figure 4.6: Bottom hole Pressure and Temperature results varying the reservoir number of nodes in vertical direction

Table 4.7: Mesh grid test, variation in reservoir element number in vertical direction

Parameter	Test1	Test2	Test3	Test4	Test5	Test6
NEX	50	50	50	50	50	50
NEY	6	24	36	48	52	60
CF	8	8	8	8	8	8
Ny	62	264	372	496	620	744

As can be seen through the analysis of Figures 4.4, 4.5 and 4.6 results became mesh independent setting appropriate values of CF, NEX and NEY.

In the next step, the mesh is tested with a stratified reservoir. The tables 4.8 and 4.9 shows the properties and parameters of the layers and nodes variation for a stratified reservoir. It was fixed the permeability and the height for the layers and vary the number of nodes in vertical direction. Using 55 nodes in vertical direction, the result became independent of the mesh grid, as can be seen in Fig. 4.7. Here, the temperature derivative was obtained using the Eq.(1-3).

Table 4.8: Layer properties and parameter for stratified reservoir mesh grid test.

Property	Layer 1	Layer 2
Permeability	10 mD	190 mD
Height	25 m	25 m

Table 4.9: Variation in reservoir nodes number in vertical direction for stratified reservoir.

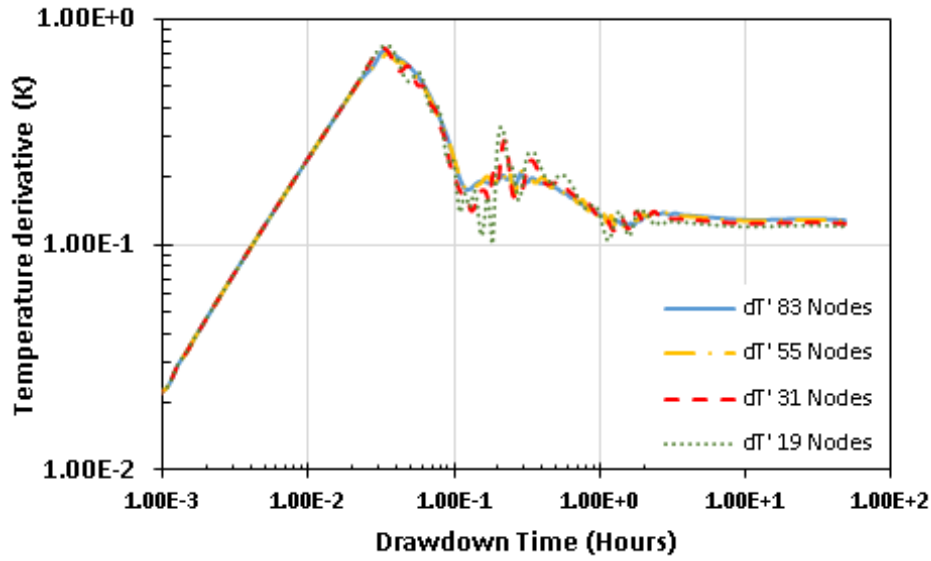| Test	Nodes number
Test 1y	19
Test 2y	31
Test 3y	55
Test 4y	83

Figure 4.7: Derivative temperature, variation as a function of the number of nodes in the vertical direction for stratified reservoir.

4.2
Validation

In this section, the numerical code implemented was validated by using analytical solutions or literature data taken into account the coupled system wellbore-reservoir. Since most works treat the reservoir in a one-dimensional way, we expect to find differences in the results, however, since one-dimensional models have shown good results in practice, we expect the behavior of the responses to be similar.
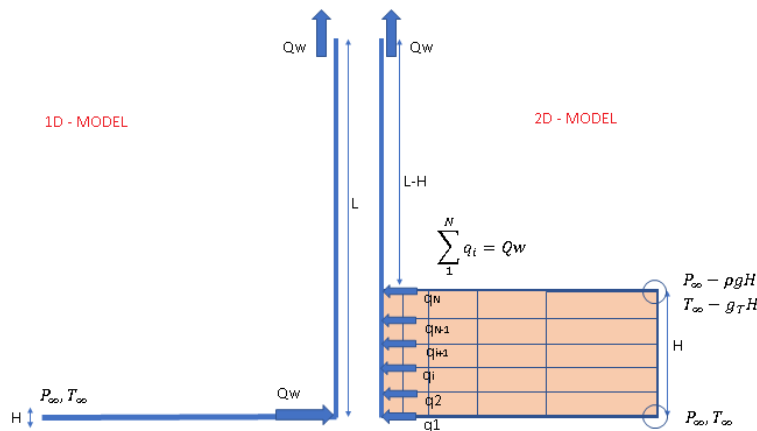
Figure 4.8: Comparative scheme of one and two-dimensional analyzes.

Fig 4.8 shows a comparative scheme of one and two-dimensional models. In the one-dimensional model, the fluid enters the reservoir through a single position, in the lower part of the wellbore, whereas in the two-dimensional model, the fluid enters the reservoir along a region of size equal to the height of the reservoir.

4.2.1
Temperature Validation

For temperature validation, the same wellbore-reservoir-fluid system used for the mesh test is used.

The results of this work are compared with one analytical and other numerical obtained by a commercial simulator CMG-Star, both from Galvão et al (2019) [40]) .

Figure 4.9 presents the evolution of pressure and temperature for a one-dimensional and a two-dimensional simulators over drawdown and builldup times, measured at the bottom hole (z=0m), both under the same conditions described above.
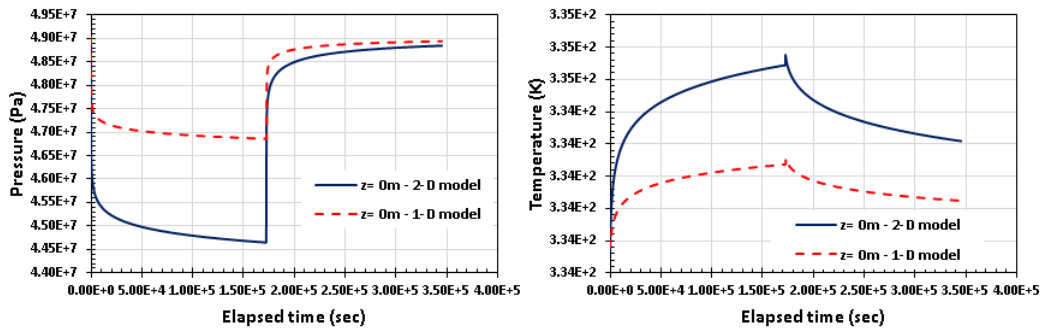

Figure 4.9: Evolution of pressure and temperature in the wellbore over the flow period, at the bottom hole for 1D and 2D models.

The largest differences between the temperature solutions is expected to occur near the bottom of the well. In the 1-D reservoir model, the entire flow enters the well at the same temperature, flows into the well through single position. In the 2-D reservoir model, the flow from the reservoir to the well is distributed in an area at different temperatures. Moreover, temperature variations due to adiabatic compression/expansion effects and by Joule-Thompson effect have different values. More information about J-T effect is shown in App (2010) [33].

The pressure boundary condition imposed on the reservoir (one and two dimensional), close to the wellbore is a flow condition, given by:

$$\lim_{r \to r_w} (r\frac{\partial p}{\partial r}) = \frac{q(z=0)\mu_o}{2\pi Kh}$$

The q/h ratio for the one dimensional analysis of the reservoir is the quotient between the total flow rate (Q_w) measured at the top of the wellbore and the total height of the reservoir (h). The q/h ratio for the two-dimensional analysis of the reservoir is the quotient between the flow of each element of the reservoir adjacent to the wellbore and its respective height, given by : $q_r(r = r_w, z)/\Delta z$.

The relationship between q/h defines that greater decrease in pressure in the two dimensional reservoir, consequently greater temperature rise.

Although we do not directly calculate the flow rate inside the reservoir, it is provided through the Darcy law in the radial direction. Table 4.10 presents the values of the flow rate $(q(z = 0))$, height(Δz), flow rate/height ratio $(q(z = 0)/\Delta z)$ for the first element of a two-dimensional reservoir as a function of the number of nodes in the vertical direction of this reservoir and a comparison with a one-dimensional analysis.

Figure 4.10 shows the flow rate variation as function of number of nodes in the vertical direction. Flow rate results above 83 nodes are independent of the mesh and the q/h ratio becomes constant, as shown in figure 4.11. We also observed that the one and two dimensional analyzes differ by a multiplication factor, in the case of the reservoir under study of approximately 0.496 .

Table 4.10: Relation of $q/(\delta z)$ as a function of number of nodes.

Nodes	Flow rate m^3/sec	Element height m	q(1)/ dz	Relation $q/\Delta z$ 1D/2D
11	13.59e-4	4.45455	2.99e-4	0.618
23	7.34e-4	2.17000	3.38e-4	0.547
35	5.03e-4	1.428571	3.52e-4	0.525
43	4.16e-4	1.162791	3.57e-4	0.517
63	2.9e-4	0.793651	3.65e-4	0.506
83	2.22e-4	0.60241	3.69e-4	0.500
103	1.8e-4	0.485437	3.71e-4	0.497
123	1.51e-4	0.406504	3.72e-4	0.496
163	1.14e-4	0.306748	3.72e-4	0.496

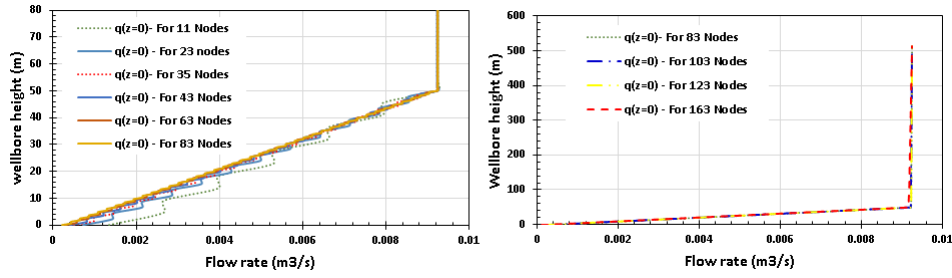Figure 4.10: Variation of element height, flow rate in the first node of the reservoir.

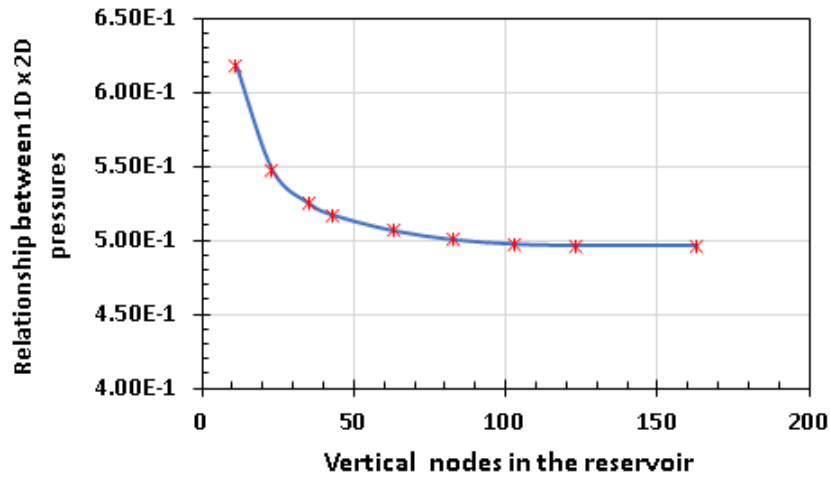Figure 4.11: Comparison between q / h ratio for one and two-dimensional analysis of the reservoir.

4.2.1.1
Case 1, At $z = 0$ m

At the bottom hole ($z = 0m$), although the reference temperature are the same T_{ini}, the flow rates in the 1-D and 2-D models at this location are different. This important difference explains the discrepancy between the 1-D and 2-D solutions, as illustrated in see Figure 4.12. However, it is important to note that the general behavior of the temperature evolution is similar.
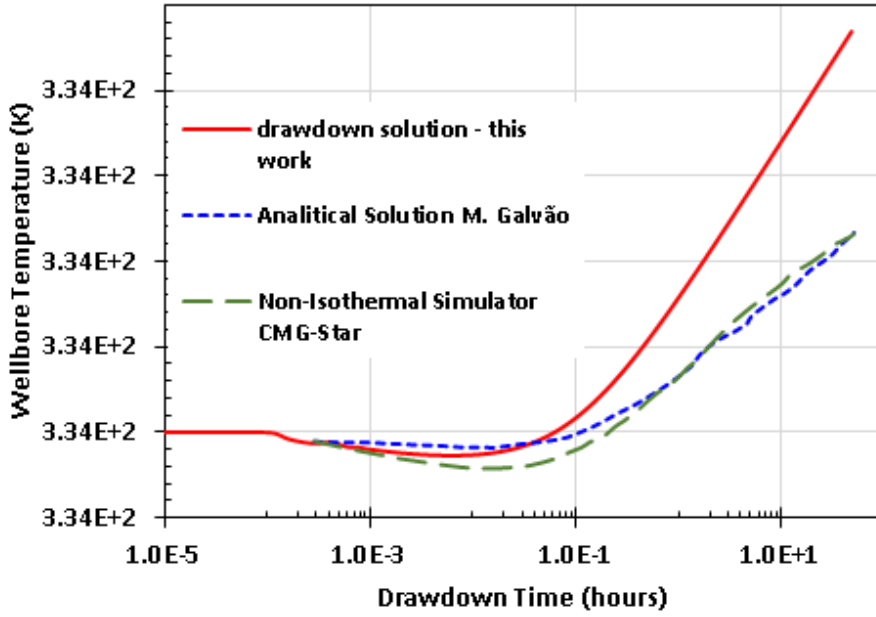
Figure 4.12: Gauge at Bottom hole, Temperature Validation.

4.2.1.2
Case 2, At Z = 100 m

At this gauge position, the flow from different layers of the reservoir at different flow rate and temperature have already been mixed, the most significant effect is the heat loss to the outside environment.

In Fig. 4.13, there is a transition in the drawdown period around 0.2h where a discontinuity in the temperature is observe. As mentioned by Galvao et. al. (2019), the physical explanation for this phenomenon is that when the well is opened to flow, the fluid below the sensor gauge starts flowing upwards, heating the gauge by a simple process of elevation, i.e., a deeper and warmer fluid continuously reaches the gauge over time. This heating effect dominates the gauge-temperature changes until the fluid originally at the bottom sandface reaches the gauge depth, suddenly ending the process of heating by vertical lifting. After this moment, the changes in temperature are caused by Joule-Thomson heating effect and by heat loss to the surroundings caused by radial diffusion. In Fig. 4.15, numerical solution are in good agreement at this position with analitical solution and results obtained using non-isothermal simulator, Galvão et al (2019) [40].
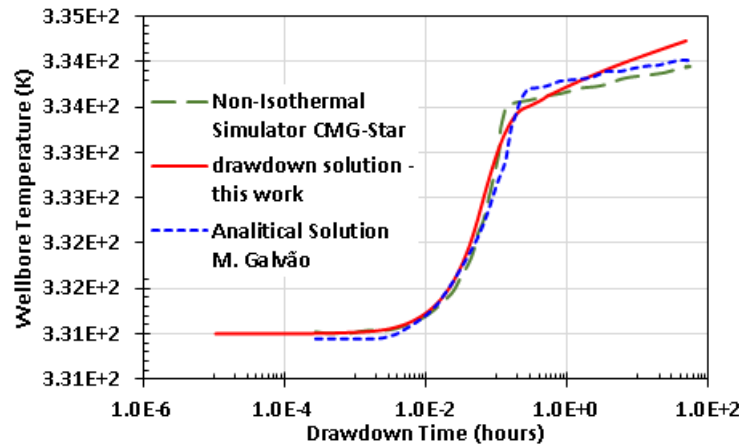
Figure 4.13: Gauge at z=100 m, Drawdown temperature Validation.

During the build up period, the temperature evolution at initial time is not the same because the final temperature achieved during the drawdown period are slightly different. However, after approximately 1h, the present solution and the non-isothermal solution present good agreement until they reach the temperature related of the geothermal gradient at this position, as shown in Figure 4.14.
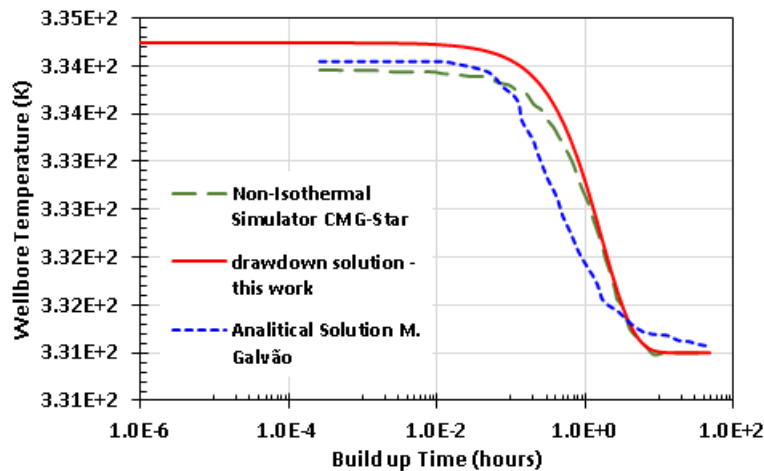

Figure 4.14: Gauge at z=100 m, Build up temperature Validation.

4.2.1.3
Case 3, At Z = 512.5 m

The same analysis that was performed for case 2 was done, but with a gauge position further up the well. In this case, a good agreement is obtained, both for drawdown, Figure 4.15 and for build up , Figure 4.16
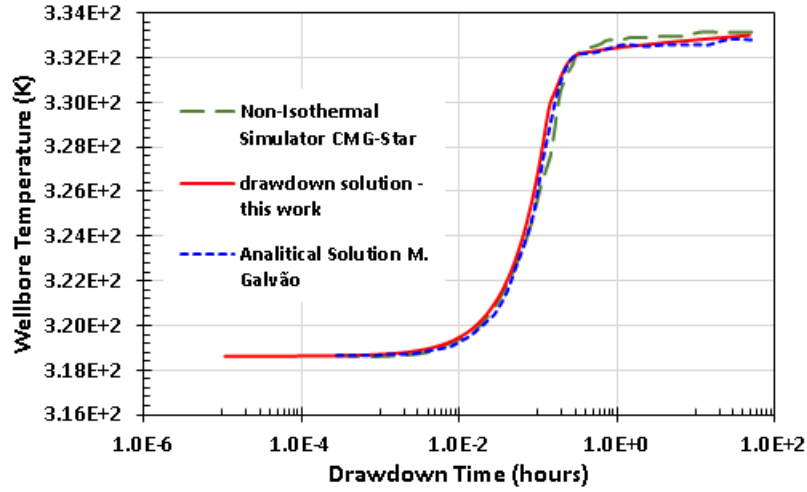
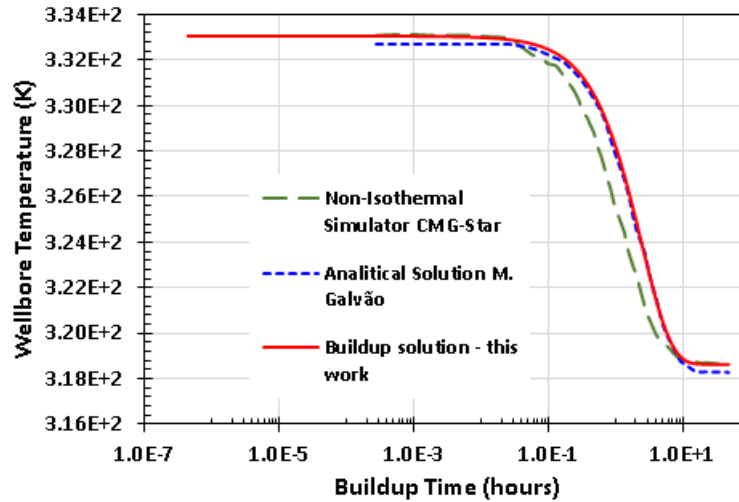Figure 4.15: Gauge at z=512.5 m, drawdown temperature validation.

Figure 4.16: Gauge at z=512.5 m, build up temperature validation.

4.2.2
Pressure Validation

For the validation of the pressure, a reservoir with high transmissibility is used. The same data from the reservoir, wellbore and fluid of the previous section is used with the following modifications:

Permeability:$K = 3000mD$

Reservoir height: $h = 75m$

Flow rate : $Q_w = 1400m^3/D$

Drawdown Period : $24 hours$

Build up Period : $48 hours$

Wellbore lenght : $262.5 meters$

As discussed before, the 1-D and 2-D problems are not exactly the same, so the validation must take these differences into account.

The validation is carried out by comparing the predictions of the proposed 2-D model with a numerical model already validated [53], based on the equations proposed by Onur and Cinar (2017) of a transient and non-isotherm model of a uni dimensional coupled wellbore-reservoir. The pressure values in the wellbore measured at 212.5m from the bottom of the reservoir are compared.

Figures 4.17 and 4.18 present the derivative plots for one dimensional simulators and the results obtained in this work. The derivative method plot for one-dimensional (green in discontinuous line) and two dimensional simulations (blue in continuous line). The divergence between those results were explained before where the drop pressure in two dimension analysis is greater than 1D due to relation $q/(\Delta z)$. Using the asymptotic value of the plot obtained in the Fig. 4.11 is possible to adjust and compare both 1D and 2D results multiplying the value of the 2D result (blue in continuous line) by 0.5. The new plot obtained (red in discontinuous line) allows to observe the good agreement of both results during drawdown and buildup period.
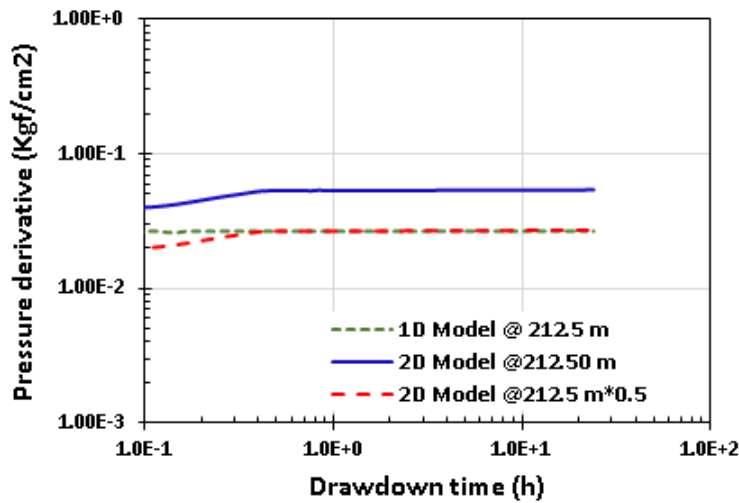

Figure 4.17: Drawdown pressure validation at 212.5 m.

It is important to note that in the buildup period, the phenomenon caused by the variation in density due to thermal effects described by Galvão et al (2019) [40] can be observed in Figure 4.18 at $z = 212.5m$.
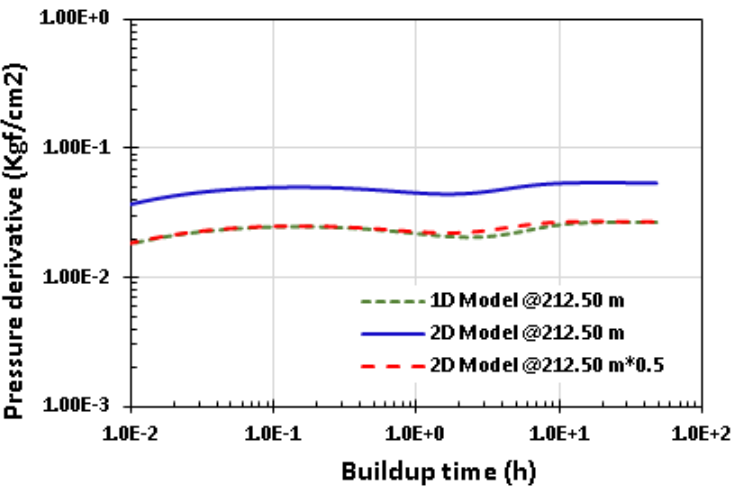
Figure 4.18: Build up pressure validation at 212.5 m.

5
Results and Discussion

In this chapter, several reservoir configurations and flow conditions are studied. Pressure and temperature behavior during a complete drawdown and buildup period are compared for homogeneous and stratified reservoirs, with and without vertical flow (crossflow). Crossflow between stratified layers will be analyzed considering an isotropic medium to different vertical permeability.

Wellbore-reservoir parameters and fluid properties described in section 4.1 are used. The vertical permeability and the thickness of each stratified layer will be set according to the analyzed case.

The simulation test comprises 48 hours of production followed by 48 hours buildup. The constant oil production rate was set at $800 m^3/$day and the total reservoir thickness is 50 meters.

Figures 5.1, 5.2 and 5.3 show the evolution of the temperature, flow rate and pressure profiles for the analyzes of a homogeneous and a stratified reservoir during the drawdown period, respectively.

The flow rate profile quickly reaches the steady state in both analyzes, and, as can be seen, in the reservoir region, emphasis in blue, the flow rate profile of the homogeneous reservoir presents a straight line. The same behavior does not occur in the stratified reservoir, where the difference in permeability of each layer gives rise to two straight lines with different slopes.

The evolution of the temperature profile, as well as the flow profile, show differences, whereas in the reservoir region, emphasis in blue, the homogeneous reservoir has a continuous profile, while the stratified reservoir has a discontinuity, resulting from different flows rate due to the difference in permeability between the layers. Another discontinuity appears on the temperature graph, at the gauge position of 100 meter, however it is due to the presence of tubing and this occurs in both models.

As can be seen, the evolution of the pressure profile for both reservoirs are similar. 125

Although the numerical model delivers information of transient data of flow rate, pressure and temperature at any position along the wellbore, and as we explained above, the analysis of flow rate and temperature graphs, at different gauge positions in the reservoir region, allows the identification of the

reservoir, the present work leads to identify the configuration of the reservoir by using of transient information of pressure and temperature in one single place just above the thickness of the reservoir.
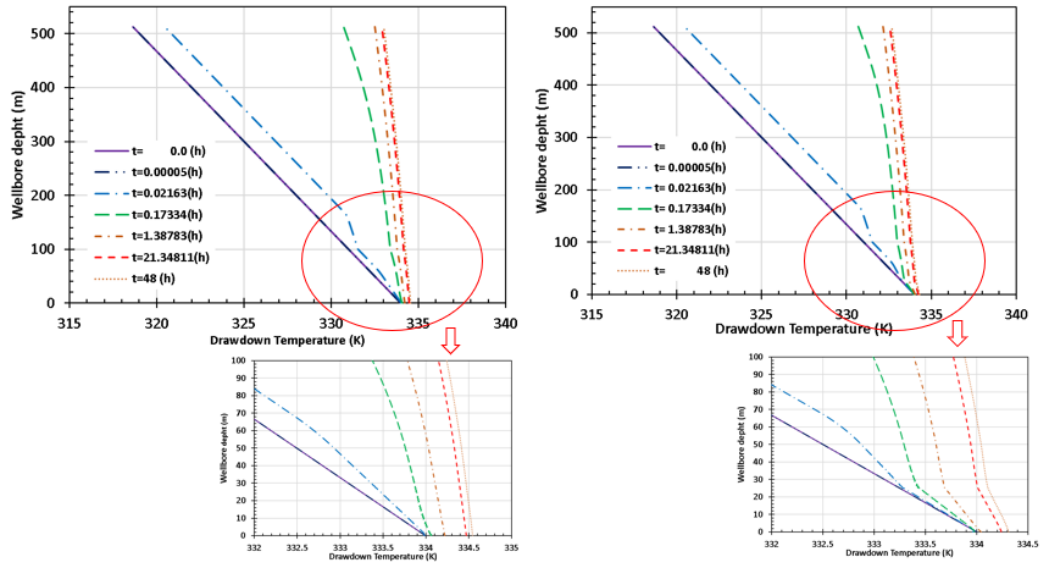

Figure 5.1: Temperature profile along the wellbore for different step times for an homogeneous and a stratified reservoirs.
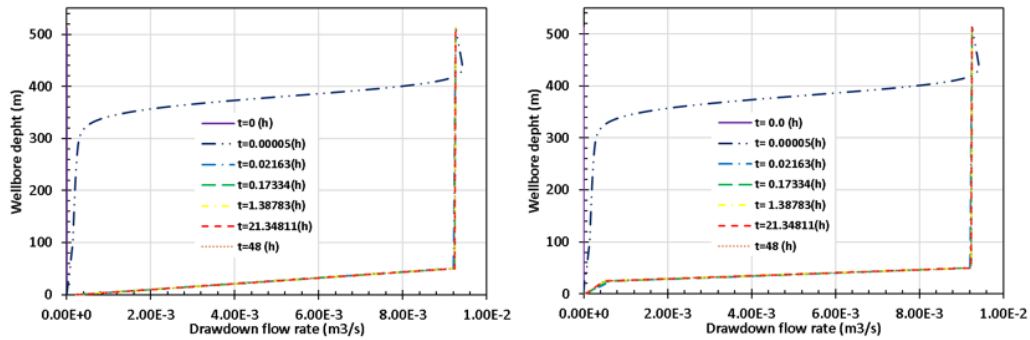

Figure 5.2: Flow rate profile along the wellbore for different step times for an homogeneous and a stratified reservoirs.
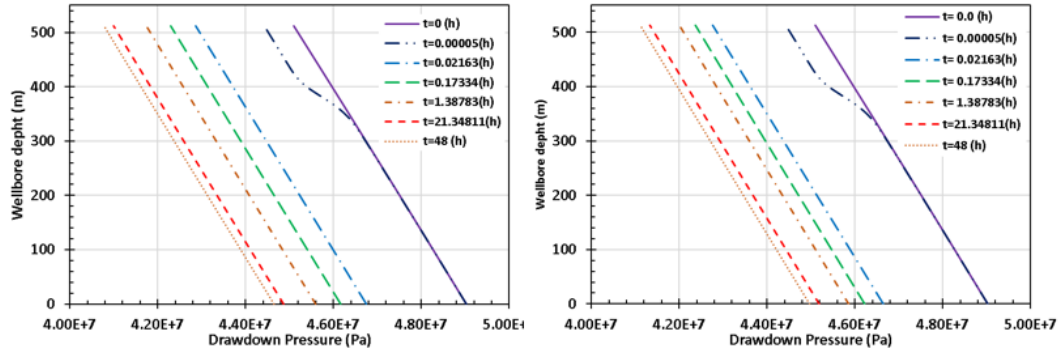
Figure 5.3: Pressure profile along the wellbore for different step times for an homogeneous and a stratified reservoirs.

In order to compare the flow behavior of homogeneous and stratified reservoirs, the transmissibility will be the same in both cases, as sketched in Figure 5.4.
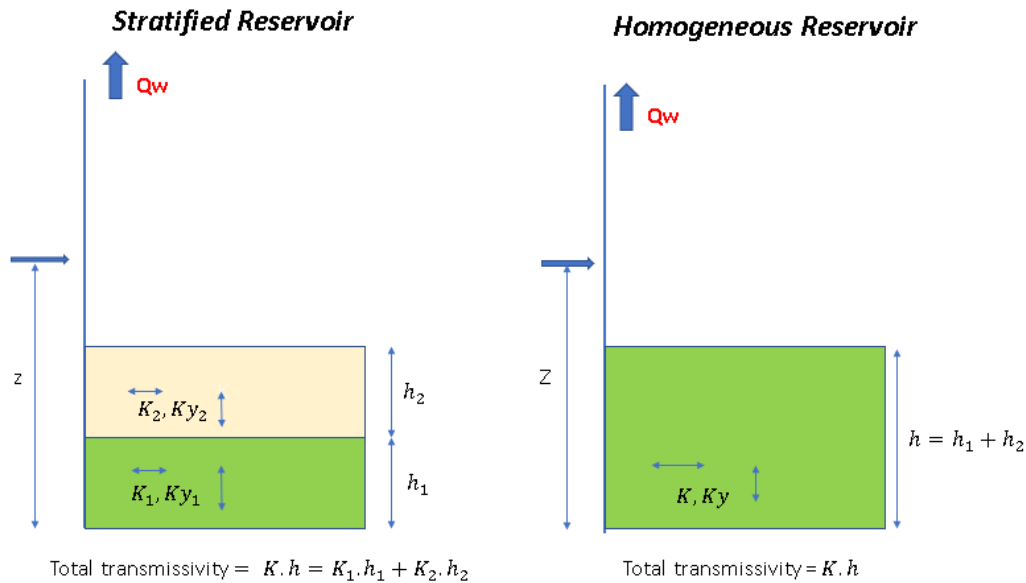

Figure 5.4: Homogeneous x Stratified Reservoir

5.1
Homogeneous reservoir

In this section we will compare the evolution of the pressure and temperature results for three different reservoirs: homogeneous and isotropic medium, homogeneous and non-isotropic medium with $Ky = 0$ and homogeneous and non-isotropic medium with $Ky = 200mD$, summarized in Table 5.1.

Table 5.1: Permeability values of the porous medium.

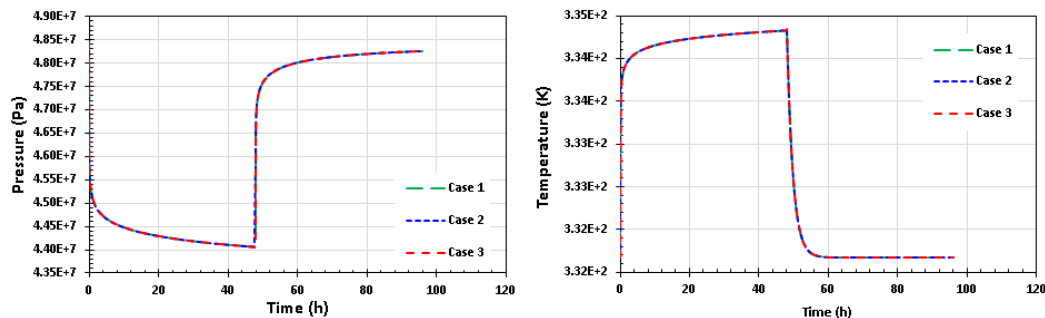| Case	Radial permeability mD	Vertical permeability mD
Case 1	100	100
Case 2	100	0
Case 3	100	200

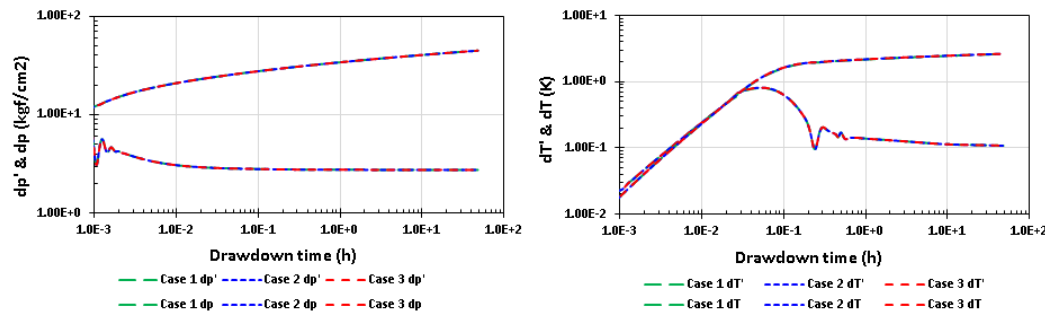Figure 5.5: Pressure and temperature for homogeneous reservoir (z=0 m).

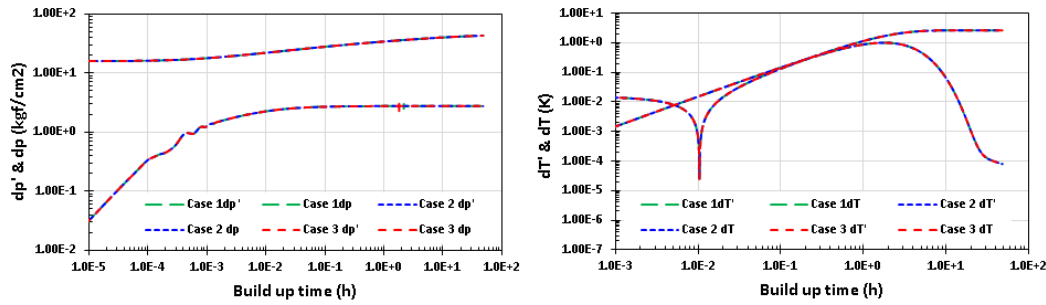Figure 5.6: Drawdown pressure and temperature derivative for homogeneous reservoir (z=86m).

Figure 5.7: Build up pressure and temperature derivative for homogeneous reservoir (z=86m).

As can be seen in Figures 5.5 to 5.7, all three cases show the same pressure and temperature evolution during the drawdown and buildup period. The flow is only in the radial direction, and the value of the vertical permeability does not affect the response.

5.2
Stratified reservoirs

Three different configurations of reservoirs were tested: an homogeneous and isotropic medium, a stratified and isotropic on each layer with crossflow and a stratified without crossflow. Table 5.2 presents the permeability values for the reservoirs. The flow rate, drawdown and build up times are the same as in the previous section. In all those cases, the thickness of each layer are also the same $(h_1 = h_2)$.

Table 5.2: Parameters of different configuration of porous medium.

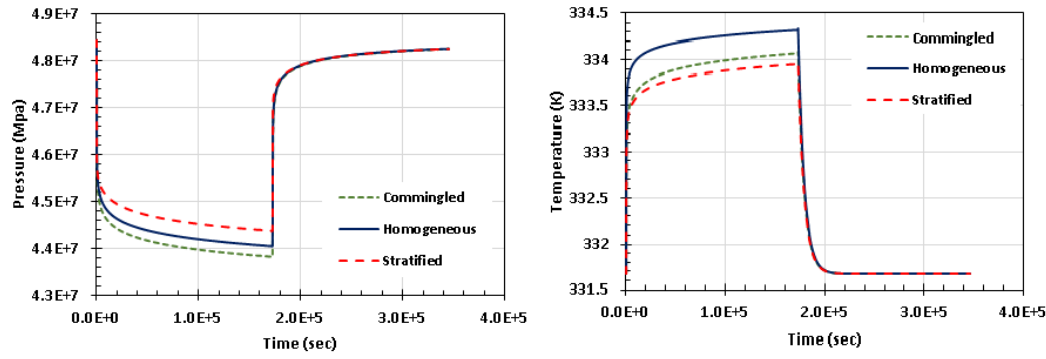| Property	Case 1	Case 2	Case 3
Description	Homogeneous	Stratified	Commingled
K_1 (mD)	100	10	10
h_1 (meters)	25	25	25
K_2 (mD)	100	190	190
h_2 (meters)	25	25	25
$TotalKh$ (mD)	5000	5000	5000
Ky_1 (mD)	100	10	0
Ky_2 (mD)	100	190	0

Figure 5.8: Pressure and temperature for homogeneous and stratified reservoir with and without crossflow ($z = 78m$).

Figure 5.8 presents the pressure and temperature evolution measured at the gauge position of $z = 78m$ for the three cases. Despite the differences in results presented by the different reservoirs, the pressure by time and temperature by time graphs do not show a behavior or signature that differentiates a homogeneous from a stratified reservoir. Actually, we observed differences in the pressure and temperature values that can be explained by the flow rate in the lower layers.
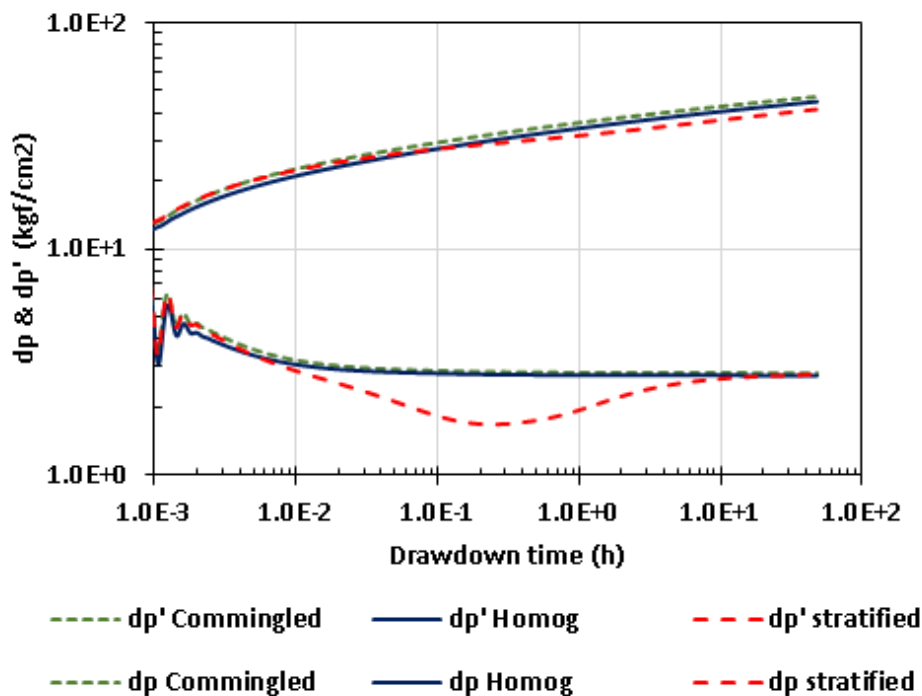

Figure 5.9: Drawdown derivative pressure for homogeneous and stratified reservoir with and without crossflow.

As we mentioned in the Chapter 1, the derivative method log-log plot is used to identify different configuration of the reservoir. Figure 5.9 shows the Bourdet derivative curve of the pressure for the same three different cases. The stratified reservoir without crossflow (commingled) and the homogeneous reservoir present similar pressure derivative plots. The stratified reservoir with vertical flow recovers the homogeneous radial regime, with a constant value of dp', for $t \geq 10^{+1}$. The curve from stratified reservoir presents a valley between about $10^{-1} \leq t \leq 1$. This pressure behavior is similar to reservoirs that have a flow barrier at a certain distance from the well.
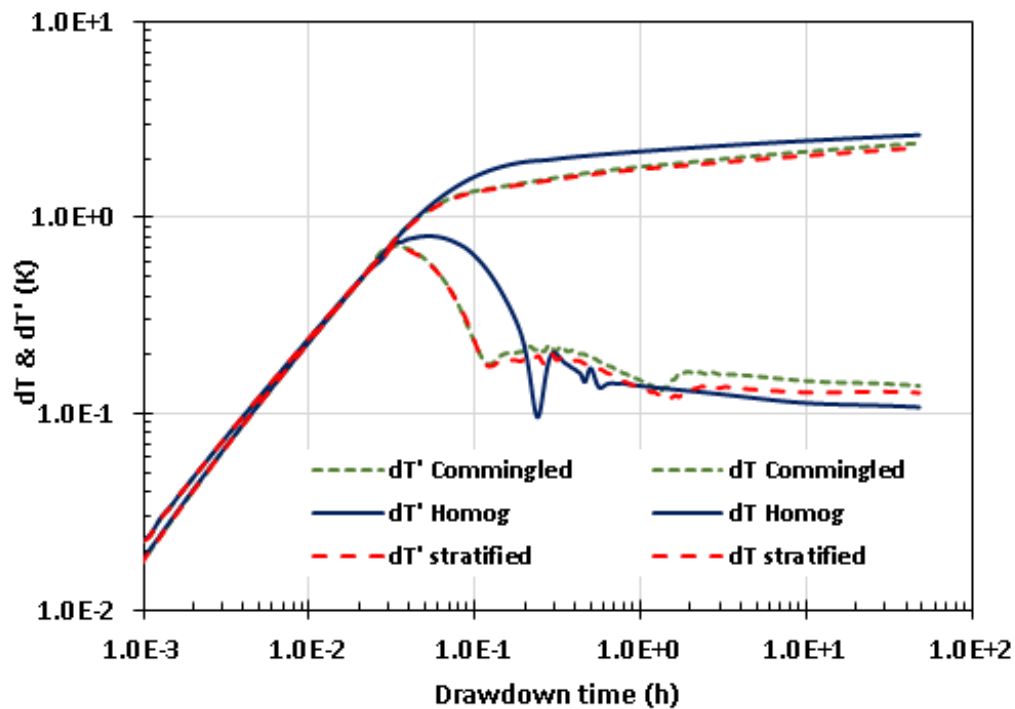
Figure 5.10: Drawdown derivative temperature for homogeneous and stratified reservoir with and without crossflow.

Differently from the pressure derivative graphs, in the temperature derivative graph, the presence of stratification anticipates the radial regime behavior, which identifies the presence of stratification in the reservoir, Figure 5.10.
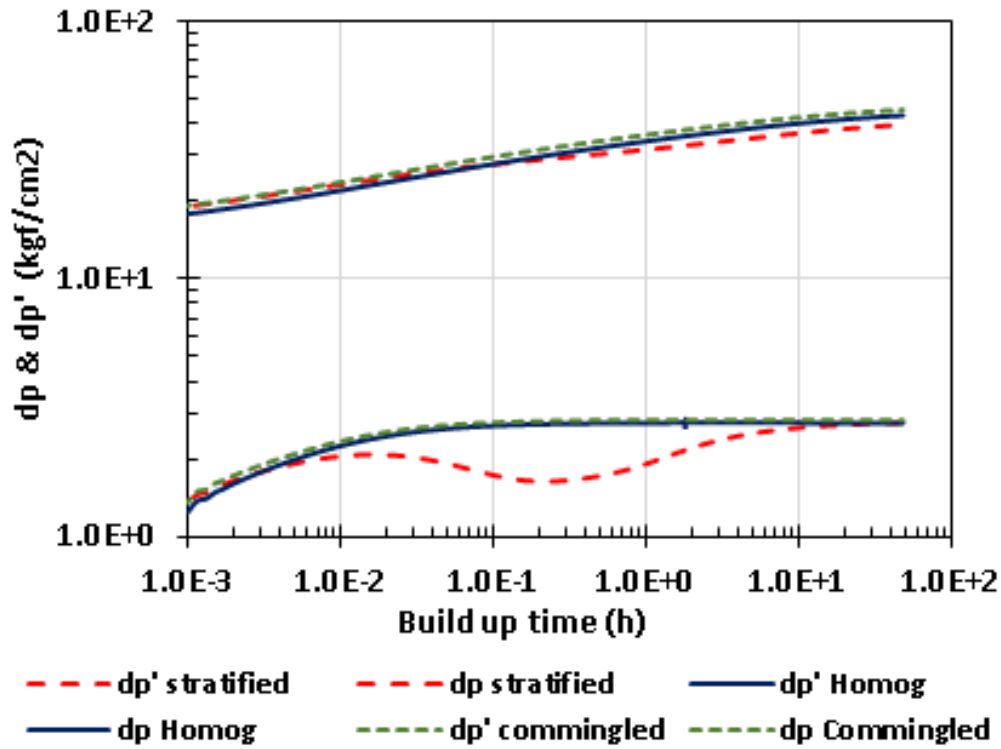
Figure 5.11: Build up derivative pressure for homogeneous and stratified reservoir with and without crossflow.

During the buildup regime, the derivative log-log pressure can be used to identify the stratified configuration of the reservoir, as shown in Fig. 5.9. On the other hand, the derivative log-log temperature in this regime can not give useful information about the stratified configuration. The log-log temperature are similar in all those three cases, as shown in Figure 5.12.

For that reason, the buildup regime is not considered in the analysis of temperature derivatives plots for the identification of stratified reservoirs.
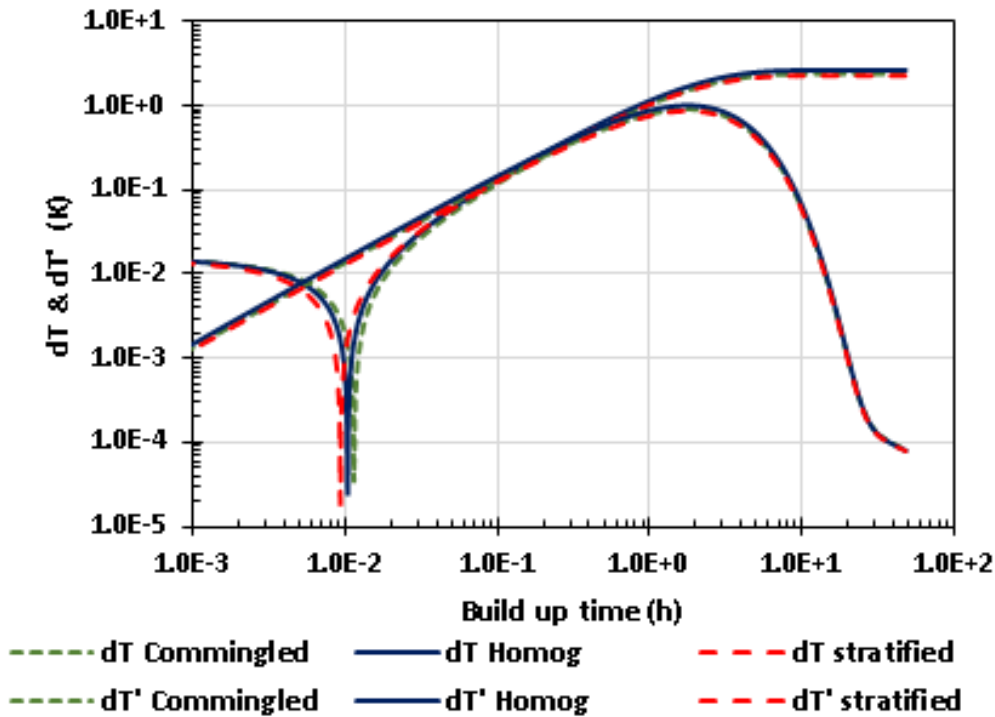
Figure 5.12: Build up derivative temperature for homogeneous and stratified reservoir with and without crossflow.

5.3
Impacts on PTA interpretation results.

Pressure transient analysis (PTA) is used to characterize reservoirs. However, only pressure data is not enough, there are different reservoir configurations that lead to similar pressure signal. As an example, three different reservoir configurations are tested: homogeneous (case1), stratified (case2) and another homogeneous vertically reservoir with internal region of high permeability in the radial direction (case3), as shown in Fig. 5.13. All data are measured at the certain gauge depth in the wellbore above the reservoir. Pressure transient behavior of case 2 and case 3 are similar and can lead to a misinterpretation, as shown in Fig. 5.14. This misinterpretation can be avoided by evaluating the temperature derivative data as shown in Fig 5.15. Case 2 and 3 have different behavior and the combined use of pressure and temperature can be explored to estimate the correct configuration of the reservoir.
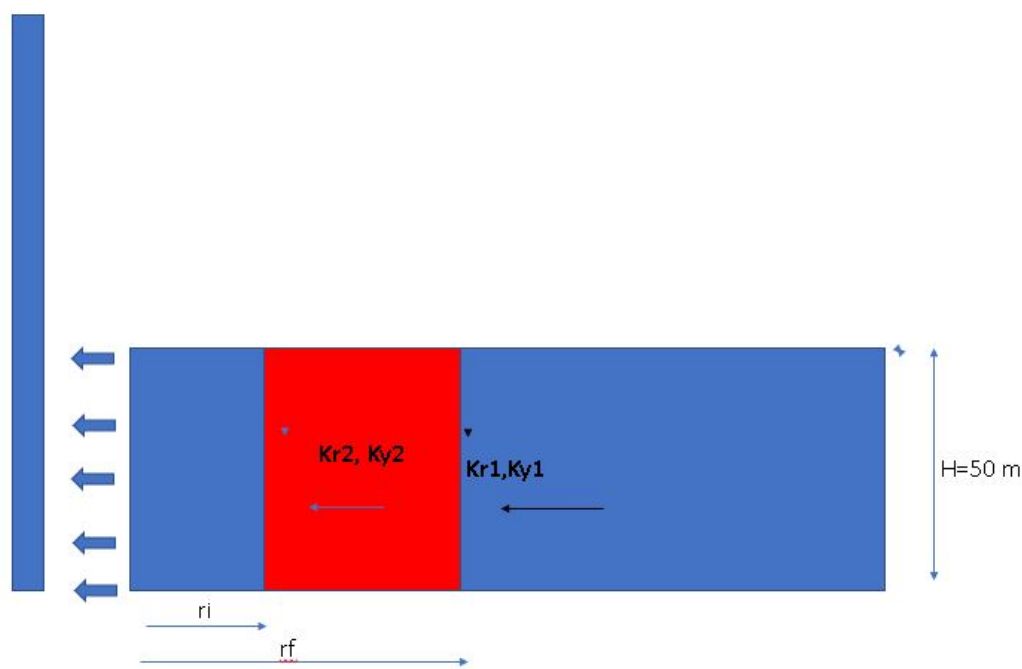
Figure 5.13: Reservoir with high permeability inside r_i and r_f.

Table 5.3: Table of parameters of a reservoirs with a central region of high permeability.

Property	Value
K_1 (mD)	100
Ky_1 (mD)	100
K_2 (mD)	200
Ky_2 (mD)	200
r_i (m)	16.92
r_f (m)	43.92

The table 5.4 presents the parameters of a stratified reservoir with flow between layers that presents the pressure derivative graph similar to the reservoir described above.

Table 5.4: Table of parameters of a stratified reservoirs.

Property	Value
K_1 (mD)	10
Ky_1 (mD)	10
h_1 (m)	25
K_2 (mD)	190
Ky_2 (mD)	190
h_2 (m)	25

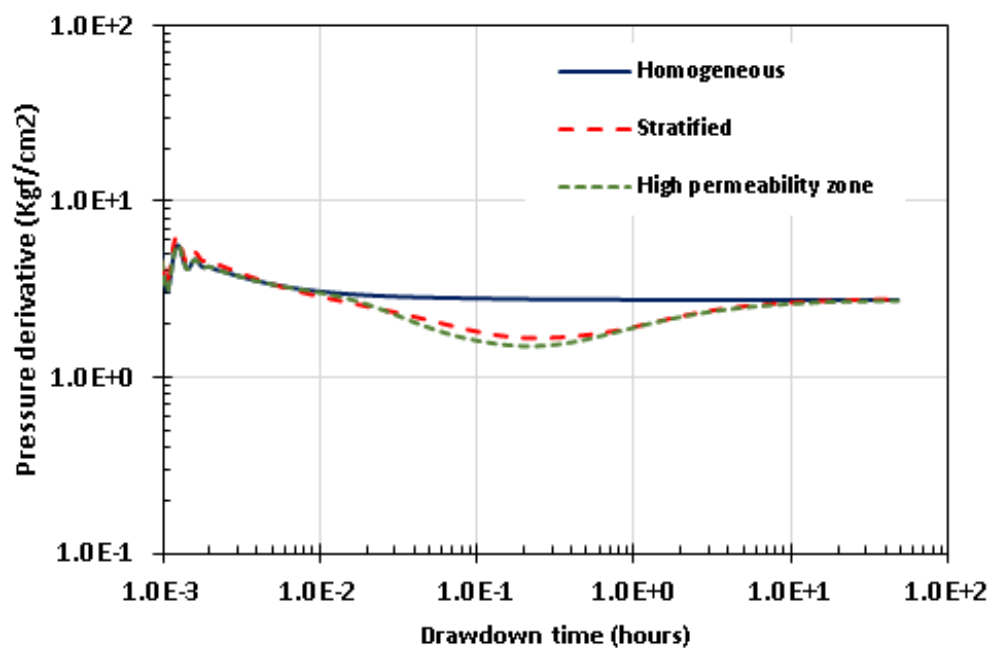Figure 5.14: Drawdown derivative pressure for a stratified reservoir (case 2), a reservoir with high permeability zone (case 3) and an homogeneous reservoir (case 1) .
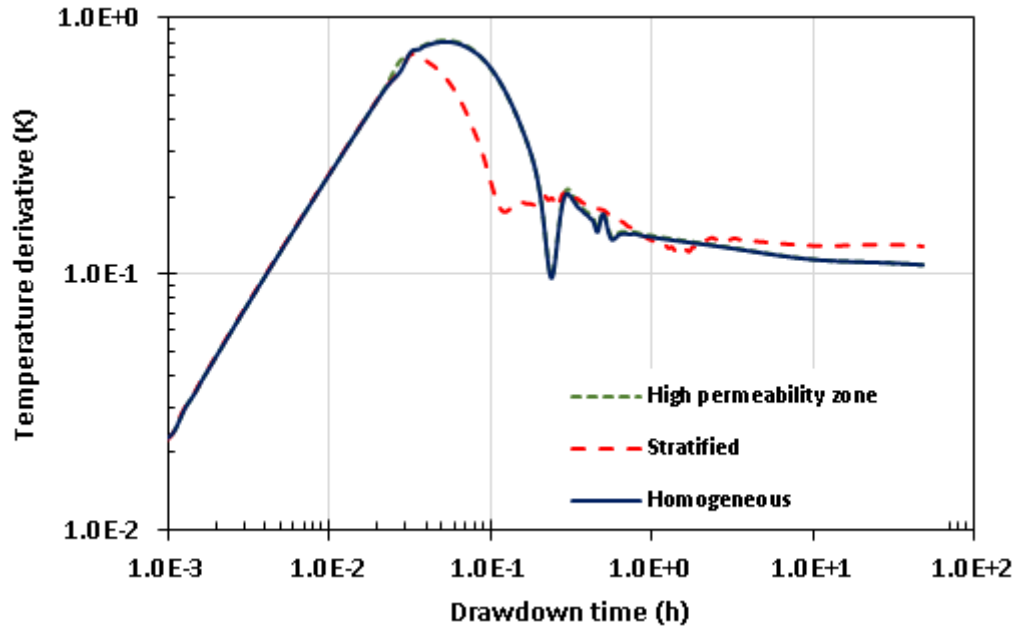
Figure 5.15: Drawdown derivative temperature for a stratified reservoir (case 2), a reservoir with high permeability zone (case 3) and an homogeneous reservoir (case 1) .

The heterogeneity along the radial direction with a high permeability region does not change the temperature derivative plot, which makes the differentiation with respect to the stratified case easy to be observed.

Temperature transient analysis (TTA) in a two-dimensional reservoir coupled with a wellbore can be used to distinguish different reservoir configuration in addition to pressure transient analysis (PTA).

5.4
Effect of permeability in Stratified reservoir

In this section, stratified reservoirs formed by isotropic layers are studied.

We present a series of derivative plots for different stratified reservoirs, always keeping the same total effective oil flow capacity value. The transmissibility of all cases are the same. The derivative pressure plots present the behavior discussed before, similar to one-dimension double porosity and double permeability, as described in previous section.

The parameter and properties of the reservoir and fluid are the same, except the permeability value of each layer. Flow rate is constant at 800 m^3/day and drawdown and buildup times are set at 48 hours.

Table 5.5 shows a combination of permeabilities for a stratified reservoir, keeping constant the height of each layer and the value of the total effective oil flow capacity. The results for the drawdown period are shown in the Figure 5.16.

Table 5.5: Table of properties of different stratified reservoirs with crossflow with the same total effective oil flow capacity.

K_1 (mD)	h_1 (m)	K_2 (mD)	h_2 (m)	$K_1 h_1 + K_2 h_2$ (mD.m)
100	25	100	25	5000
10	25	190	25	5000
30	25	170	25	5000
50	25	150	25	5000
70	25	130	25	5000
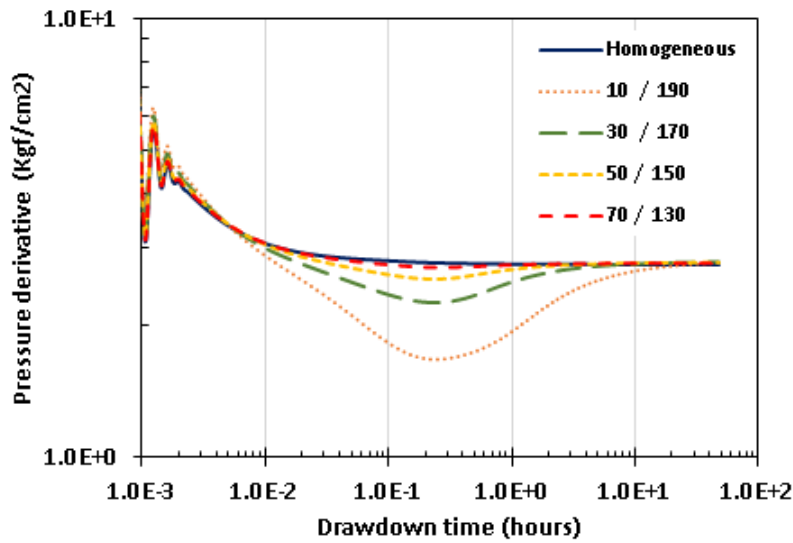
Figure 5.16: Derivatives Pressure of different stratified reservoirs with crossflow with the same total effective oil flow capacity value.

The results in Figure 5.16 show that the smaller the difference between layers permeability, the lower the dp' valley of the pressure derivative plot.

The higher depression of the pressure derivative curve in the diagnostic graph evidences an increase in crossflow transmissibility, which should be understood as an increase in vertical flow, from the layer with lower permeability to the layer with the higher permeability.

Figure 5.17: Derivatives temperature for different stratified reservoirs with vertical permeabilities, Drawdown period.

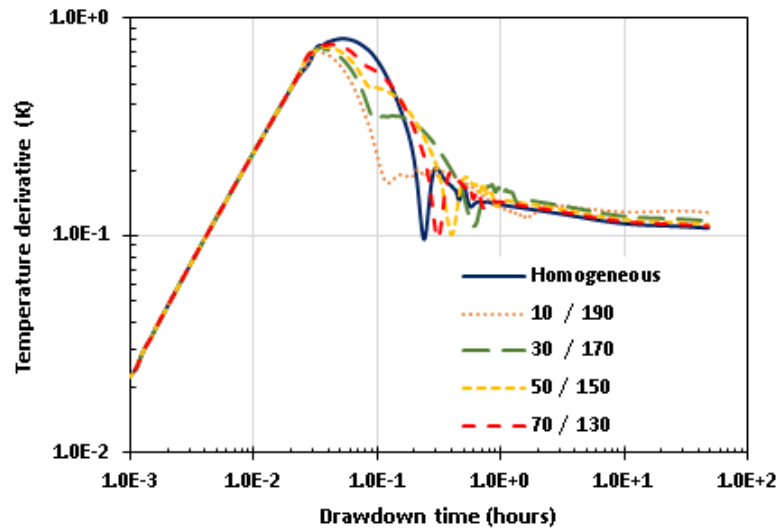The temperature derivative graphs for the different reservoir configurations, shown in Fig. 5.17, we can observe in initial times that the greater the permeability difference between the layers, the greater the deviation of the graph in relation to the homogeneous behavior.

5.5
Effect of vertical permeability changes in stratified reservoirs

In this section, we explore the effect of the vertical permeability in the flow response.

The table 5.6 shows the analyzed reservoirs and the variation in vertical permeability.

Figure 5.18 shows that increasing the vertical permeability leads to a shift to the left in the depression of the pressure derivative curve of a stratified reservoir. Conversely, the reduction in the vertical permeability value causes a shift to the right in the diagnostic graph, delaying the infinity acting radial flow regime (IARF).

Table 5.6: Table of properties of a stratified reservoirs with different vertical permeability.

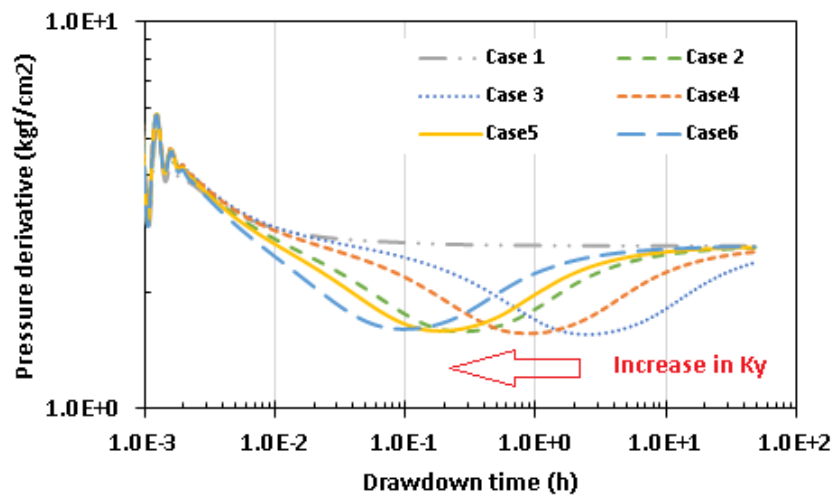| Case	K1 mD	K2 mD	Ky1 mD	Ky2 mD	h1 m	h2 m
Case 1	100	100	100	100	25	25
Case 2	10	190	10	190	25	25
Case 3	10	190	0.1×10	0.1×190	25	25
Case 4	10	190	0.5×10	0.5×190	25	25
Case 5	10	190	1.5×10	1.5×190	25	25
Case 6	10	190	3×10	3×190	25	25

Figure 5.18: Stratified reservoir, changes in vertical permeability

The position where the minimum in the pressure derivative appears in stratified reservoir changes to the left as the vertical permeability value of each layer increase, as shown in Fig. 5.18.

As discussed later, this shift is associated with the vertical flow between the layers with different permeability's. Low vertical permeability delays the flow communication between the layers of a stratified reservoir, shifting the valley to longer times.

The temperature derivative is not very sensitive to changes in vertical permeability, as can be seen in Fig. 5.19.
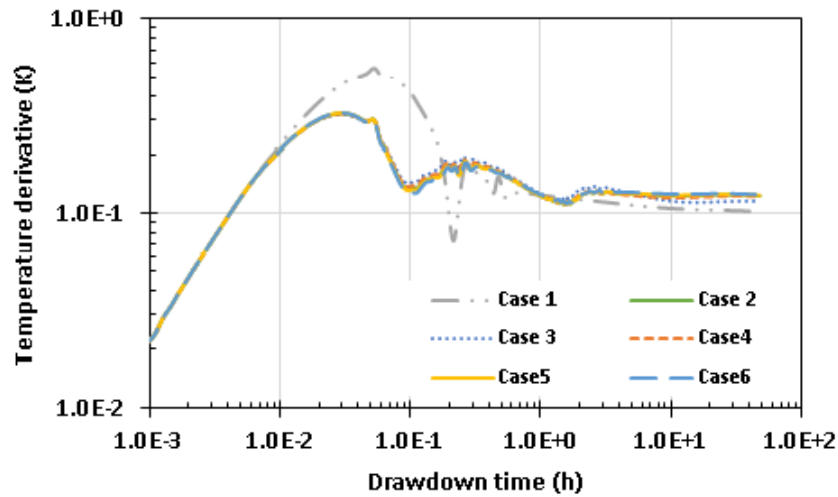
Figure 5.19: Temperature derivative for a stratified reservoir, changes in vertical permeability

5.6
Effect of reservoir permeability on the flow behavior

As seen in the previous section, the increase of vertical permeability shifts to the left the characteristic curve of the stratified reservoir in pressure derivative plots.

The average permeability was changed to $3000mD$. The reservoir height changed to 150 meters and the flow rate was increased to $1400m^3/day$. Pressure and temperature are measure along the time at the same distance above the reservoir (28 m), i.e. gauge position 178m, during a 24 hours of drawdown period. Parameters and properties of the wellbore/system are the same as used in section 4.2.2 .

Table 5.7 shows the permeability of five high permeability stratified reservoirs, with constant total transmissibility and one homogeneous reservoir as basis of comparison. The thickness of the layers was kept constant and equal to 75m.

Table 5.7: Table of properties of a high permeability stratified reservoirs.

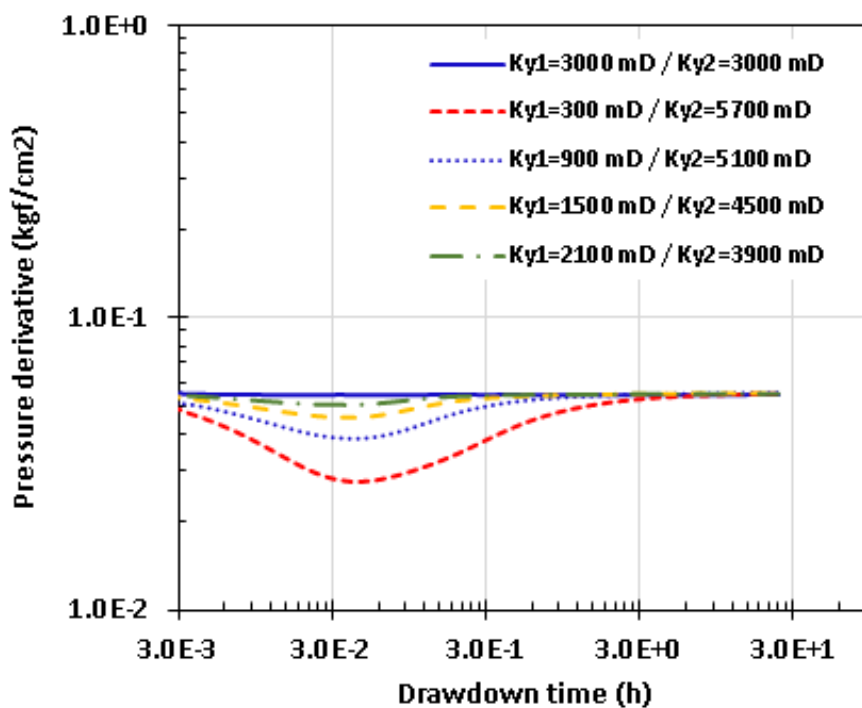| Case	K_1 mD	K_2 mD	Ky_1 mD	Ky_2 mD	h_1 m	h_2 m
Case 1	3000	3000	3000	3000	75	75
Case 2	300	5700	300	5700	75	75
Case 3	900	5100	900	5100	75	75
Case 4	1500	4500	1500	4500	75	75
Case 5	2100	3900	2100	3900	75	75

Figure 5.20: Stratified reservoir, high permeability.

In reservoirs with high permeability it is possible to observe the signature of the stratified reservoir were moved to the left, as shown in Fig. 5.20, when compared to the results presented in Fig. 5.16. The shift of the dp' valley to earlier times is associated with the stronger crossflow. This anticipation could hide the signature of the stratified reservoir if the valley occurs at very early times, where the effect of storage and skin are present. However, TTA remains less sensitive to the high permability reservoir effect,as shown in Fig. 5.21
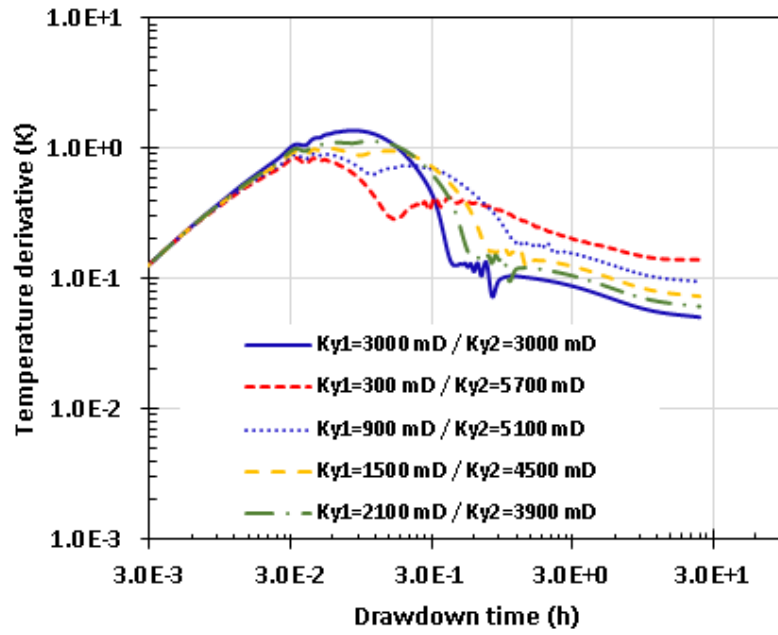
Figure 5.21: Derivative temperature for stratified reservoir, high permeability.

5.7
Transient cross-flow analysis

The purpose of this section is to analyze the flow behavior between adjacent layers during a drawdown test. The wellbore-reservoir system described in section 5.6 is used.

As discussed in the previous sections, the time at which the valley in the dp' occurs is directly associated with the vertical permeability and its amplitude is a function of the difference in permeability between the layers.

Figure 5.22 and 5.23 shows a sequence of surface plots of pressure and vertical velocity fields inside the reservoir at intervals that vary from the early times to the end of the test.
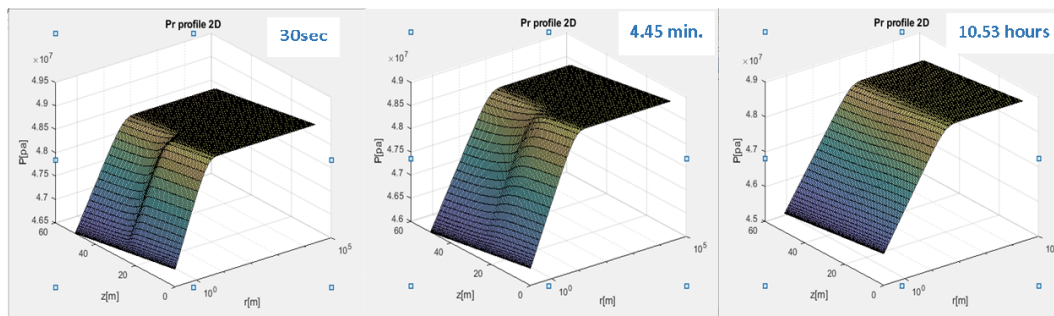

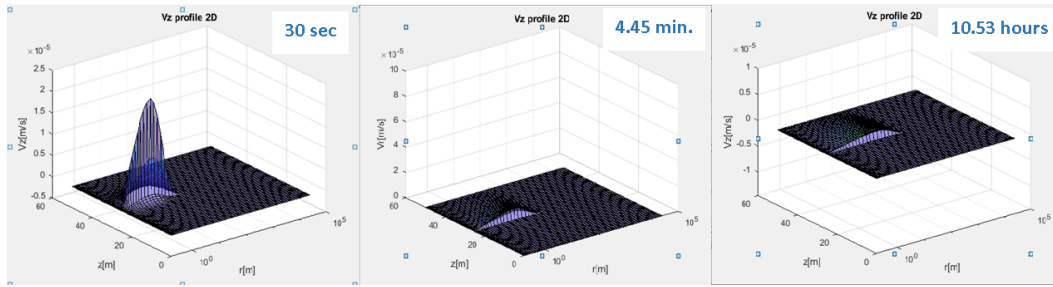Figure 5.22: Pressure evolution inside the reservoir

Figure 5.23: Crossflow evolution inside the reservoir

As soon as the reservoir starts to produce, the difference in permeability between the two layers leads to a stronger pressure gradient in the radial direction in the less permeability layer (bottom). As a consequence, a pressure gradient in the vertical direction is created, driving flow from the less permeable to the more permeable layer. As the flow progresses, the pressure stabilizes, and the flow in vertical direction vanishes. After this stabilization, the reservoir behavior is similar to a homogeneous reservoir, since there is no vertical flow.

The pressure difference between two layers of a stratified reservoirs was monitored during a drawdown test inside the resrvoir, at a position 1.5 meters far from the wellbore.

In the beginning of the test (early times), the stratified reservoir behaves as if there was no flow between layers, as time goes up, due to the differences in radial velocities between the layers, there is the appearance of a pressure differential greater than the hydrostatic gradient and this gives rise to a vertical flow between the layers.Advancing a little more in time, the hydrostatic gradient, which dominates the well's behavior, is also extended to the reservoir, ceasing the vertical flow. At this point, the reservoir starts to behave as if it were homogeneous .

The higher the vertical permeability, the faster the reservoir approaches the hydrostatic gradient and inversely, the lower the vertical permeability, more time the reservoir needs to equilibrate the pressure.

Figure 5.24 shows the evolution of the pressure differential over time, this test was repeated for similar reservoirs, but only with different vertical permeabilities.
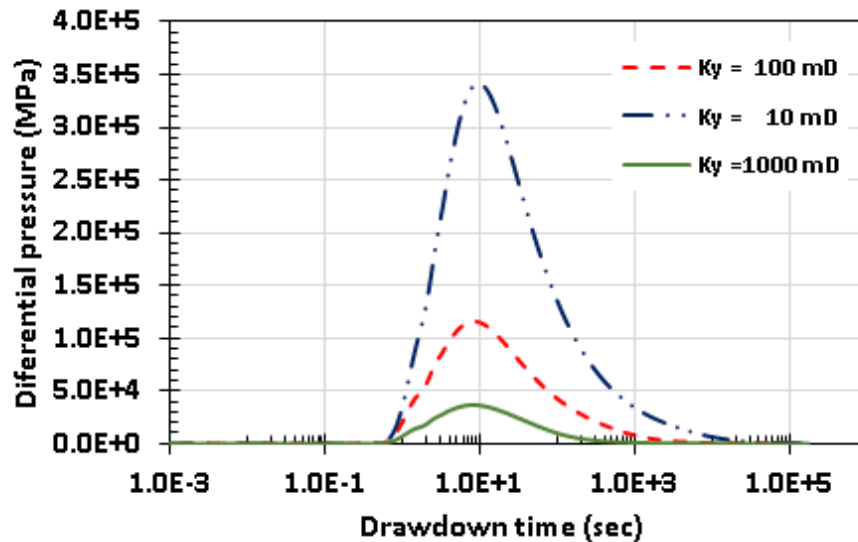
Figure 5.24: pressure differential in the reservoir

5.8
Effect position of the most permeable layer.

The pressure derivative plots are slightly affected by the order of the layers and shows the same behavior, as illustrated in Figure 5.25 (a).

Due to the geothermal gradient, the lower layer feeds the wellbore with a fluid at a higher temperature, when this layer has higher permeability it dominates the temperature behavior of the wellbore and it has a thermal behavior closer to that of an homogeneous reservoir, however, the maximum of the temperature derivative graph is higher and not smooth, a characteristic that differs it from the homogeneous reservoir. This effects is shown in Figure 5.25 (b). Again, the temperature diagnostic graph must be used to complement the analysis and characterization of the reservoir.
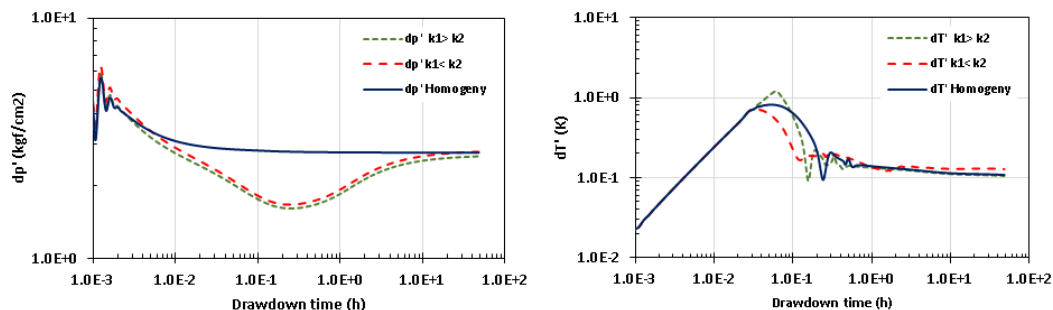

Figure 5.25: Effect of layer order on derivative graphs.

5.9
Gauge position effect.

In this section, pressure and temperature measurements are taken at different gauge positions along the wellbore, above the reservoir. As can be seen in Figure 5.26, the pressure derivative plots are the same for any gauge position, but the temperature derivative plots exhibit the differences caused by the influence of the relationship between the flows of the layers and their temperature as shown in Figure 5.27.

The difference between the derivative temperature plots for homogeneous and stratified reservoirs is minimized as we evaluate the temperature in gauge positions away from the reservoir. The temperature effect is minimized due to heat exchange with the neighborhood as this measurement is made at higher positions. The best gauge positions to characterize the reservoir are those located just above it, Figure 5.28 shows that the shift disappear far away from the reservoir.
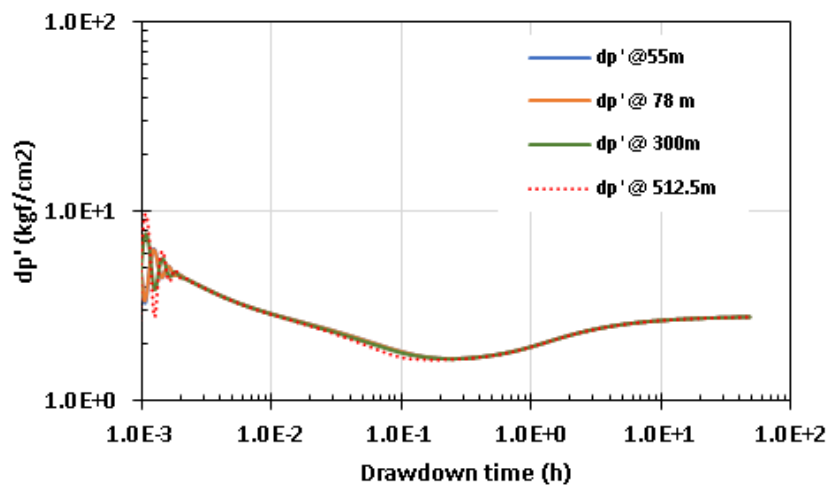
Figure 5.26: Effect of gauge position on pressure derivative graphs.
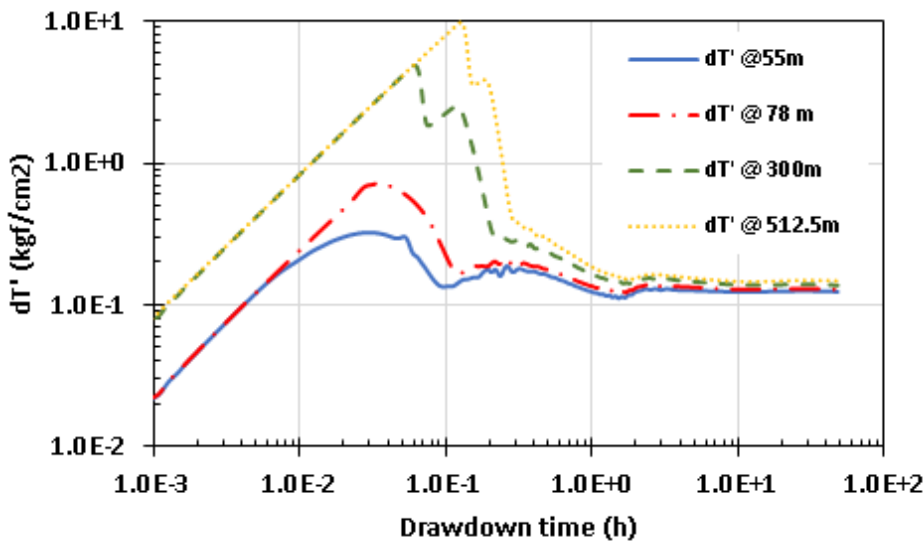
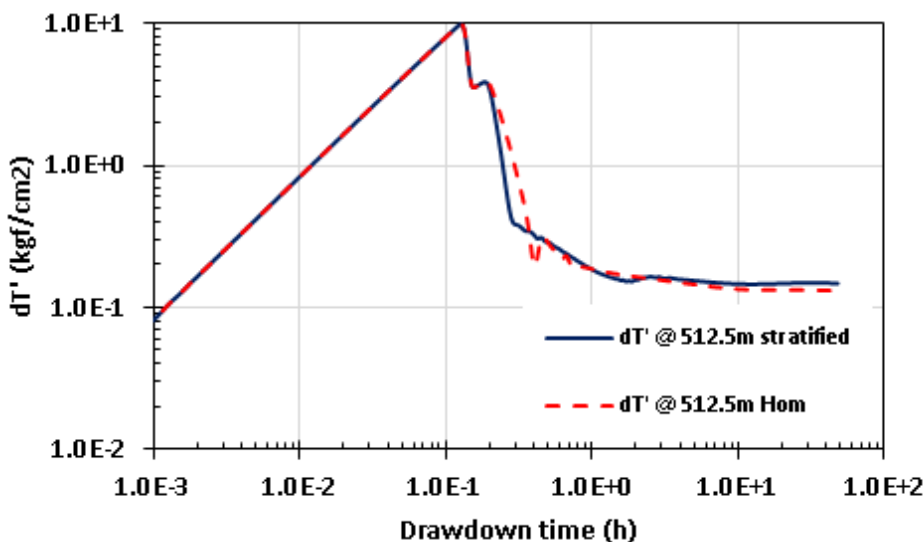Figure 5.27: Effect of gauge position on temperature derivative graphs.

Figure 5.28: Effect on temperature derivative graphs at the top of the wellbore.

6
Conclusions and Suggestions

This work presented a numerical modeling for a coupled wellbore-stratified reservoir system. The reservoir is treated in a two-dimensional way and the presence of heterogeneity in the vertical direction is analyzed. A non-isothermal modeling was used, where the effects of conduction, convection, adiabatic fluid expansion-compression and Joule-Thompson were considered. Density and porosity were treated as a function of pressure and temperature.

The proposed numerical model shows good agreement with the results of commercial software both for temperature and pressure.

The analysis of the temperature transient together with the analysis of the pressure transient can help in the identification of stratified, double porosity or reservoirs with heterogeneities.

6.1
Contributions of this work

In this work we focus on the vertical variation of permeability, leading to the following results:

1. In a two dimensional analysis of an homogenous reservoir the value of the vertical permeability does not affect the flow. There is no vertical flow.

2. The derivative method is used to identify different configuration of the reservoir. PTA and TTA show characteristic signatures of a stratified reservoir.

3. PTA obtain good results for identifying stratified reservoirs during drawdown and buildup periods. However, TTA during buildup period can not give useful information about the stratified configuration.

4. During drawdown period, the temperature transient analysis (TTA) in a two-dimensional reservoir coupled with a wellbore can be used to distinguish different reservoir configurations in addition to pressure transient analysis (PTA).

5. Higher difference between permeability of each layer, higher the curvature of the PTA log-log plot. In TTA log-log plot is observed difference from the behavior of a homogeneous reservoir.

6. The position where the signature appears in typical stratified reservoir changes to the left when the vertical permeability value of each layer increase.

7. For high permeability reservoir, TTA log-log plots shows clear results comparatively to PTA log-log plots.

8. TTA log-log plots can be used to characterize the position of the most permeable layer.

9. The best gauge positions to characterize the reservoir are those located just above it.

6.2
Future work

The main goal achieved by this work was the development of a tool for a two-dimensional analysis of a non-isothermal reservoir. The behavior of the pressure transient has been widely studied, but the use of the temperature transient to complete the analysis is in the beginning. Some configurations were analyzed, however, there is a need for further details:

1. Vertical porosity variations.

2. Skin effects in stratified reservoirs.

3. Injection test.

4. An inverse problem model that identifies the stratification and properties of each layer.

Bibliography

[1] RN Horne. Modern well test analysis: A computer-aided approach.–4th printing.–palo alto, california, usa: Petroway, 1990.

[2] Alain C Gringarten. From straight lines to deconvolution: The evolution of the state of the art in well test analysis. *SPE Reservoir Evaluation & Engineering*, 11(01):41–62, 2008.

[3] Dominique Bourdet, JA Ayoub, and YM Pirard. Use of pressure derivative in well test interpretation. *SPE Formation Evaluation*, 4(02):293–302, 1989.

[4] HC Lefkovits, P Hazebroek, EE Allen, and CS Matthews. A study of the behavior of bounded reservoirs composed of stratified layers. *Society of Petroleum Engineers Journal*, 1(01):43–58, 1961.

[5] D Bourdet. Pressure behavior of layered reservoirs with crossflow. In *SPE California Regional Meeting*. Society of Petroleum Engineers, 1985.

[6] Heungjun Park and RN Horne. Well test analysis of a multilayered reservoir with formation crossflow. In *SPE Annual Technical Conference and Exhibition*. Society of Petroleum Engineers, 1989.

[7] Cheng-tai Gao. Determination of parameters for individual layers in multi layer reservoirs by transient well tests. In *Annual Technical Meeting*. Petroleum Society of Canada, 1986.

[8] DG Russell and M Prats. Performance of layered reservoirs with crossflow–single-compressible-fluid case. *Society of Petroleum Engineers Journal*, 2(01):53–67, 1962.

[9] JD Pendergrass and VJ Berry Jr. Pressure transient performance of a multilayered reservoir with crossflow. *Society of Petroleum Engineers Journal*, 2(04):347–354, 1962.

[10] F Kucuk and L Ayestaran. Well test analysis of commingled zones without crossflow. Technical report, Schlumberger, Well Services, 1984.

[11] F Kucuk, M Karakas, and L Ayestaran. Well testing and analysis techniques for layered reservoirs. *SPE Formation Evaluation*, 1(04):342–354, 1986.

[12] Christine A Ehlig-Economides and Jeffrey Joseph. A new test for determination of individual layer properties in a multilayered reservoir. *SPE Formation Evaluation*, 2(03):261–283, 1987.

[13] Plyush C Shah, Metin Karakas, Fikri Kuchuk, and Luis C Ayestaran. Estimation of the permeabilities and skin factors in layered reservoirs with downhole rate and pressure data. *SPE formation evaluation*, 3(03):555–566, 1988.

[14] Fikri J Kuchuk and David J Wilkinson. Transient pressure behavior of commingled reservoirs. *SPE formation evaluation*, 6(01):111–120, 1991.

[15] Weibo Sui, Ding Zhu, Alfred Daniel Hill, and Christine Ehlig-Economides. Model for transient temperature and pressure behavior in commingled vertical wells. In *SPE Russian Oil and Gas Technical Conference and Exhibition*. Society of Petroleum Engineers, 2008.

[16] R Vicente, C Sarica, and T Ertekin. A two-phase model coupling reservoir and horizontal well flow dynamics. in {SPE} latin american and caribbean petroleum engineering conference. society of petroleum engineers ({SPE}), 2001.

[17] ED Nennie, GJN Alberts, SPC Belfroid, E Peters, and GJP Joosten. An investigation into the need of a dynamic coupled well-reservoir simulator. In *SPE Annual Technical Conference and Exhibition 2007, ATCE 2007, 11 November 2007 through 14 November 2007, Anaheim, CA, USA, Conference code: 71497, 4, 2461-2469*, 2007.

[18] Khafiz Muradov and David Davies. Temperature transient analysis in horizontal wells: Application workflow, problems and advantages. *Journal of Petroleum Science and Engineering*, 92:11–23, 2012.

[19] Obinna O Duru and Roland N Horne. Simultaneous interpretation of pressure, temperature, and flow-rate data using bayesian inversion methods. *SPE reservoir evaluation & engineering*, 14(02):225–238, 2011.

[20] M Sidorova, V Shako, V Pimenov, and B Theuveny. The value of transient temperature responses in testing operations. In *SPE Middle East Oil & Gas Show and Conference*. Society of Petroleum Engineers, 2015.

[21] Maurice Schlumberger, AA Perebinossoff, and Henri-Georges Doll. *Temperature measurements in oil wells*. 1936.

[22] Frans Barends. Complete solution for transient heat transport in porous media, following lauwerier. In *SPE Annual Technical Conference and Exhibition*. Society of Petroleum Engineers, 2010.

[23] GE Malofeev and AB Scheinman. The calculation of oil recovery from a stratum upon injecting hot water into it. *Neft. Khoz*, 41:31–35, 1963.

[24] RH Al-Hussainy. Ramey, jr, and crawford, p, 1966. *The flow of real gases through porous media journal of Petroleum Technology*, 18(05):624–636.

[25] PG Atkinson and Henry J Ramey Jr. Problems of heat transfer in porous media. In *SPE Annual Fall Technical Conference and Exhibition*. Society of Petroleum Engineers, 1977.

[26] RN Horne and K Shinohara. Wellbore heat loss in production and injection wells. *Journal of Petroleum Technology*, 31(01):116–118, 1979.

[27] RB Crookston, WE Culham, and Wen H Chen. A numerical simulation model for thermal recovery processes. *Society of Petroleum Engineers Journal*, 19(01):37–58, 1979.

[28] DH Brownell Jr, SK Garg, and JW Pritchett. Governing equations for geothermal reservoirs. *Water Resources Research*, 13(6):929–934, 1977.

[29] KC Shiu and HD Beggs. Predicting temperatures in flowing oil wells. 1980.

[30] Frederic Maubeuge, Eric Arquis, and O Bertrand. Mother: A model for interpreting thermometrics. In *SPE Annual Technical Conference and Exhibition*. Society of Petroleum Engineers, 1994.

[31] EB Chekalyuk. Thermodynamics of the oil-bearing bed. *Nedra, Moscow*, 1965.

[32] A Sh Ramazanov and VM Nagimov. Analytical model for the calculation of temperature distribution in the oil reservoir during unsteady fluid inflow. *Oil and Gas Business Journal*, 1(1), 2007.

[33] Jeffrey F App. Nonisothermal and productivity behavior of high-pressure reservoirs. *Spe Journal*, 15(01):50–63, 2010.

[34] Obinna O Duru and Roland N Horne. Modeling reservoir temperature transients and reservoir-parameter estimation constrained to the model. *SPE Reservoir Evaluation & Engineering*, 13(06):873–883, 2010.

[35] Ayrat Ramazanov, Rim Abdullovich Valiullin, Valery Shako, Vyacheslav Pimenov, Alexandr Sadretdinov, Vyacheslav Fedorov, and Kirill Belov. Thermal modeling for characterization of near wellbore zone and zonal allocation. In *SPE Russian Oil and Gas Conference and Exhibition*. Society of Petroleum Engineers, 2010.

[36] Jeffrey App and Keita Yoshioka. Impact of reservoir permeability on flowing sandface temperatures: dimensionless analysis. *Spe Journal*, 18(04):685–694, 2013.

[37] Mustafa Onur and Yildiray Palabiyik. Nonlinear parameter estimation based on history matching of temperature measurements for single-phase liquid-water geothermal reservoirs. In *World Geothermal Congress, Melbourne, Australia*, pages 19–25, 2015.

[38] Mustafa Onur and Murat Çinar. Temperature transient analysis of slightly compressible, single-phase reservoirs. In *SPE Europec featured at 78th EAGE Conference and Exhibition*. Society of Petroleum Engineers, 2016.

[39] Yilin Mao and Mehdi Zeidouni. Temperature transient analysis for characterization of multilayer reservoirs with crossflow. In *SPE Western Regional Meeting*. Society of Petroleum Engineers, 2017.

[40] Mauricio SC Galvao, Marcio S Carvalho, and Abelardo B Barreto Jr. A coupled transient wellbore/reservoir-temperature analytical model. *SPE Journal*, 2019.

[41] Omer Izgec, Birol Demiral, Henri Jacques Bertin, and Serhat Akin. Experimental and numerical modeling of direct injection of co2 into carbonate formations. In *SPE annual technical conference and exhibition*. Society of Petroleum Engineers, 2006.

[42] Ibrahim Kocabas. Thermal transients during nonisothermal fluid injection into oil reservoirs. *Journal of Petroleum Science and Engineering*, 42(2-4):133–144, 2004.

[43] M Enamul Hossain, S Hossein Mousavizadegan, and M Rafiqul Islam. Rock and fluid temperature changes during thermal operations in eor processes. *Journal of nature science and sustainable technology*, 2(3):347–378, 2007.

[44] Pinan Dawkrajai, Larry Wayne Lake, Keita Yoshioka, Ding Zhu, and Alfred Daniel Hill. Detection of water or gas entries in horizontal wells from temperature profiles. In *SPE/DOE Symposium on Improved Oil Recovery*. Society of Petroleum Engineers, 2006.

[45] Mustafa Onur, Gonca Ulker, Serhat Kocak, and Ihsan M Gok. Interpretation and analysis of transient-sandface-and wellbore-temperature data. *SPE Journal*, 22(04):1–156, 2017.

[46] A Rashid Hasan and C Shah Kabir. A simple model for annular two-phase flow in wellbores. In *SPE Annual Technical Conference and Exhibition*. Society of Petroleum Engineers, 2005.

[47] AF Van Everdingen. The skin effect and its influence on the productive capacity of a well. *Journal of petroleum technology*, 5(06):171–176, 1953.

[48] A Rashid Hasan, C Shah Kabir, and Cem Sarica. *Fluid flow and heat transfer in wellbores*. Society of Petroleum Engineers Richardson, TX, 2002.

[49] Rajiv Sagar, DR Doty, and Zelimar Schmidt. Predicting temperature profiles in a flowing well. *SPE production engineering*, 6(04):441–448, 1991.

[50] Onur M. Turuyen O. I. Palabiyik, Y. and M. çinar. *Journal of Petroleum Science and Engineering*, 2016.

[51] Keith W Morton and David Francis Mayers. *Numerical solution of partial differential equations: an introduction*. Cambridge university press, 2005.

[52] Marcel Vinokur. On one-dimensional stretching functions for finite-difference calculations. *Journal of Computational Physics*, 50(2):215–234, 1983.

[53] M.S. Silva, V.R.M.;Carvalho and D.M. Quinones. Estimativa da permeabilidade de reservatórios com base em dados transientes de pressão e temperatura., 2019. Monografia (Bacharel em Engenharia Mecânica), PUC (Pontificia Universidade Católica), Rio de Janeiro, Brazil.